ENERGY CONSERVATION

ORNL/Sub/86-47985/1

Free-Piston Stirling Engine Diaphragm-Coupled Heat-Actuated Heat Pump Component Technology Program

Phase 1C Final Report

R. A. Ackermann

Report Prepared by

MECHANICAL TECHNOLOGY, INC.
968 Albany-Shaker Road
Latham, New York 12110

under
Subcontract 86X-47985V

for

OAK RIDGE NATIONAL LABORATORY
operated by
MARTIN MARIETTA ENERGY SYSTEMS, INC.
for the

U.S. DEPARTMENT OF ENERGY

OFFICE OF BUILDINGS AND COMMUNITY SYSTEMS

Printed in the United States of America. Available from
National Technical Information Service
U.S. Department of Commerce
5285 Port Royal Road, Springfield, Virginia 22161
NTIS price codes—Printed Copy: A08 Microfiche A01

This report was prepared as an account of work sponsored by an agency of the United States Government. Neither the United States Government nor any agency thereof, nor any of their employees, makes any warranty, express or implied, or assumes any legal liability or responsibility for the accuracy, completeness, or usefulness of any information, apparatus, product, or process disclosed, or represents that its use would not infringe privately owned rights. Reference herein to any specific commercial product, process, or service by trade name, trademark, manufacturer, or otherwise, does not necessarily constitute or imply its endorsement, recommendation, or favoring by the United States Government or any agency thereof. The views and opinions of authors expressed herein do not necessarily state or reflect those of the United States Government or any agency thereof.

ORNL/Sub/86-47985/1
Dist. Category UC-95d

FREE-PISTON STIRLING ENGINE DIAPHRAGM-COUPLED HEAT-ACTUATED HEAT PUMP COMPONENT TECHNOLOGY PROGRAM

PHASE 1C FINAL REPORT

R. A. Ackermann

Date Published—July 1987

Report Prepared by

MECHANICAL TECHNOLOGY, INC.
968 Albany-Shaker Road
Latham, New York 12110

under
Subcontract 86X-47985V

for the

ENERGY DIVISION
OAK RIDGE NATIONAL LABORATORY
Oak Ridge, Tennessee 37831
operated by
MARTIN MARIETTA ENERGY SYSTEMS, INC.
for the
U.S. DEPARTMENT OF ENERGY
under contract DE-AC05-84OR21400

TABLE OF CONTENTS

SECTION		PAGE
	LIST OF FIGURES	v
	LIST OF TABLES	ix
	EXECUTIVE SUMMARY	xi
	ABSTRACT	xv
1.0	INTRODUCTION	1-1
2.0	TECHNICAL DISCUSSION	2-1
	2.1 Design and Analysis of the External Vibration Absorber	2-1
	2.1.1 Absorber Assembly	2-3
	2.1.2 Theory of Operation	2-4
	2.1.3 Dynamic Behavior - Six-Degree-of-Freedom Model	2-9
	2.1.4 Leaf Spring Design	2-21
	2.1.5 Summary of Absorber Design	2-27
	2.2 Transmission Design Modifications and Checkout Testing	2-27
	2.2.1 Hydraulic Transmission and Compressor Checkout Test Results	2-30
	2.3 Breadboard Heat Pump Baseline Testing	2-35
	2.3.1 Breadboard Heat Pump Test Facility	2-35
	2.3.2 Breadboard Heat Pump Test Plan	2-40
	2.3.2.1 Test Procedure Guidelines	2-40
	2.3.2.2 Breadboard Heat Pump Data Reduction and Performance Evaluation	2-43
	2.3.2.3 Transmission Efficiency As a Function of Transmission Fluid Viscosity	2-53
	2.3.3 Performance Data Presentation	2-53
	2.3.4 Energy Balance Results	2-54
	2.3.5 Performance Test Results	2-59
	2.3.5.1 Steady-State Ambient Temperature Tests	2-67
	2.3.5.2 Transmission Oil Viscosity Tests	2-81
	2.3.6 Conclusions and Recommendations	2-89
	APPENDIX A: DESCRIPTION OF A FPSE HEAT PUMP	A-1
	APPENDIX B: HEAT PUMP PERFORMANCE DATA	B-1
	APPENDIX C: FPSE DATA ACQUISITION SYSTEM	C-1

LIST OF FIGURES

NUMBER		PAGE
1	Mark I Free-Piston Stirling Engine Breadboard Heat Pump with Direct-Drive Transmission	xii
1-1	Original Heat Pump Compressor and Hydraulic Transmission Layout with Internal Couterweight	1-2
1-2	Representative Lower End and EM FPSE Power Characteristics	1-4
1-3	EM No. 4 Free-Piston Stirling Engine Heat Pump with Internal Counterweight Removed from Transmission	1-5
2-1	Top View of Absorber	2-5
2-2	Side View of Absorber	2-6
2-3	End View of Absorber	2-7
2-4	Two-Degree-of-Freedom Schematic	2-8
2-5	Two-Degree-of-Freedom System Absorber Response vs. Frequency	2-10
2-6	Dynamic Model of HAHP with Vibration Absorbers: Top View Schematic	2-11
2-7	System Equations of Motion	2-12
2-8	Values of Dynamic Parameters	2-13
2-9	Eigenvalue - Eigenvector Results	2-15
2-10	System Tolerance to Unequal Absorber Masses ($m_1 \neq m_2$)	2-16
2-11	System Behavior with f_{n_1} = 120 Hz	2-17
2-12	Measured and Predicted Absorber Stroke vs. Frequency Predicted Housing Acceleration vs. Frequency	2-19
2-13	Compressor Housing and Combustor Lateral Acceleration Traces	2-20
2-14	Compressor Lateral Vibration and Tipping about Center of Gravity	2-22
2-15	Superposition of Lateral and Rotational Vibration	2-23
2-16	Leaf Spring Design	2-24
2-17	Rectangular vs. Tapered Leaves	2-25
2-18	Leaf Spring Bending Stress: Margin of Safety	2-26
2-19	Heat-Actuated Heat Pump with Vibration Absorbers	2-28
2-20	Direct-Drive Hydraulic Transmission and Compressor Assembly	2-29
2-21	Mark I Free-Piston Stirling Engine Breadboard Heat Pump Power Module with Direct-Drive Transmission	2-32
2-22	HAHP Breadboard Hydraulic Transmission Loss	2-33
2-23	HAHP Breadboard Hydraulic Transmission Efficiency	2-33
2-24	Compressor PV Diagram for R-22 Refrigerant	2-34
2-25	Breadboard System Oil Cavity Temperature Rise for the Internal Counterweight Compressor	2-36
2-26	Breadboard System Oil Cavity Temperature Rise for the Direct-Drive Compressor	2-36
2-27	HAHP System Schematic Showing Interface Parameters	2-38
2-28	HAHP Refrigerant Calorimeter	2-42
2-29	Refrigerant Test Loop State Points	2-42
2-30	Flow Schematic for Heat Pump Lower End	2-46
2-31	Breadboard Heating and Cooling Capacity As a Function of Ambient Temperature for a Home in the Mid-Atlantic Region	2-48
2-32	Schematic of Refrigeration Cycle	2-49
2-33	HAHP Engine Schematic Showing Parameters for Engine Energy Balancer	2-52

LIST OF FIGURES (Continued)

NUMBER		PAGE
2-34	Entire System Energy Balance	2-56
2-35	Upper End Energy Balance	2-57
2-36	Upper End Energy Balance After Instrumentation Calibration	2-58
2-37	Heat Pump Mapping of Refrigerant Flow As a Function of Time	2-60
2-38	Heat Pump Mapping of Compressor Stroke As a Function of Time	2-61
2-39	Heat Pump Mapping of Drive Piston Loss As a Function of Time	2-62
2-40	Diaphragm Life Prediction	2-65
2-41	Breadboard Heating and Cooling Capacity as a Function of Ambient Temperature for a Home in the Mid-Atlantic Region	2-68
2-42a	Breadboard Heat Pump Cooling Capacity As a Function of Compressor Piston Stroke and Ambient Temperature	2-69
2-42b	Breadboard Heat Pump Heating Capacity As a Function of Compressor Piston Stroke and Ambient Temperature	2-69
2-43	Breadboard Heat Pump System Coefficient of Performance As a Function of Ambient Temperature	2-71
2-44	Breadboard Heat Pump System Coefficient of Performance As a Function of Compressor Piston Stroke	2-71
2-45	Composite of Compressor Efficiency As a Function of Compressor Piston Stroke at All Ambient Temperatures	2-72
2-46	Breadboard Heat Pump Compressor Efficiency As a Function of Ambient Temperature	2-74
2-47	Hydraulic Transmission Power Loss As a Function of Compressor Piston Stroke	2-74
2-48	Compressor Measured Energy Flow	2-75
2-49	Hydraulic Transmission Efficiency As a Function of Compressor Piston Stroke	2-76
2-50	Hydraulic Transmission Efficiency As a Function of Ambient Temperature	2-76
2-51a	Breadboard Heat Pump Engine PV Power As a Function of Compressor Piston Stroke for the Heating Ambient Temperatures	2-78
2-51b	Breadboard Heat Pump Engine PV Power As a Function of Compressor Piston Stroke for the Cooling Ambient Temperatures	2-78
2-52	Breadboard Heat Pump Refrigerant (R-22-) Flow Rate As a Function of Compressor Piston Stroke and Ambient Temperature	2-79
2-53	Breadboard Heat Pump Hydraulic Transmission Efficiency As a Function of Compressor Piston Stroke and Hydraulic Fluid Viscosity	2-79
2-54	Transmission Power Loss As a Function of Compressor Piston Stroke and Hydraulic Fluid Viscosity	2-84
2-55	Breadboard Heat Pump Compressor Efficiency As a Function of Compressor Piston Stroke and Hydraulic Fluid Viscosity	2-84
2-56	Corrected Compressor Efficiency As a Function of Compressor Pison Stroke and Hydraulic Fluid Viscosity	2-86
2-57	Hydraulic Fluid Temperature Rise with Time for a 22-mm Displacer Stroke	2-87
A-1	Mark I Free-Piston Stirling Engine-Driven Heat Pump	A-4
A-2	Free-Piston Stirling Engine Combustor Schematic	A-6
A-3	Free-Piston Stirling Engine External Heat System	A-7

LIST OF FIGURES (Continued)

NUMBER		PAGE
A-4	Displacer Rod Dynamics	A-8
A-5	Free-Piston Stirling Engine Displacer Gas Spring Design	A-10
A-6	Monolithic Heater Head Configuration for Engineering Model Engine	A-12
A-7	Hydraulic Transmission and Compressor Schematic	A-13
A-8	Compressor Housing	A-14
C-1	Free-Piston Data Acquisition System	C-4
C-2	Error Associated with DAS Phase Angle Calculations	C-7

LIST OF TABLES

NUMBER		PAGE
1	FPSE Heat Pump Performance Data	xiv
2-1	Phase IB Breadboard Heat Pump Performace Results	2-2
2-2	Code Analytical Routines	2-14
2-3	Comparison of HAHP Breadboard Heat Pump Module with and without Internal Counterweight (95°F Ambient Temperature Conditions)	2-37
2-4	HAHP Performance Measurement Instruments	2-39
2-5	Compressor Description - Build 1	2-41
2-6	Heat Pump Test Conditions for R-22 Refrigerant	2-44
2-7	Test Plan Matrix for Different Ambient Temperatures and Displacer Strokes	2-45
2-8	Key Parameter Comparisons for Tests Conducted with the Oil Accumulation in the Refrigerant Loop	2-63
2-9	Actual Matrix of Test Data for Different Ambient Temperatures and Displacer Strokes	2-66
2-10	Heat Pump Mapping for Steady-State Performance Parameters (for 10-cs Silicon Oil)	2-80
2-11	Heat Pump Mapping - Compressor Transmission Oil Properties	2-82
2-12	Heat Pump Mapping Compressor Chevron Seal Leakage From Oil Viscosity Tests	2-88

EXECUTIVE SUMMARY

During Phase I of the Heat-Actuated Heat Pump Development Program, a Breadboard Heat Pump power module consisting of a free-piston Stirling engine (FPSE), a hydraulic transmission, and a linear-resonant refrigerant compressor was designed and fabricated. The essential ground rule of this development was the use of an existing Mechanical Technology Incorporated FPSE. During testing, this breadboard heat pump fell far short of its design capacity of 3.0 tons of cooling at 95°F ambient conditions. In Phases IA and IB, excessive losses in the hydraulic transmission were identified as the cause of the shortfall in capacity and the hydraulically driven counterweight inside the transmission as the major cause of the high loss. The object of Phase IC of the program was to replace the internal counterweight with an external vibration absorber and to test the breadboard heat pump, shown in Figure 1, over a broad range of ambient conditions from 0 to 95°F.

The work elements of the Phase IC program addressed the design, fabrication, and test of the external absorber, the development of a comprehensive test plan for the breadboard heat pump, and the steady-state testing of the heat pump to determine its performance in both the heating and cooling modes. The specific objectives of the testing were, first, to operate the heat pump over a range of ambient conditions from 0 to 95°F; second, to establish the steady-state performance of the unit at each of these points; and third, to achieve a minimum cooling capacity of 2.5 tons at the 95°F ambient conditions. The following results were achieved:

1. The external absorber performed very well and improved performance by significantly reducing the losses in the hydraulic transmission. The breadboard heat pump achieved its performance goal of 2.5 tons of cooling at the 95°F ambient condition. At this operating point, the hydraulic transmission efficiency was 88%, and the COP of the hydraulic transmission and compressor (lower end) was 3.75.

2. The vibration measurements on the combustor with the external absorber were lower than with the internal counterweight. The maximum vibration recorded on the combustor was 0.3 g; the goal was to

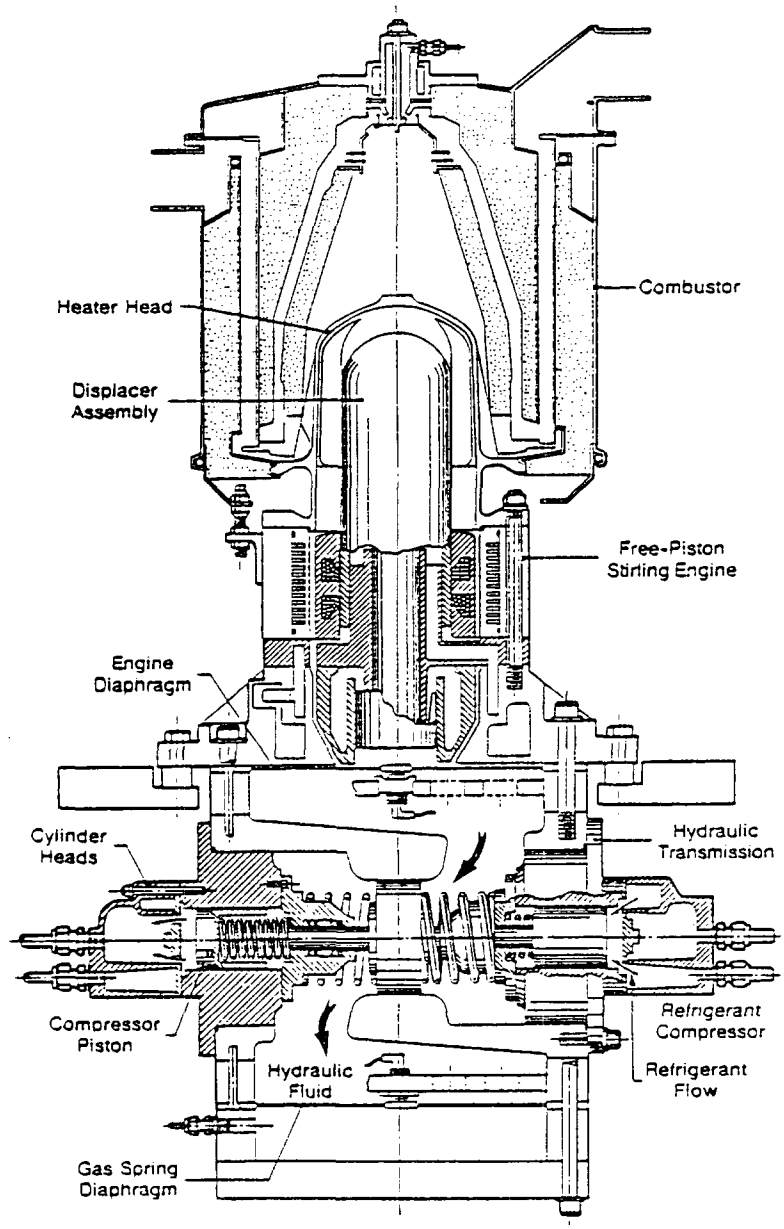

Figure 1 Mark I Free-Piston Stirling Engine Breadboard Heat Pump with Direct-Drive Transmission (Mark I engine configuration shown is similar to EM No. 4 FPSE)

853393

obtain less than 1.0 g, which was the vibration level measured on the combustor of the FPSE used during the 5000 hours of endurance testing.

3. Breadboard heat pump performance testing over a range of ambients from 0 to 95°F was completed. Over this entire range of ambients, the engine was stable; and accurate, repeatable, steady-state data were obtained. A summary of the results of this testing is given in Table 1.

Table 1

FPSE Heat Pump
Performance Data

Parameter	Measured Data (R-22) Ambient Temperature °F (°C) 95 (35)	47 (8.3)	Precision (±)
Evaporating Temperature, °F (°C)	44 (6.7)	34 (1.1)	2.0 (1.1)
Condensing Temperature, °F (°C)	121 (49.4)	100 (37.8)	1.5 (0.8)
Pressure Ratio	3.09	2.82	—
System Capacity (Maximum) Btu/h (MJ/h)	28,950 (30.5)	62,342 (65.8)	1,000 (1.0)
Transmission Efficiency (%)	88	83	3.0
Compressor Efficiency (%)	75	76	2.0
Lower End COP	3.75	4.92	0.12
System COP*	0.64	1.39	0.20

*Based on HHV of fuel

ABSTRACT

The Heat-Actuated Heat Pump Program has consisted of three previous phases: Phase I, IA, and IB. Each of these phases has been documented in a final report published for the U.S. Department of Energy (DOE), Office of Building Energy Research and Development. The objective of this phase, Phase IC, was to demonstrate the performance of the breadboard free-piston Stirling engine heat pump (FPSE/HP) over a range of ambient temperature conditions from 0 to 95°F. This testing was performed successfully.

During Phase IC, the counterweight inside the hydraulic transmission was replaced with an external vibration absorber. The vibration absorber is a passive, resonant spring mass unit mounted to the compressor housing. The absorber exhibits a fairly broad frequency bandwidth over which it effectively reduces lateral housing vibrations. The performance of the heat pump was substantially improved by eliminating the internal counterweight. The capacity was increased by 25% to 2.5 tons of cooling at the 95°F ambient conditions, and the transmission efficiency was increased from about 63% to 88%.

Phase IC completes the development and testing of the first generation of breadboard hardware. The program has been successful in that all of the goals, with the exception of 3.0 tons of cooling capacity at the 95°F ambient conditions, have been achieved. The follow-on to this work will be to replace the FPSE used on the breadboard system with a second generation FPSE, the Mark I, and to repeat the baseline breadboard performance testing. The Mark I FPSE is being developed under a parallel program sponsored by the Gas Research Institute (GRI). The Mark I includes several improvements that should improve the breadboard performance and enable the FPSE/HP to achieve its capacity goal of 3.0 tons of cooling.

1.0 INTRODUCTION

During 1980, Mechanical Technology Incorporated (MTI) identified the diaphragm-coupled hydraulic transmission as the best means for providing hermetic coupling between a free-piston Stirling engine (FPSE) and a refrigerant compressor. The essential features of the MTI concept were positive seal (diaphragm), hydraulically powered transmission, and vibration balance (counterweight).

The first-generation diaphragm-coupled compressor was developed during Phase I of the program as part of a breadboard configuration. The original transmission and compressor (shown in Figure 1-1) included a hydraulically driven counterweight inside the transmission for vibration balance. The breadboard system consisted of a natural gas combustor, the "Engineering Model" FPSE, and the transmission/compressor lower end. The object of this work was to prove the technical feasibility of the design approach. The initial Phase I development program addressed the following points:

- Efficiency
- Stability
- Capacity
- Vibration balance
- Capacity modulation
- Durability.

The Phase I program resulted in good technical progress, which verified the technical feasibility of the diaphragm-coupled hydraulic design and provided operational data on several key items; namely,

- Stable operation of the engine and compressor
- Vibration-free operation
- Capacity modulation
- Durability of the diaphragms.

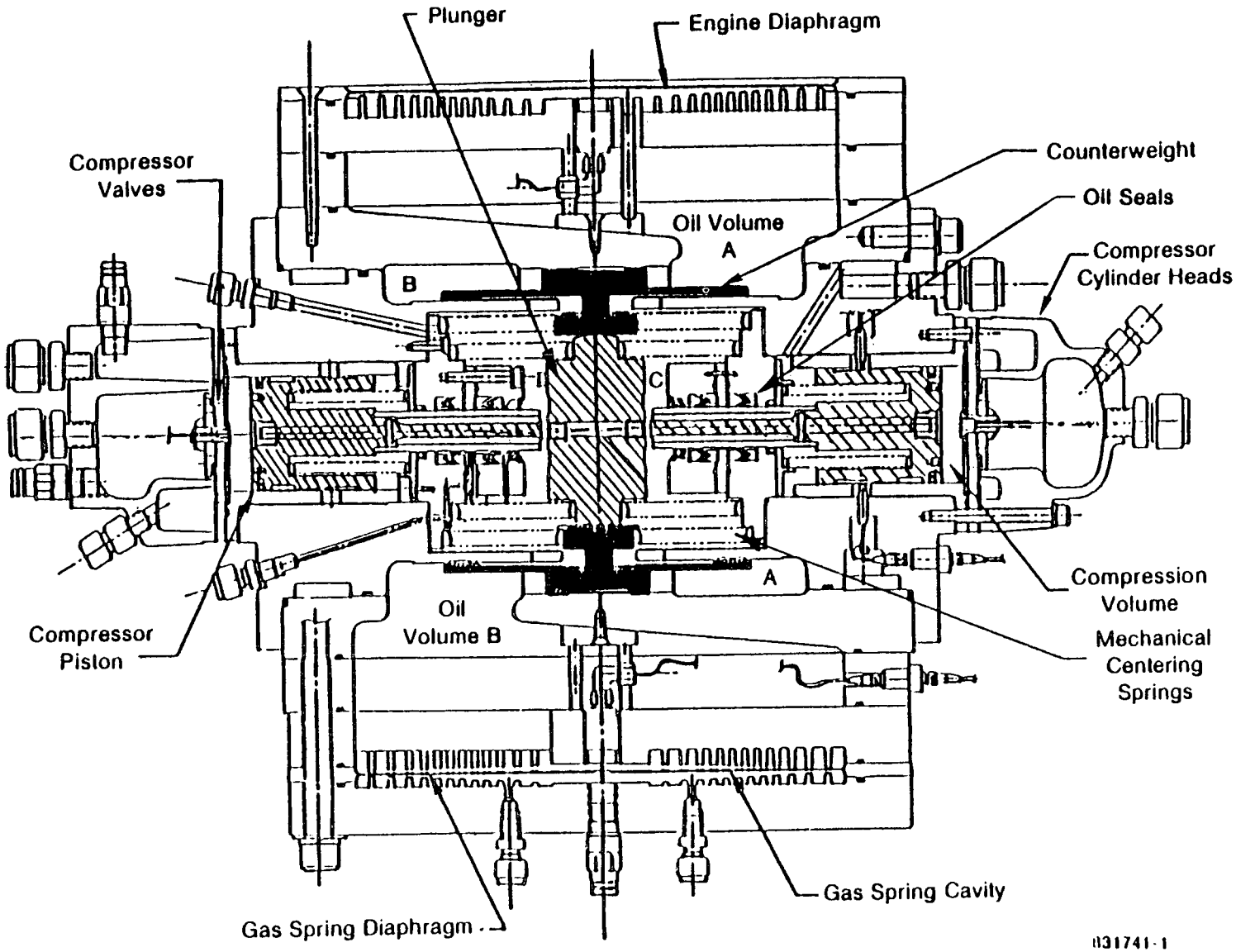

Figure 1-1 Original Heat Pump Compressor and Hydraulic Transmission Layout with Internal Counterweight

At the end of Phase I the major outstanding problem with the breadboard heat pump was difficulty in achieving the 3.0 ton full-rated capacity with the compressor at 95°F ambient conditions.

In two subsequent Phases, IA and IB, extensive analysis and experimentation convinced the MTI program team that the compressor design was neither geometrically nor thermodynamically limited from achieving its rated capacity. Further, the engine was known to provide ample power output to drive the compressor to its rated capacity. More specifically, the compressor requires ~3500 W of pressure volume (PV) at rated capacity, and the engine had been measured to provide up to 4200 W of PV power when coupled to an electric alternator load.

Analysis and test data showed that the original hydraulic transmission did not meet its design specification because of excessive losses. That is, the hydraulic transmission, with high loss, absorbed too much energy and did not allow the engine/compressor system to operate at the design piston stroke. This is shown in Figure 1-2, where the hydraulic transmission and compressor load characteristics are plotted along with the engine's power output characteristics. The intersection of these two curves represents the operating point for the system. The result of the increased transmission losses is seen to raise the load line of the transmission and compressor, producing a lower piston stroke and a reduced engine PV power output. This result is analogous to a rotary prime mover where too high a starting load will prevent the machine from reaching its full speed. By reducing the load, the speed will increase and the machine will produce its rated power.

The individual losses in the hydraulic transmission were evaluated, and it was concluded that the internal counterweight (shown in Figure 1-1) was the major contributor to the excessive transmission losses. During Phase IB, the internal counterweight was removed from the transmission (see Figure 1-3), and the breadboard system was operated in an unbalanced mode. Extensive testing was not possible because of extreme vibration levels, but the testing did indicate that the direct-drive transmission would result in greatly reduced losses. A more comprehensive description of the FPSE heat pump system is presented in Appendix A.

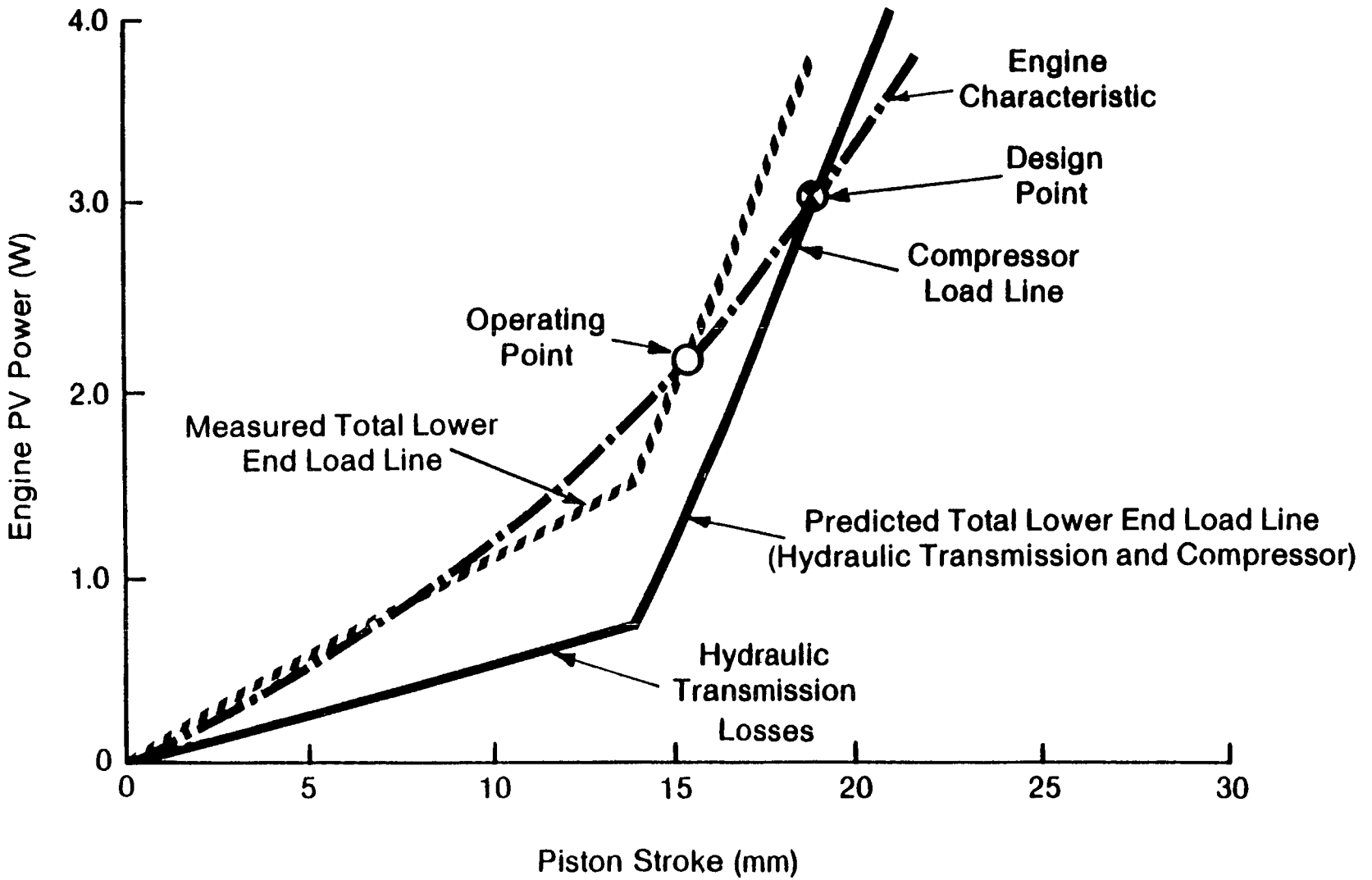

Figure 1-2 Representative Lower End and EM FPSE Power Characteristics

852206-1

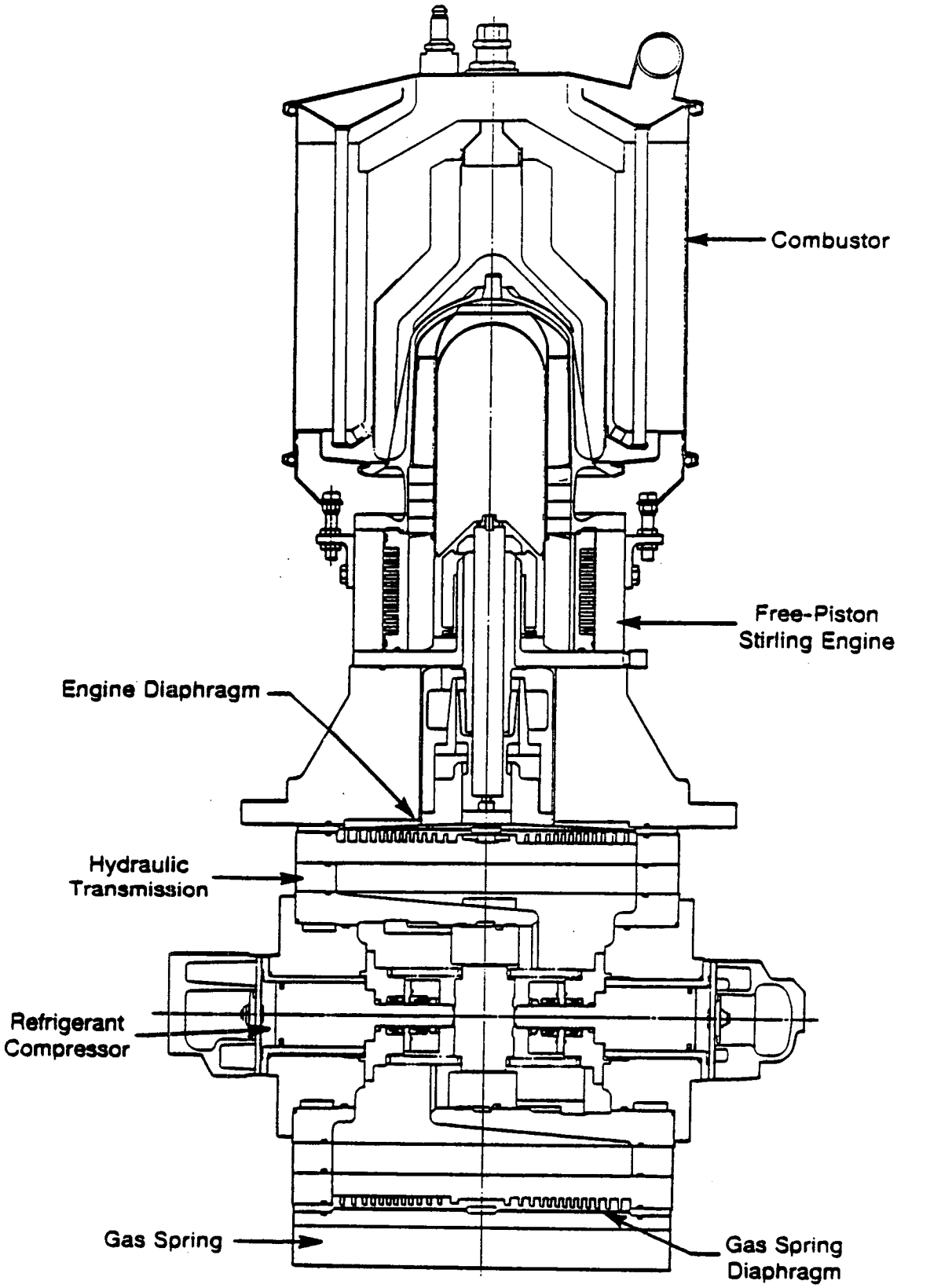

Figure 1-3 EM No. 4 Free-Piston Stirling Engine Heat Pump with Internal Counterweight Removed from Transmission

The objective of Phase IC of the program was to develop an external vibration absorber to replace the internal counterweight and thus permit long-term steady-state testing of the direct-drive transmission. The program included an evaluation of several absorber approaches, and a tuned spring mass system that could easily be mounted to the compressor housing was selected. The absorber was fabricated and tested during this phase of the program, and the results have shown that the absorber is very effective in eliminating compressor housing vibrations. This, in turn, has allowed the breadboard heat pump to achieve good steady-state operation and enabled MTI to conduct performance tests on the breadboard heat pump over a broad range of ambient conditions from 0 to 95°F. This report presents the design of the external vibration absorber and the heat pump performance results that were achieved.

2.0 TECHNICAL DISCUSSION

Phase IC consisted of three major technical tasks;

1. Design and analysis of the external vibration absorber
2. Checkout testing of the breadboard heat pump with the external vibration absorber
3. Breadboard heat pump baseline performance testing.

At the completion of Phase IB, analysis results showed that higher than predicted losses in the hydraulic transmission were preventing the breadboard heat pump from achieving its capacity goals. The cause was determined to be the clearance seals and the serpentine flow passages created by the counterweight. The best breadboard performance recorded at the end of Phase IB is given in Table 2-1, where the shortfall in capacity and the large hydraulic transmission loss associated with the counterweight are shown.

The design of the external vibration absorber and the results obtained from the breadboard heat pump performance testing are described in the following sections.

2.1 Design and Analysis of the External Vibration Absorber

To allow the use of the direct-acting refrigerant compressor, an externally tuned vibration absorber has been design, analyzed, and installed on the breadboard system. This vibration absorber consists of two 35-lb_m assemblies attached to the right and left sides of the compressor housing by means of leaf springs. The vibration absorber assemblies oscillate laterally and generate forces at their attachment points to the compressor housing which are equal and opposite to the inertia force produced by the piston and center bearing assembly. Without the absorber assemblies, a net shaking force of 2630 lb_f at 60 Hz is generated by the piston assembly moving at 22-mm stroke. Under these conditions, housing acceleration is $\sim$9.2 g and combustor life

Table 2-1

Phase IB Breadboard Heat Pump Performance Results

Mode	With Counterweight
Date	3/29/85*
Scan No.	34
Refrigerant	R-22
Hydraulic Oil	Dow Corning 200, 2 cs
Mean Pressure (bar)	62.1
Frequency (Hz)	58.0
Average Heater Head Temperature (°C)	710
Counterweight Stroke (mm)	15.25
Piston Stroke (mm)	15.25
Displacer Stroke (mm)	21.73
$\Theta_{d,p}$ (°)	89.8
Suction Pressure (psia)	89.6
Discharge Pressure (psia)	280.3
Suction Temperature (°F)	46.6
Discharge Temperature (°F)	144.5
Refrigerant Flow (lb_m/hr)	342
Refrigerant Capacity (Btu/hr)	23,000
Comp. Adiabatic Power (W)	1,258.8
Compressor PV Power (W)	1,576.3
Engine PV Power (W)	2,511.6
Counterweight Loss (W)	612.8
Piston Loss (W)	299.2
Gas Spring Loss (W)	28.7
Hydraulic Fluid Loss (W)	(5.4)
Overall Lower End Efficiency (%)	50.1
Hydraulic Transmission Efficiency (%)	62.8

*With 3-mm piston shim

would probably not exceed one hour.* With the absorber tuned to match the system's operating frequency, housing acceleration in the lateral direction becomes negligible.

This report describes in detail the design, analysis, and measured performance of the absorber assemblies mounted to the direct-acting refrigerant compressor. First, drawings illustrate the right-side absorber assembly as mounted to the compressor housing. Second, the general theory of operation for tuned vibration absorbers is given, referring to results for a two-degree-of-freedom system. Then, a computer model is described in which six-degrees-of-freedom are used to represent

- Lateral motion of each absorber independently
- Translation and rotation of the engine/compressor
- Translation and rotation of the test stand which is connected to ground by mounts having soft lateral and rotational stiffness.

The model is used to obtain the six natural frequencies of the system with their associated mode shapes and also to obtain steady-state response of the system to applied harmonic forcing functions which represent shaking force and moment. Measured absorber strokes are compared to computer predictions over a range of test frequencies. The design of the absorber leaf springs is covered in Section 2.1.4, and a summary of system specifications and performance is presented in Section 2.1.5.

2.1.1 Absorber Assembly

Each absorber assembly is mounted to the side of the compressor housing using two leaf spring packs clamped together and also clamped to a vertical gusset, which is part of the transmission casting. Aluminum spacer strips, 0.040-in. thick, are used between each leaf spring to maintain separation. The top view

---

*Because of the system geometry relative to center of gravity location, combustor lateral acceleration is significantly less than compressor housing acceleration. Combustor analysis has established an upper limit of 1 to 1.5 g lateral acceleration for long life.

of the right-side absorber assembly is shown in Figure 2-1, and the side view and end view are shown in Figures 2-2 and 2-3, respectively. The leaf spring packs support the assembly by attachment to the center mass (Figure 2-1). The remaining weights for the assembly (top plate, bottom plate, and end plates) are then bolted to the center mass in a way designed to conserve space. Two support brackets for each absorber assembly are used to transmit most of the cyclic load, due to leaf spring deflection, directly to the wall of the compressor housing. Without these brackets, analysis indicates that fatigue of the gusset would probably occur. Tuning plates can be attached to the outside surface of each absorber assembly to adjust its design frequency, as shown in Figure 2-1.

2.1.2 Theory of Operation

The basic principle of operation, see Figure 2-4, can be stated simply: design a mass-spring system to be mounted to the main mass which will oscillate with an amplitude and phase such that the spring force K_A $(x_A - x_E)$ exactly opposes the applied shaking force F at all times. The amplitude of the absorber mass, m, for these conditions equals F_0/K_A, and it can be shown that this amplitude occurs when m and K_A are chosen such that $\sqrt{K_A/m}$ equals ω, the angular frequency of the applied shaking force.*

In the case where the absorber 'natural frequency' $(\frac{1}{2\pi})\omega_A$ equals 60 Hz, note that neither of the two natural frequencies for the coupled two-degree-of-freedom system equals 60 Hz, provided that the mass ratio m/M_E is not equal to zero. For m/M_E equal to 1.0, the higher system resonance equals $\sqrt{2}$ times 60 Hz assuming the spring to ground is relatively soft. For the mass ratio used in the actual absorber design, 0.246, the higher system resonance becomes approximately 67 Hz. The lower system resonance is governed by the soft spring to ground and generally will be less than 10 Hz if isolators are used to mount the engine/compressor assembly.

---

*Den Hartog, J. P. Mechanical Vibrations. 4th Ed. Section 3.2. New York: McGraw-Hill, 1956.

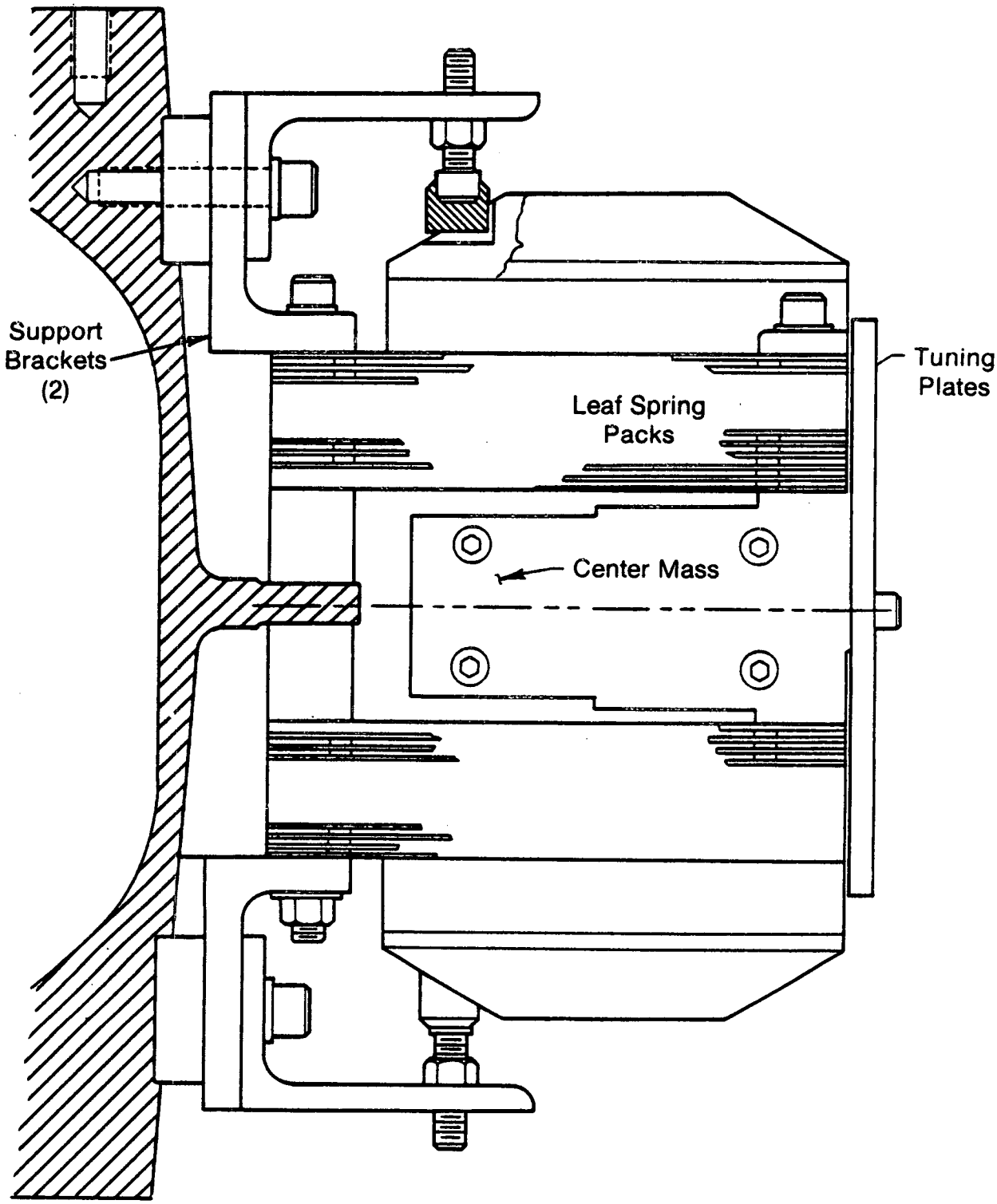

Figure 2-1 Top View of Absorber

852949-1

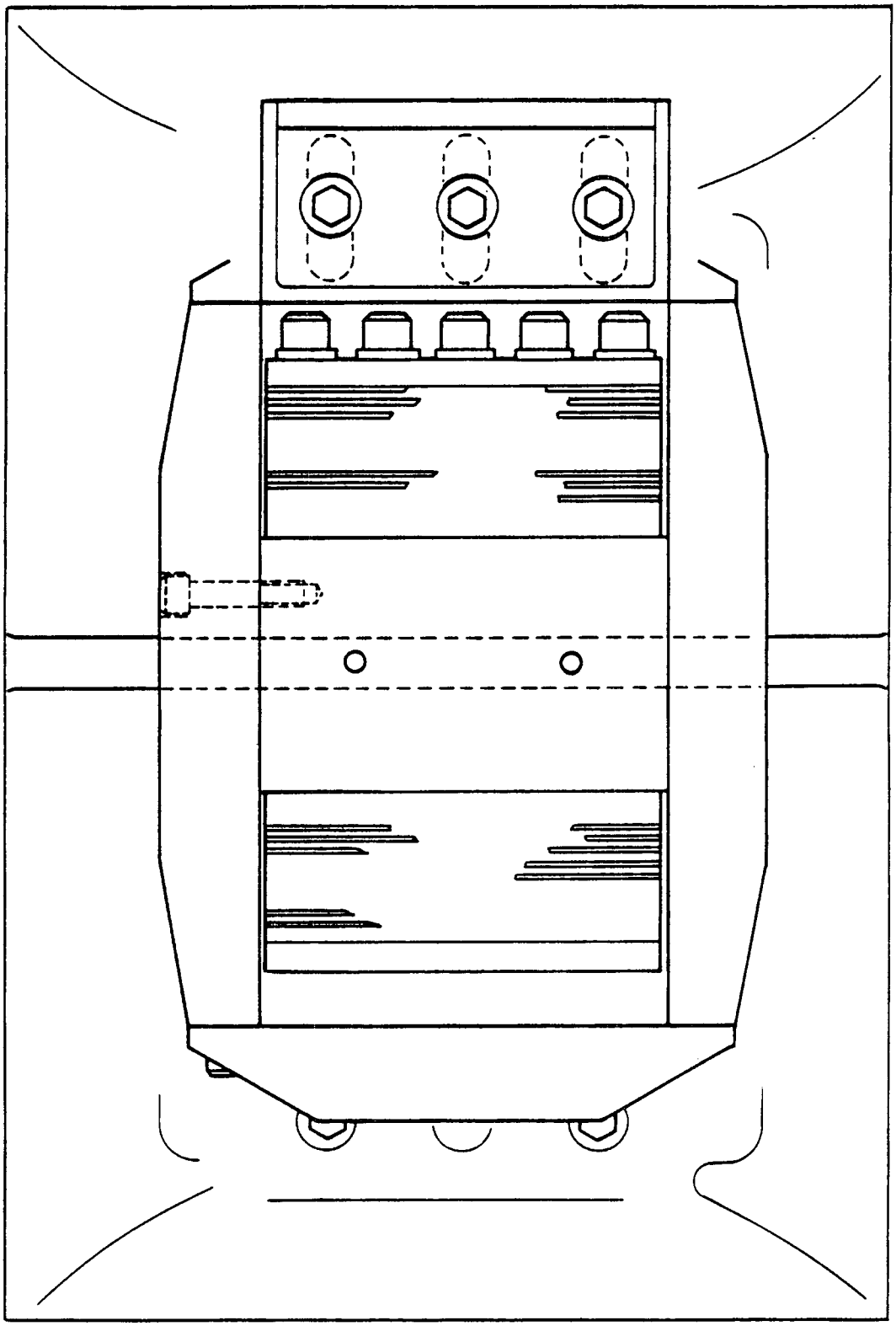

Figure 2-2 Side View of Absorber

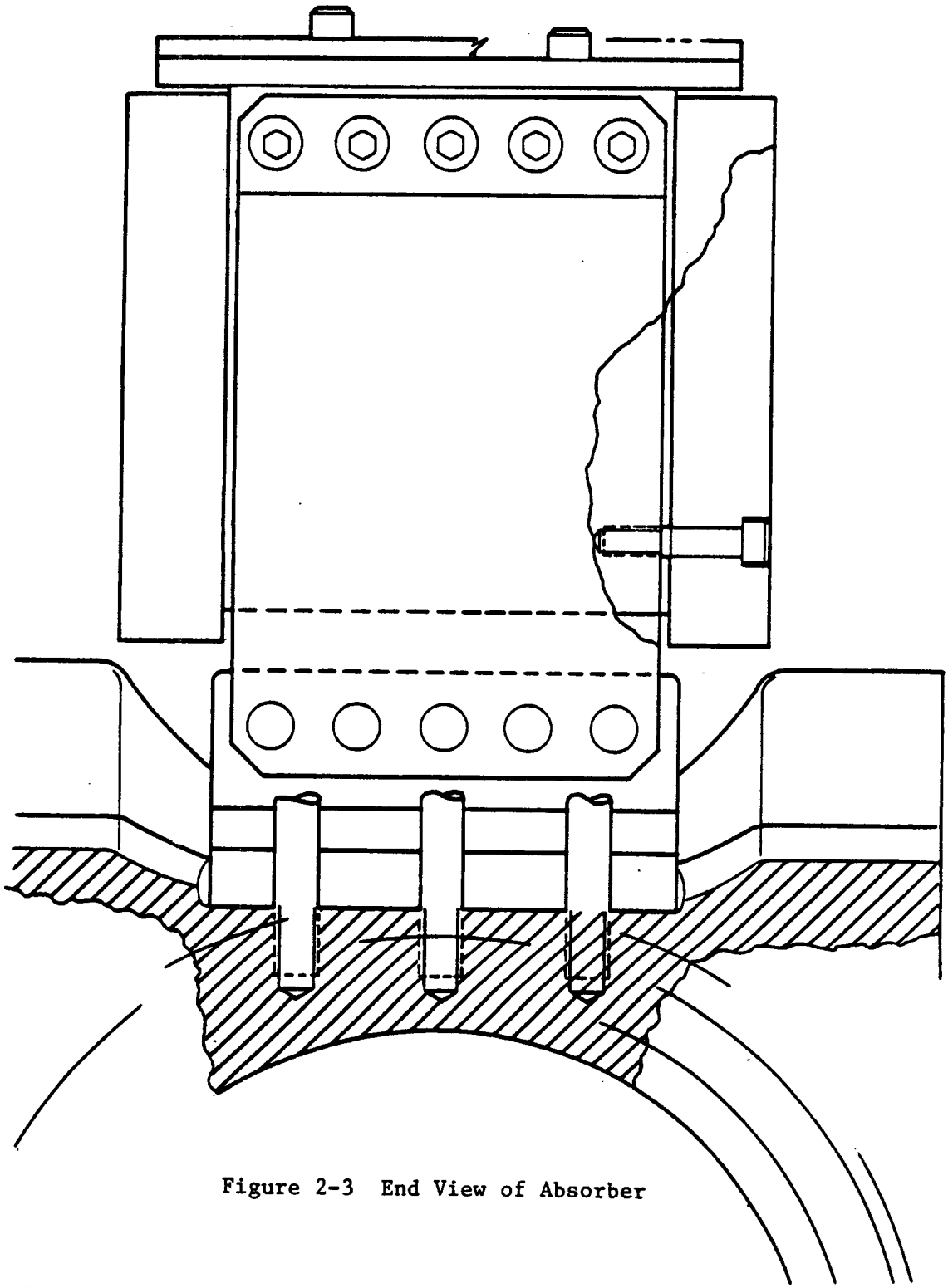

Figure 2-3 End View of Absorber

852950

Two Degree-of-Freedom System:

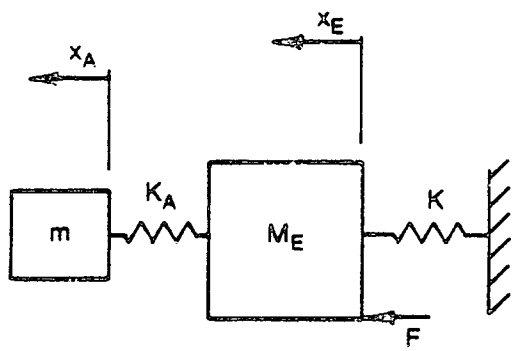

$$F = F_o \sin \omega t$$
$$x_A = X_{A_o} \sin (\omega t + \phi_1)$$
$$x_E = X_{E_o} \sin (\omega t + \phi_2)$$

Define: $M_{AR} = m/M_E$ Mass Ratio

$\omega_R = \omega/\omega_A$ Freq. Ratio

Where $\omega_A = \sqrt{K_A/m}$

$X^*_{E_o} = (-F_o / \omega^2 M_E)$ (Amplitude of Case without Absorber)

$X^*_{A_o} = (-F_o / K_A)$ (Absorber Amplitude at Ideal Tuning)

Assuming Very Soft Spring to Ground, K, Solution of Equations of Motion Yields:

$$X_{A_o} = \frac{X^*_{A_o} M_{AR}}{\omega_R^2 (M_{AR} + 1 - \omega_R^2)}, \qquad X_{E_o} = X^*_{E_o} \frac{1 - \omega_R^2}{\omega_R^4 (M_{AR} + 1 - \omega_R^2)}$$

$$\phi_1 = 180, \qquad \phi_2 = 180$$

Use m = 70 lb_m (Spring Deflections Approximately ±0.10 in. at 22 mm Stroke)

and M_E = 285 lb_m (Compressor Soft Mounted to Stand; Tuning Sensitivity Becomes Broader-Band)

Figure 2-4 Two-Degree-of-Freedom Schematic

The sensitivity of the system to operation at off-design frequencies is shown in Figure 2-5. This curve shows that absorber stroke is optimal when operating frequency is precisely 60 Hz. For operation at 4 Hz less than nominal, the absorber understrokes by 75%. However, at 4 Hz greater than nominal, the absorber overstrokes by nearly 100%. This indicates that if broadband operation is desired, operation at frequencies somewhat less than the tuned frequency of the absorber should be attempted.

2.1.3 Dynamic Behavior - Six-Degree-of-Freedom Model

The dynamic behavior of the refrigerant compressor, mounted to an existing test stand and with absorber assemblies attached, has been simulated using a six-degree-of-freedom computer model. This model considers motion in a horizontal plane and allows independent motion of the absorber assemblies. Rotation, as well as fore and aft lateral translation, of both the engine/compressor and test stand is also considered. A top view schematic of the actual system (Figure 2-6) illustrates the degrees-of-freedom considered: x_1, x_2 (motion of the absorber assemblies); x_3, θ_3 (lateral shaking of the compressor and rotation about the vertical axis); and x_4, θ_4 (lateral shaking of the test stand and rotation about the vertical axis). The six equations of motion for the system and the values of all dynamic parameters are given in Figures 2-7 and 2-8, respectively; the computer analytical routines used are described in Table 2-2. Damping in the system was added at the isolators between the compressor and the test stand and also at the floor mount isolators for the test stand. Damping coefficients were calculated such that damping ratios for these low frequency motions are $\sim$0.2.

Results from the model are given in Figures 2-9 through 2-11. Figure 2-9 gives the six undamped natural frequencies for the system and the associated mode shapes. The damped natural frequencies were also calculated, and these are shown in parentheses on the figure. No problems with system stability are indicated from these results, since none of the system natural frequencies are close to the operating frequency of 60 Hz.

Other results of the analysis involve steady-state response to an applied harmonic forcing function. The tolerance of the system to unequal absorber

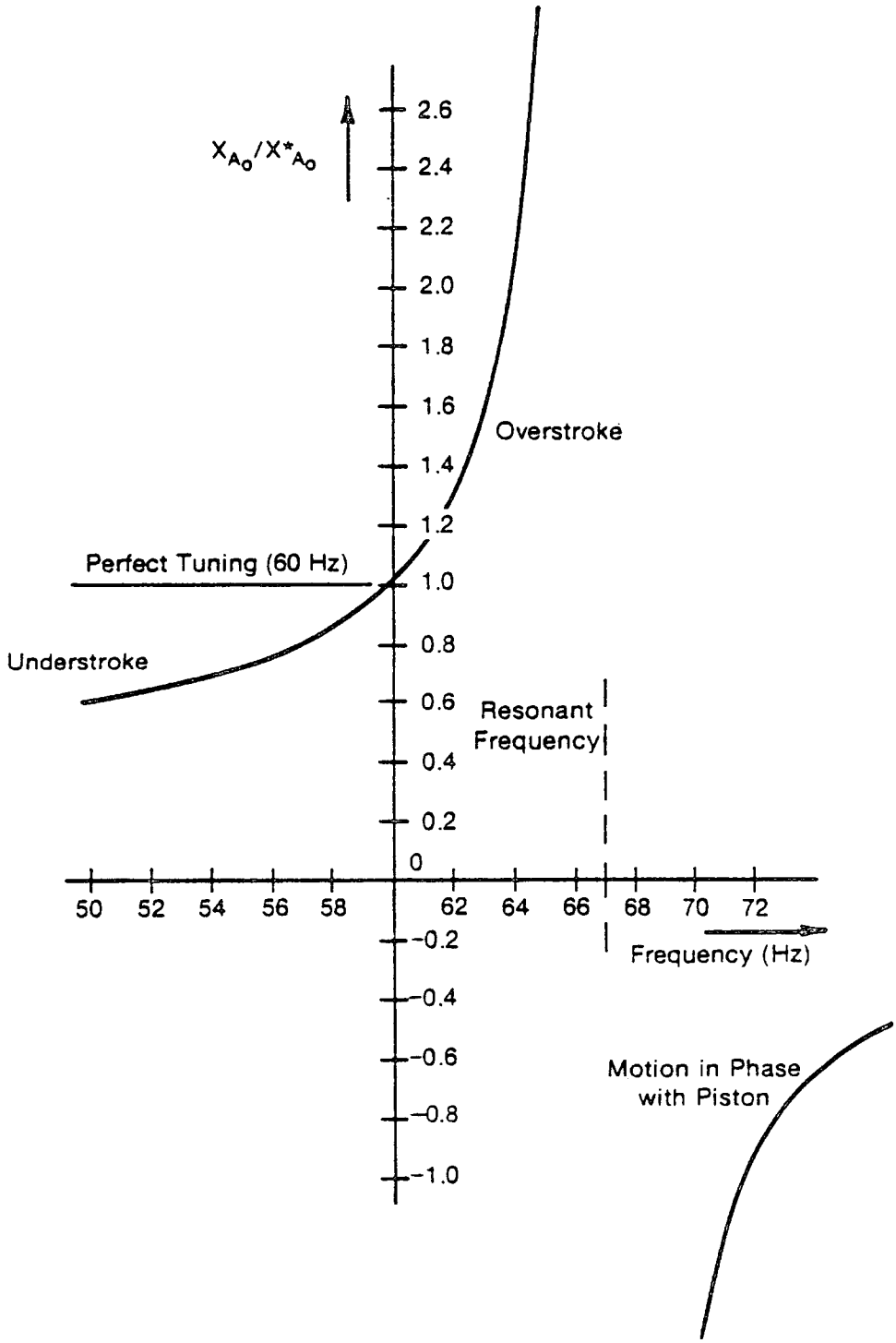

Figure 2-5 Two-Degree-of-Freedom System Absorber Response vs. Frequency

852942

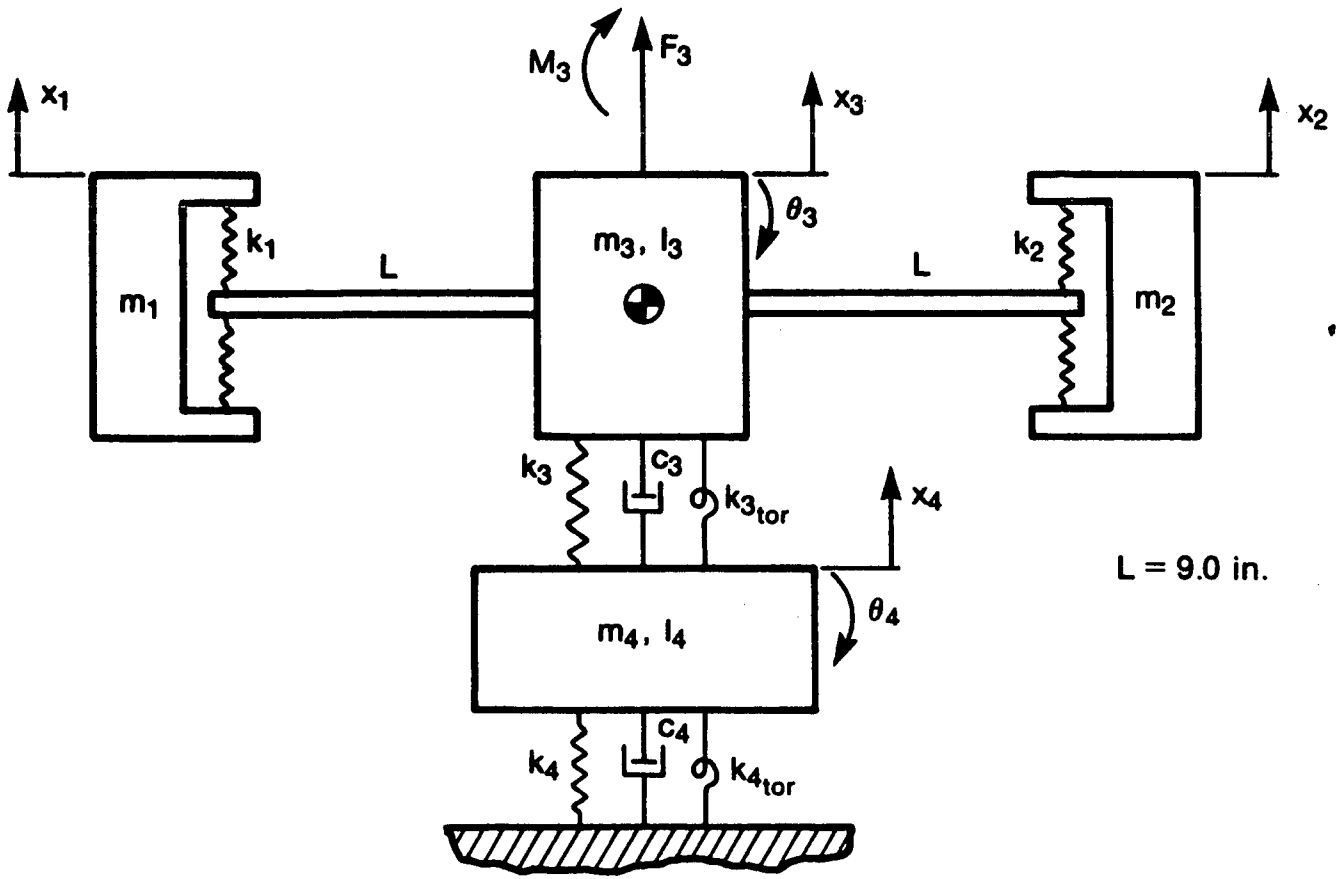

Figure 2-6 Dynamic Model of HAHP with Vibration Absorbers: Top View Schematic

852444

$$\underline{m}\,\underline{\ddot{x}} + \underline{c}\,\underline{\dot{x}} + \underline{k}\,\underline{x} = \underline{F}.$$

$$\begin{bmatrix} m_1 & 0 & 0 & 0 & 0 & 0 \\ 0 & m_2 & 0 & 0 & 0 & 0 \\ 0 & 0 & m_3 & 0 & 0 & 0 \\ 0 & 0 & 0 & m_4 & 0 & 0 \\ 0 & 0 & 0 & 0 & I_3 & 0 \\ 0 & 0 & 0 & 0 & 0 & I_4 \end{bmatrix} \begin{bmatrix} \ddot{x}_1 \\ \ddot{x}_2 \\ \ddot{x}_3 \\ \ddot{x}_4 \\ \ddot{\theta}_3 \\ \ddot{\theta}_4 \end{bmatrix} + \begin{bmatrix} 0 & 0 & 0 & 0 & 0 & 0 \\ 0 & 0 & 0 & 0 & 0 & 0 \\ 0 & 0 & c_3 & -c_3 & 0 & 0 \\ 0 & 0 & -c_3 & c_3 + c_4 & 0 & 0 \\ 0 & 0 & 0 & 0 & c_{3_t} & -c_{3_t} \\ 0 & 0 & 0 & 0 & -c_{3_t} & (c_{3_t} + c_{4_t}) \end{bmatrix} \begin{bmatrix} \dot{x}_1 \\ \dot{x}_2 \\ \dot{x}_3 \\ \dot{x}_4 \\ \dot{\theta}_3 \\ \dot{\theta}_4 \end{bmatrix}$$

$$+ \begin{bmatrix} k_1 & 0 & -k_1 & 0 & -k_1L & 0 \\ 0 & k_2 & -k_2 & 0 & +k_2L & 0 \\ -k_1 & -k_2 & (k_1 + k_2 + k_3) & -k_3 & (k_1L - k_2L) & 0 \\ 0 & 0 & -k_3 & (k_3 + k_4) & 0 & 0 \\ -k_1L & +k_2L & (k_1L - k_2L) & 0 & (k_1L^2 + k_2L^2 + k_{3_t}) & -k_{3_t} \\ 0 & 0 & 0 & 0 & -k_{3_t} & (k_{3_t} + k_{4_t}) \end{bmatrix} \begin{bmatrix} x_1 \\ x_2 \\ x_3 \\ x_4 \\ \theta_3 \\ \theta_4 \end{bmatrix} = \begin{bmatrix} 0 \\ 0 \\ F_3 \\ 0 \\ M_3 \\ 0 \end{bmatrix}$$

Figure 2-7 System Equations of Motion

861361

$m_1 = 9.067 \times 10^{-2}$ lb_f $sec^2/in.$

$m_2 = 9.067 \times 10^{-2}$ lb_f $sec^2/in.$

$m_3 = 0.7383$ lb_f $sec^2/in.$

$m_4 = 2.202$ lb_f $sec^2/in.$

$I_3 = 18.90$ in. lb_f $sec.^2$

$I_4 = 936.1$ in. lb_f $sec.^2$

$k_1 = 12{,}887$ $lb_f/in.$

$k_2 = 12{,}887$ $lb_f/in.$

$k_3 = 1560$ $lb_f/in.$

$k_4 = 530$ $lb_f/in.$

$k_{3t} = 8.892 \times 10^4$ in. lb_f/rad

$k_{4t} = 3.445 \times 10^5$ in. lb_f/rad

$c_3 = 15.15$ lb_f sec/in

$c_4 = 16.87$ lb_f sec/in

$c_{3t} = 691.4$ in. lb_f sec

$c_{4t} = 7311$ in. lb_f sec

$L = 9.0$ in.

$\frac{1}{2\pi}\sqrt{k_1/m_1} = 60$ Hz

damping ratio, $\xi = 0.2$ for motion on engine mounts and floor mounts.

spring rates k_4 and k_{4t} calculated to give frequencies equal 2 and 3 Hz, respectively

Figure 2-8 Values of Dynamic Parameters

Table 2-2

Code Analytical Routines

1. EIGENVALUES - EIGENVECTORS

   a. IMSL routine EIGZF - used to analyze undamped and damped systems

   b. Performs matrix operations on the equations $\underline{K}\ \underline{X} = \omega^2\ \underline{M}\ \underline{X}$ to find values of ω^2 and associated $\underline{X}$ which satisfy. Operations are equivalent to finding roots of the characteristic equation.

2. STEADY-STATE RESPONSE TO APPLIED HARMONIC FORCING FUNCTION

   a. Forms set of coupled linear complex equations which result for a given frequency, amplitude, and phase of $\underline{F}$.

$$\underline{F} = -\omega\ \underline{M}^2\underline{X} + j\omega\ \underline{C}\ \underline{X} + \underline{K}\ \underline{X}$$

   b. Performs Gauss elimination to solve for magnitude and phase of response.

   c. Requests new frequency for subsequent evaluation if desired.

$\bar{X}_1$	$\bar{X}_2$	$\bar{X}_3$	$\bar{X}_4$	$\bar{X}_5$	$\bar{X}_6$
$\begin{bmatrix} -.0020 \\ +.0020 \\ 0.0 \\ 0.0 \\ +1.7 \times 10^{-3} \\ -6.5 \times 10^{-8} \end{bmatrix}$	$\begin{bmatrix} +.0024 \\ +.0024 \\ -5.9 \times 10^{-4} \\ +2.4 \times 10^{-6} \\ 0.0 \\ 0.0 \end{bmatrix}$	$\begin{bmatrix} +.019 \\ -.019 \\ 0.0 \\ 0.0 \\ 2.07 \times 10^{-3} \\ -8.52 \times 10^{-5} \end{bmatrix}$	$\begin{bmatrix} -.020 \\ -.020 \\ -.019 \\ +.0092 \\ 0.0 \\ 0.0 \end{bmatrix}$	$\begin{bmatrix} -.078 \\ -.078 \\ -.078 \\ -.070 \\ 0.0 \\ 0.0 \end{bmatrix}$	$\begin{bmatrix} -.053 \\ +.053 \\ 0.0 \\ 0.0 \\ -.0059 \\ -.0052 \end{bmatrix}$
80.33 Hz (80.26)*	67.05 Hz (67.04)	8.38 Hz (8.20)	7.92 Hz (7.64)	2.04 Hz (2.00)	3.00 Hz (2.94)

f_{n_1} = 80.33 Hz - absorbers out of phase with rotation of housing

f_{n_2} = 67.05 Hz - lateral shaking; abosrbers out of phase with housing

f_{n_3} = 8.38 Hz - rotation of housing on shear mounts; absorbers in phase with housing

f_{n_4} = 7.92 Hz - lateral motion of housing and absorbers on shear mounts

f_{n_5} = 2.04 Hz - lateral motion of stand on floor mounts

f_{n_6} = 3.00 Hz - rotation of stand on floor mounts

* Frequencies in parentheses result when damping is included

Figure 2-9 Eigenvalue - Eigenvector Results

861363

- SIX-DEGREE-OF-FREEDOM MODEL EXERCISED WITH $m_2 = 0.9 \times m_1$

  RESULTS: 1) Optimum Operating Frequency Increases 1.48 Hz

  2) Absorber Strokes Differ by 2.2%

  3) Housing Rotation Produces 1.22 g at 9-in. Radius

- MODEL AGAIN EXERCISED, BUT I_3 INCREASED BY A FACTOR OF 100

  RESULTS: 1) Absorber Strokes Differ by a Factor of 12.8 at Design Frequency

Figure 2-10 System Tolerance to Unequal Absorber Masses ($m_1 \neq m_2$)

861364

- Six-Degree-of-Freedom model with damping exercised for $I_3 = 4.978$ in.-lb_f-sec^2

  1. f_{n_1} goes to 120.0 Hz.

  2. Shaking moment applied over frequency range 59 to 60 Hz.
     Moment (M_3) equals 1315-in.-lb_f (0.5 in. offset; 22-mm piston stroke).
     No peak in response seen at 60 Hz.
     Amplitude of absorber deflection at 60 Hz equals 0.0057 in. (housing rotation equals zero).

  3. Shaking moment (10% of fundamental amplitude) applied at 120 Hz.
     Peak observed in housing rotation at 120 Hz.
     Peak amplitude of absorber deflection equals 0.0003 in. at 120 Hz.

- Absorber amplitude due to full shaking force (60 Hz) equals 0.102 in.

- Total amplitude of absorber deflection due to shaking moment (60 Hz and 120 Hz components) equals 0.006 in., 5.9% of full deflection.

- Conclusion: no special problems arise if first natural frequency equals 120 Hz.

Figure 2-11 System Behavior with f_{n_1} = 120 Hz

861365

tuning conditions are indicated in Figure 2-10. With normal values of compressor inertia, the absorber strokes at the optimum tuning condition (i.e., minimum lateral shaking of the compressor) differ by only 2.2%. With compressor inertia increased by a factor of 100, absorber strokes differ by a large factor, since the absorber with correctly tuned frequency tends to absorb nearly all of the applied shaking force. This shows that coupling of the absorber assemblies through rotation of the compressor housing has the beneficial effect of tending to equalize absorber strokes.

In Figure 2-11, results are presented for the case where compressor inertia, I_3, is set equal to 4.978 in.-lb_f-sec^2. The first natural frequency of the system with damping equals 120.01 Hz rather than the normal value of 80.26 Hz. Because of damping in the system provided by the rubber isolator mounts, motions are relatively small, even when a 10% component of the shaking moment is assumed to act at 120 Hz. The investigations summarized in Figure 2-11 indicate that no problems would arise with absorber motion or housing rotation if a lighter compressor housing were used and the rotational mode natural frequency went to 120 Hz.

Figure 2-12 presents predicted (two-degree-of-freedom model) and measured absorber strokes for the system when the absorber mass was increased to 38 lb_m. This change was made in the laboratory by adding 3 lb_m tuning weights so that ideal balance would occur for operation at 57.8 Hz, a frequency more consistent with engine test points previously obtained. The figure shows that over the frequency range tested, 54 to 57 Hz, the measured and predicted absorber strokes agree quite closely. Housing acceleration was very difficult to measure accurately with accelerometers because of internal noise from the engine and refrigerant compressor. Figure 2-13 shows oscilloscope traces for housing vibration, combustor vibration, and absorber vibration at 13-mm piston stroke and frequency equal to 55.4 Hz. The fundamental component of housing and combustor acceleration is difficult to see on these traces but is on the order of 0.7 g for the housing and less than 0.3 g for the combustor.

Combustor lateral acceleration was observed to be very low throughout recent testing performed on the breadboard compressor with absorber, even when compressor lower-end vibrations were in the range of 2 to 3 g due to operation

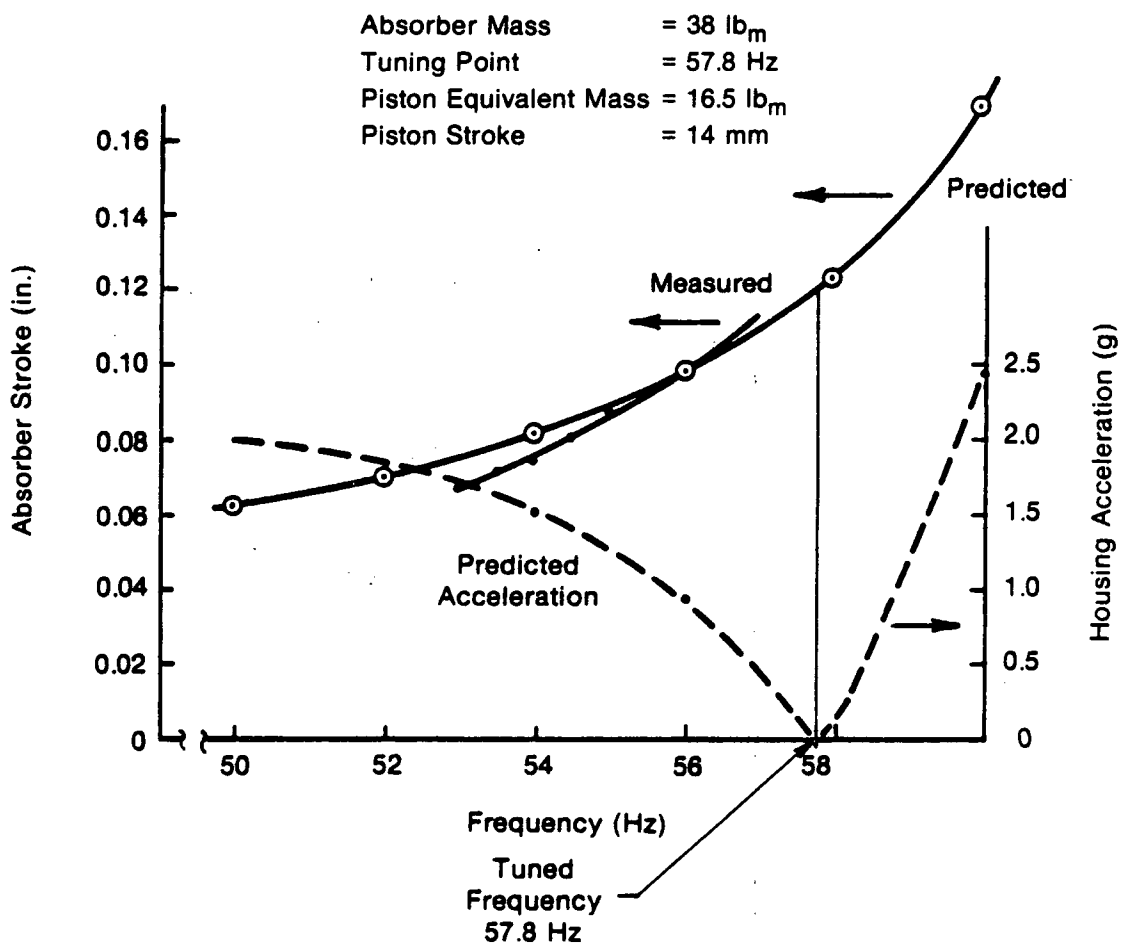

Figure 2-12 Measured and Predicted Absorber Stroke vs. Frequency
Predicted Housing Acceleration vs. Frequency

852940

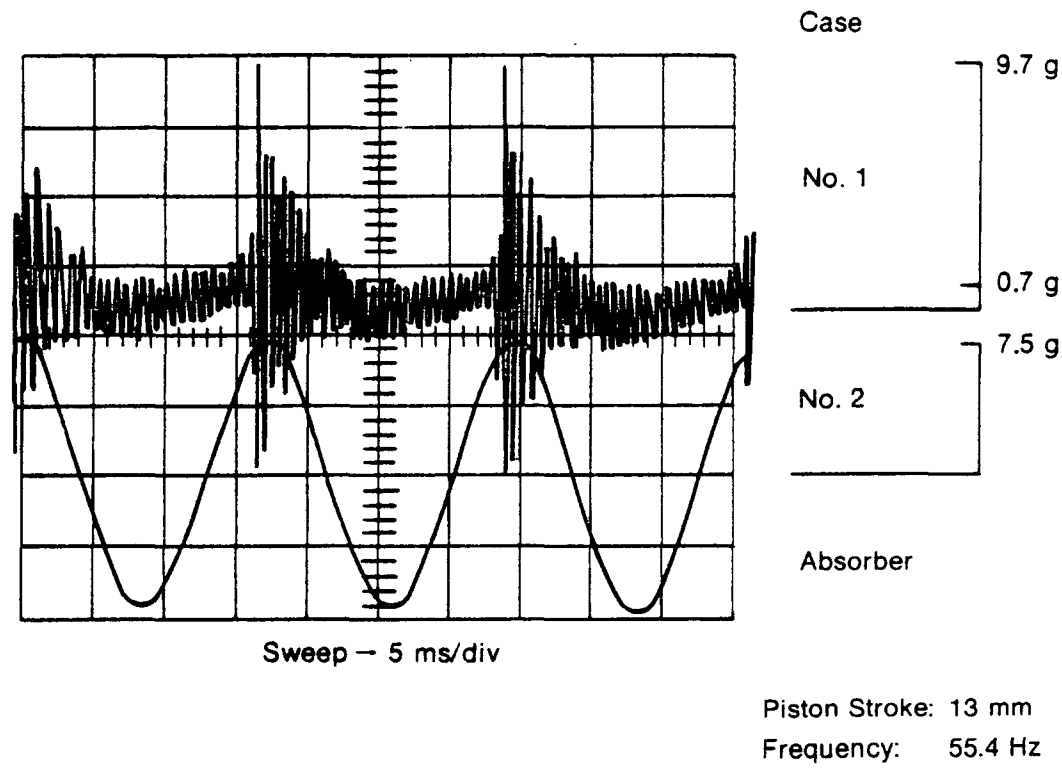

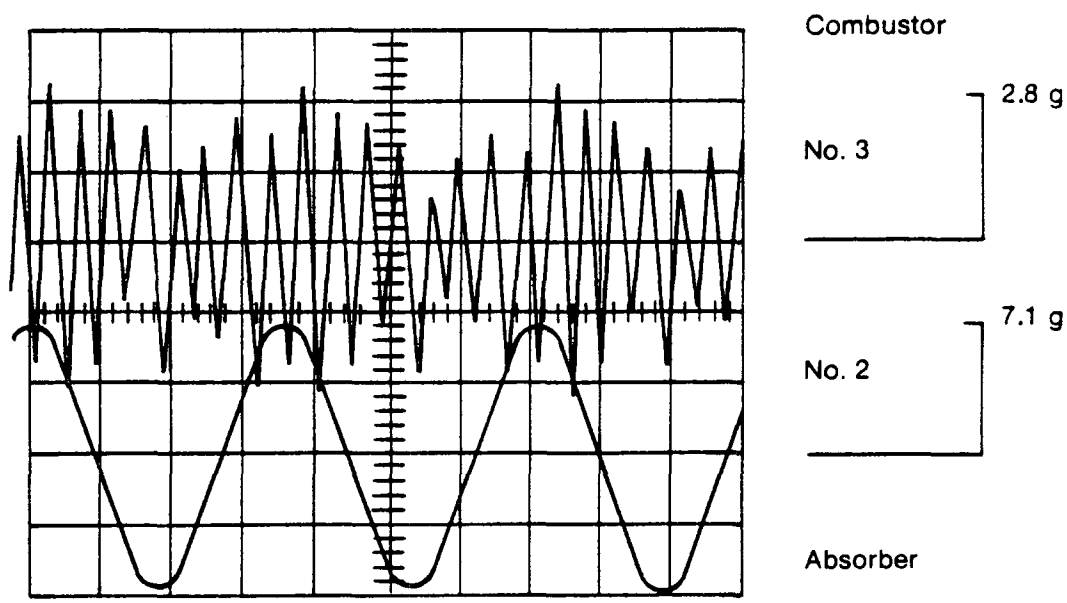

Figure 2-13 Compressor Housing and Combustor Lateral Acceleration Traces

852943

at off-design frequency with high piston stroke. Figures 2-14 and 2-15 show how compressor tipping about the center of gravity, when superimposed on lateral shaking at the center of gravity, results in a point of pure rotation for the system located near the top of the combustor. This feature has proven to be beneficial in laboratory testing so that a fairly broad range of operating frequencies may be used without retuning the absorber.

2.1.4 Leaf Spring Design

The most important aspect of this vibration absorber design is the leaf spring packs which support the absorber masses and provide springing at 60 Hz. Analyses were performed in many areas related to this design, including deflection behavior of clamped regions, fluctuating bolt stresses, loads transmitted to compressor housing, and material behavior at the interface between spacers and leaf springs, in addition to calculations for spring rate and leaf spring fatigue due to bending. The results for spring rate analysis and fatigue due to bending are presented in Figures 2-16 through 2-18.

Figure 2-16 shows how the free length of the leaf spring (2L), leaf thickness (h), and number of leaves (N) interact to allow these criteria to be met:

- Maximum bending stress at clamped edge equals 35 ksi
- Total spring rate for all the leaves supporting the absorber mass equals 12,887 lb/in.

The analysis shows that if a great number of relatively thin leaves are used, then the overhang of the absorber assembly could be reduced. Another technique for reducing overhang is shown in Figure 2-17, where the bottom sketch shows a leaf spring with tapered middle. The deflection of a cantilevered beam of tapered width is greater than that for uniform width, while bending stress at the clamped edge is unchanged for the same load. Therefore, different equations for L and N result, and the final design can be somewhat shorter by modifying beam deflection.* This approach may be pursued at a later date if overhang needs to be minimized and if quantities justify the manufacture of custom dies for cutting the leaf springs.

---

*Wahl, A. M. Mechanical Springs. 2d Ed. New York: McGraw-Hill, 1963.

— System Center of Gravity Located Approximately 5.5 in. Above Piston Centerline

— Residual Unbalance Produces Shaking Force and Moment About Center of Gravity

— Lateral Displacement and Rotation Results in Node Point Near Combustor

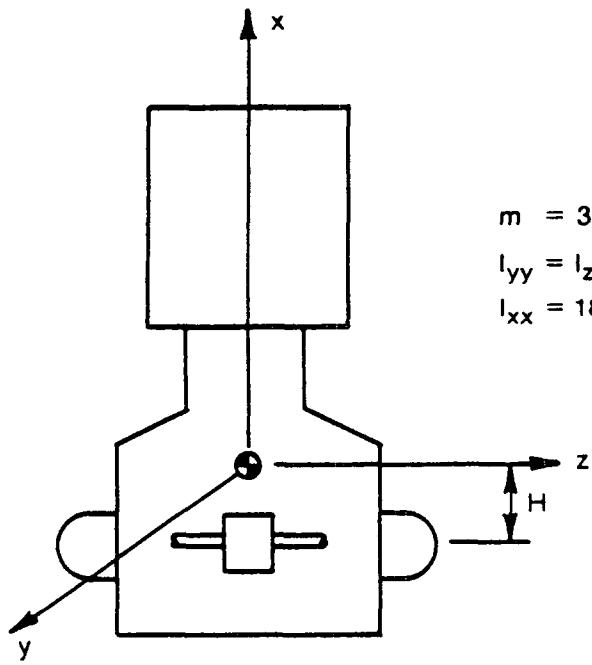

$m = 385\ lb_m$

$I_{yy} = I_{zz} = 108$ in.-lb_f sec^2

$I_{xx} = 18.9$ in.-lb_f sec^2 (used in 6 d.o.f. model)

Figure 2-14 Compressor Lateral Vibration and Tipping about Center of Gravity

852944

$F = m\ddot{X}_{cg}$ $\qquad$ $M = I\ddot{\theta}_{cg}$

$F = mX\omega^2$ $\qquad$ $FH = I\theta\omega^2$

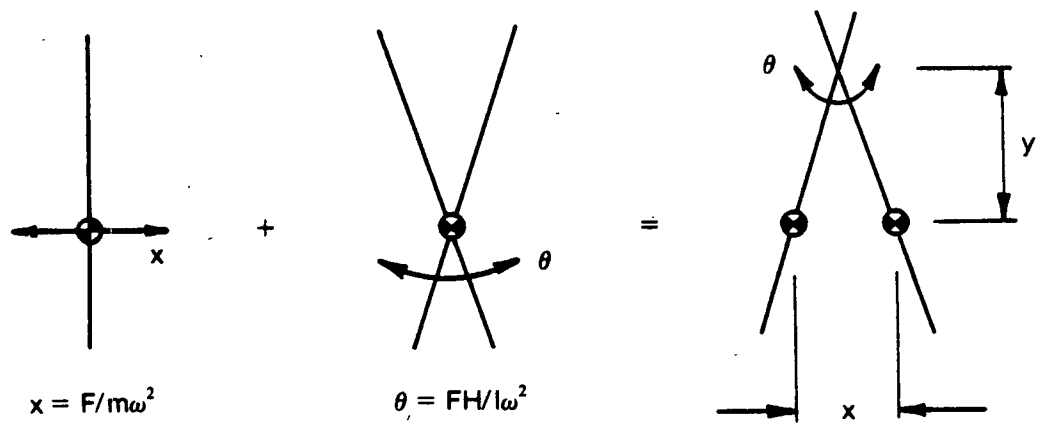

$x = F/m\omega^2$ $\qquad$ $\theta = FH/I\omega^2$

Find Location of Node, y: $\theta y = x$

$$(FH/I\omega^2)\, y = F/m\omega^2$$

$$y = I/mH$$

For $m = 385\ lb_m$, $I = 108$ in.-lb_f sec^2, and $H = 5.5$ in.

$y = 20$ in. (4 in. below top of combustor)

Figure 2-15 Superposition of Lateral and Rotational Vibration

852945 -1

— Spring Rate and Bending Stress Analysis

Allowable Bending Stress, σ_b = 35 ksi

Force Amplitude Per Absorber F_{tot} = 2634/2 = 1317 lb_f

Amplitude of Motion δ = 0.1022 in. ($\frac{1}{2\pi}\sqrt{K/m}$ = 60 Hz)

— Deflection for Beam Clamped at Both Ends

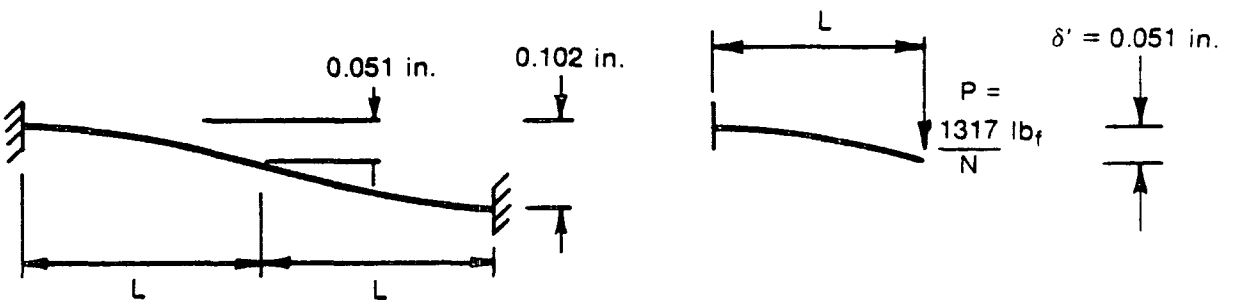

N = Number of Leaves Per Absorber

$\delta' = PL^3 / 3EI$, $\sigma_{bending} = Mh/2I = (6 \times 1317\ L) / N \times b \times h^2)$

where

b = Leaf Width

h = Leaf Thickness

$I = bh^3/12$

For δ' = 0.051 in., E = 28 × 10^6 psi, b = 3.70 in., σ_b = 35 ksi

$L = 7.831\sqrt{h}$, and $N = 0.0611\ L/h^2$

— Choose h = 0.071 in. (15 gauge), then 2 L = 4.173 in., N = 26

Figure 2-16 Leaf Spring Design

852946

Chosen Design: 0.071 in. Sheet Thickness; 13 Leaves Per Pack
0.040 in. Aluminum Spacers Between Leaves

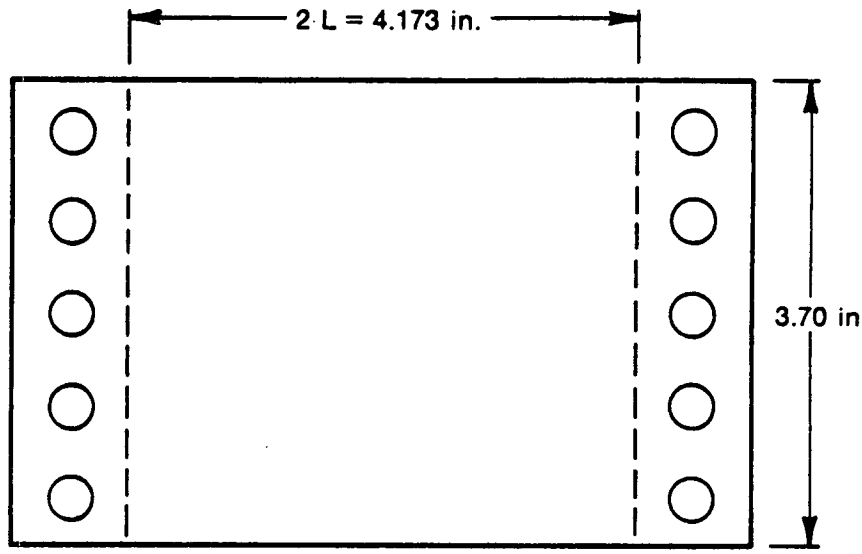

Tapered Middle: Provides Reduced Overhang, 2 L = 3.75 in.

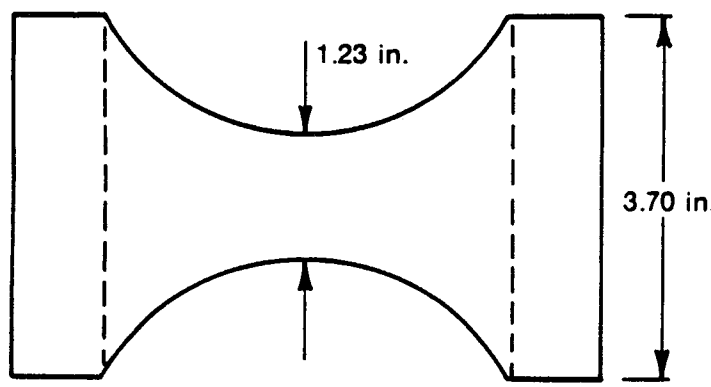

Figure 2-17 Rectangular vs. Tapered Leaves

852941

Material: 17-7 PH Stainless

Heat Treat: RH-950; σ_{yield} = 175 ksi

σ_e = 100 ksi (endurance limit, S_e')

Design for Infinite Life: $S_e = k_a\ k_b\ k_c\ k_d\ S_e'$

where S_e = corrected endurance limit

k_a = surface factor = .95 (polished surface)

k_b = size factor = .97

k_c = reliability factor = .753 (for 99.9% reliability)

k_d = factor for stress concentration = .84 (assumes K_t = 1.2 at clamped edge)

S_e = .95 x .97 x .753 x .84 x 100 ksi

= 58.3 ksi

$\sigma_{bending}$ = 35 ksi - at stroke equal 0.024 in.

Margin of Safety = .67 - conservative design

Figure 2-18 Leaf Spring Bending Stress: Margin of Safety

861366

Figure 2-18 presents a calculation for margin of safety for fatigue of the leaf springs. The material chosen for the initial build was 17-7 PH stainless steel, which provides a very conservative margin of safety for infinite life because of its superior fatigue strength. Other steels, such as 301 stainless, cold worked to 3/4 hard, display endurance limits of ~80 to 85 ksi and would probably be more suitable for eventual use in a product because of their lower cost. These alternatives to 17-7 PH can be used in future builds.

One potential problem, which has not yet been investigated with the current hardware, involves fretting of the leaf springs or spacers just behind the clamped edge. When disassembled, these parts will be carefully inspected for signs of fatigue or fretting. If indications are present that fretting (i.e., microscopic wear) has occurred at the clamped edge, development tasks will be started to solve the problem. Many options exist to combat fretting, such as anodized coating with Teflon lubricant applied to the spacers or the use of thin, compliant layers to accommodate slight relative motion. Long life of the absorber assemblies should be relatively easy to achieve.

2.1.5 Summary of Absorber Design

Specifications and performance of the vibration absorbers currently in use on the breadboard compressor are given in Figure 2-19. Performance to date has been excellent, and the broad range of acceptable operating frequencies has proven very convenient for laboratory testing. Vibration problems with the direct-acting compressor have been solved, and attention can now be focused on attaining high engine/compressor performance and good controllability at all ambient conditions.

2.2 Transmission Design Modifications and Checkout Testing

To operate the existing hydraulic transmission and compressor hardware without the internal counterweight required several modifications to the hydraulic transmission. Modifications, shown in the Compressor Drive Assembly drawing (Figure 2-20), include

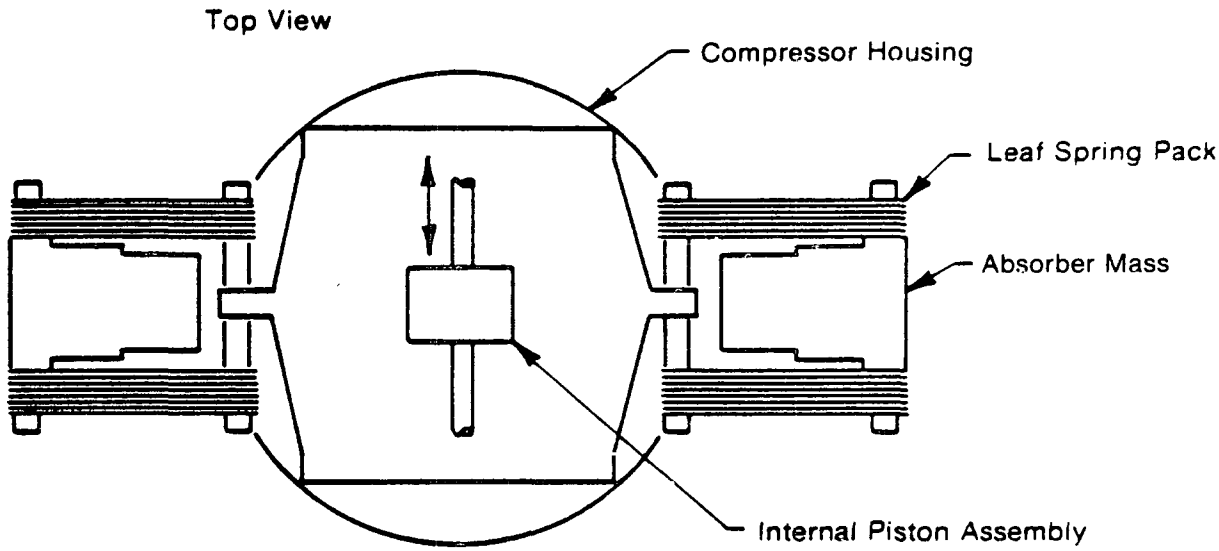

Absorber Specifications

Absorber Dynamic Mass	38 lb_m (each side)
Housing Effective Mass	285 lb_m
Unbalance Force	2442 lb_f – 57.8 Hz, Due to 16.5 lb_m Piston at 22-mm Stroke
Leaf Springs	13 Springs Per Pack; 17-7 PH, 0.071-in Sheet
Maximum Bending Stress	35 ksi at Stroke = 0.204 in.

Performance on GRI/DOE Heat Pump

Accumulated Operating Time	30 to 35 h; 7.5×10^6 Cycles
Tuned Operating Point	57.8 Hz
Operating Frequency Range	54 to 60 Hz
Housing Lateral Acceleration	< 1.5 g at 56 Hz
Combustor Lateral Acceleration	< 0.3 g at 56 Hz

Figure 2-19 Heat-Actuated Heat Pump with Vibration Absorbers

852947-1

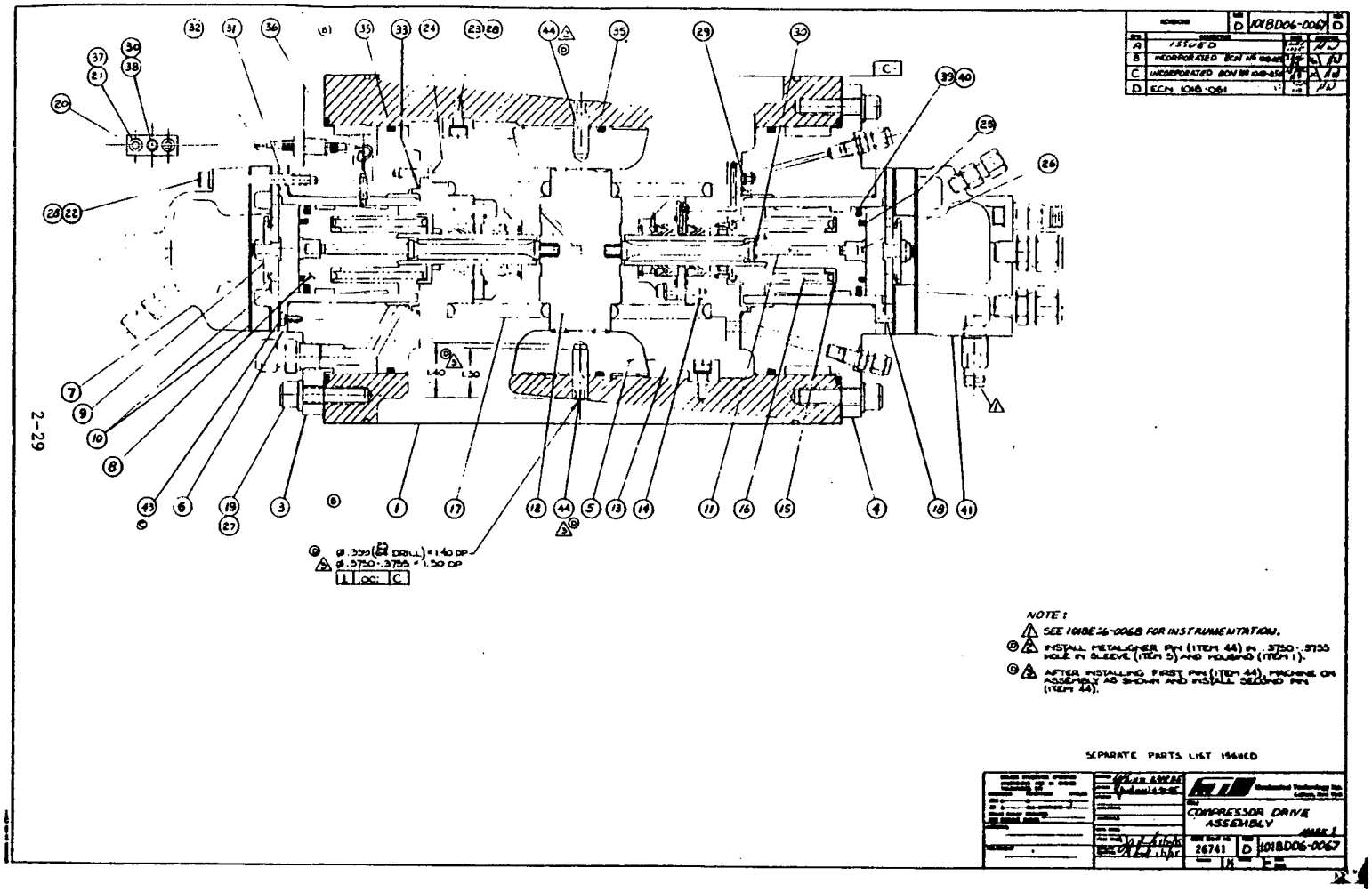

Figure 2-20 Direct-Drive Hydraulic Transmission and Compressor Assembly

861360

2-29

- The addition of a dummy bore, Item 5, to occupy the space of the counterweight. The dummy bore was also used to provide a sealing surface for the compressor drive pistons, Item 12.

- The fabrication of a new compressor drive piston made from Kennertium (type W2) to give the proper dynamic weight to the FPSE system.

- The modification of the compressor gas spring to match the compressor drive dynamics. This new gas spring was also designed to reduce the hysteresis loss from the previous variable gas spring geometry.

- The redesign of the compressor drive piston centerports to minimize porting losses and provide good centering and stability of the compressor piston. The new centerports consist of a series of slots machined into the wall of the dummy bore that short circuit the clearance seals on the drive piston when it is located at the center of the transmission housing.

In addition, several other small changes were made in the hydraulic transmission to reduce viscous flow losses by eliminating any abrupt changes in flow direction. These modifications included

- The tapering of the front edge of the seal cartridge holder, Item 14
- The streamlining of the edges of the dummy bore to match the flow paths.

With these changes and the addition of the external absorber, the breadboard system was first tested in May 1985. After several runs to check out the absorber assemblies, the unit was run on June 24, 1985, at the 95°F ambient conditions.

2.2.1 Hydraulic Transmission and Compressor Checkout Test Results

During May 1985, the tuned vibration absorber was assembled and mounted to the compressor housing of the direct-acting HAHP. Following checkout tests for

natural frequency and slight retuning for 58-Hz operation, the absorber assemblies were tested over a frequency range from 53 to 57 Hz at a constant compressor piston stroke equal to 14 mm. Performance was excellent over the entire frequency range, with combustor lateral accelerations measured at less than 0.3 g. Combustor acceleration remains low even when perfect lower end balance is not achieved because the motion that results from unbalance occurs as rotation about a point near the top of the combustor.

Installation of the external absorber assemblies enabled the compressor to be run at full stroke with no apparent difficulties, which enabled some compressor performance tests to be conducted. A layout drawing of the breadboard system configuration without the internal counterweight is shown in Figure 2-21. The breadboard system in the configuration tested consisted of

- G6 natural gas combustor
- Engineering model EM No. 4 FPSE
- Direct-drive refrigerant compressor.

The results obtained during May and June 1985 for checkout tests conducted at the 95°F ambient conditions were:

- Lower end losses were reduced by more than 70%. This result is shown in Figure 2-22, which gives the lower end loss as a function of compressor piston stroke. As shown, the total hydraulic transmission loss with the internal counterweight was 1400 W at a stroke of 16 mm, and the equivalent loss with the external absorber was 375 W.

- The maximum hydraulic transmission efficiency measured at the 95°F ambient temperature was 88%. Figure 2-23 presents the measured hydraulic transmission efficiency as a function of compressor piston stroke. The figure shows that a transmission efficiency of about 85% was achieved over a broad operating range.

- The new centerport design provides very stable compressor operation and holds the compressor piston on center very well. Figure 2-24 shows a trace of the compressor PV diagram achieved. The diagram shows that

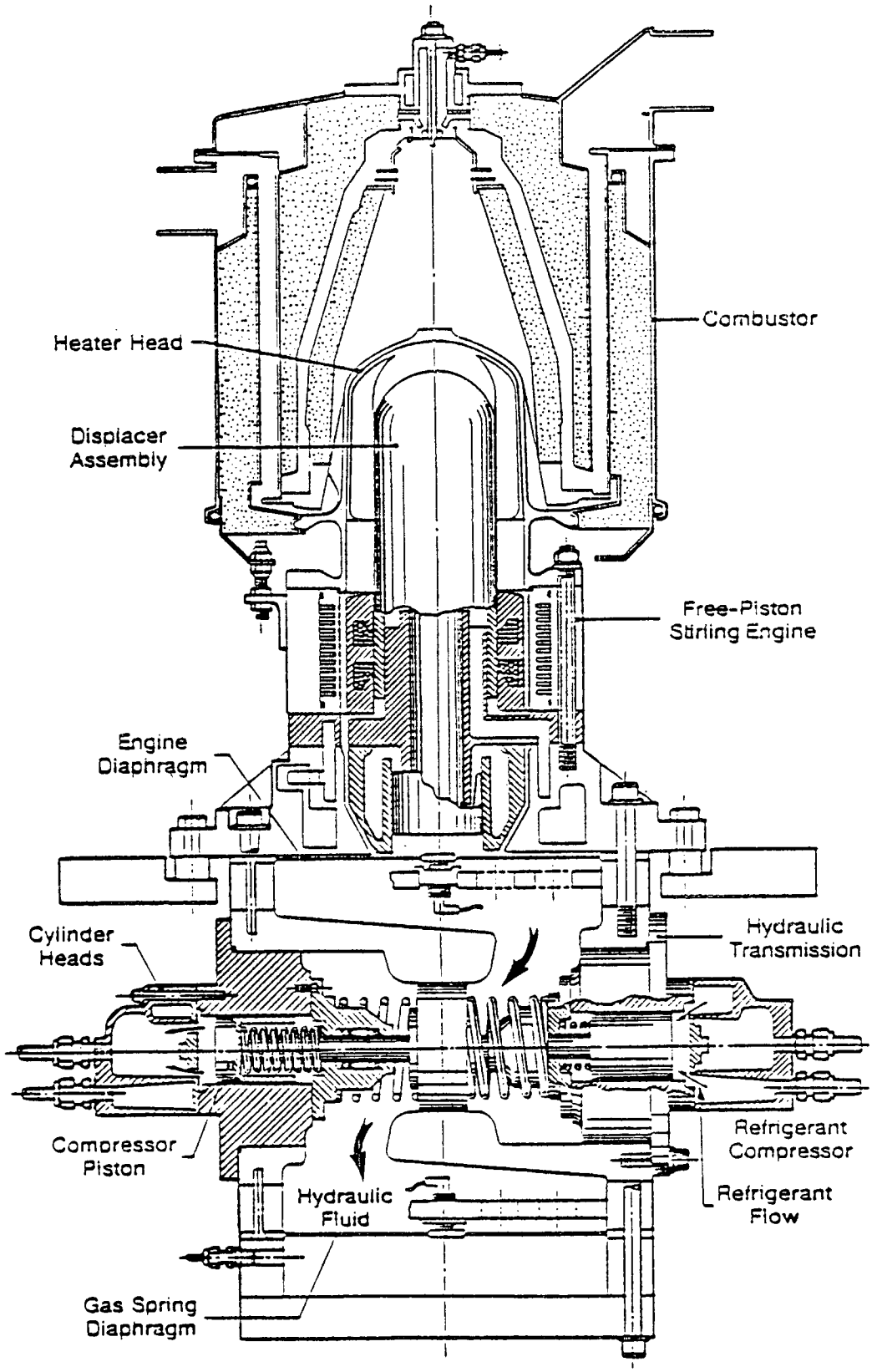

Figure 2-21 Mark I Free-Piston Stirling Engine Breadboard Heat Pump with Direct-Drive Transmission (Mark I engine configuration shown is similar to EM No. 4 FPSE)

853393

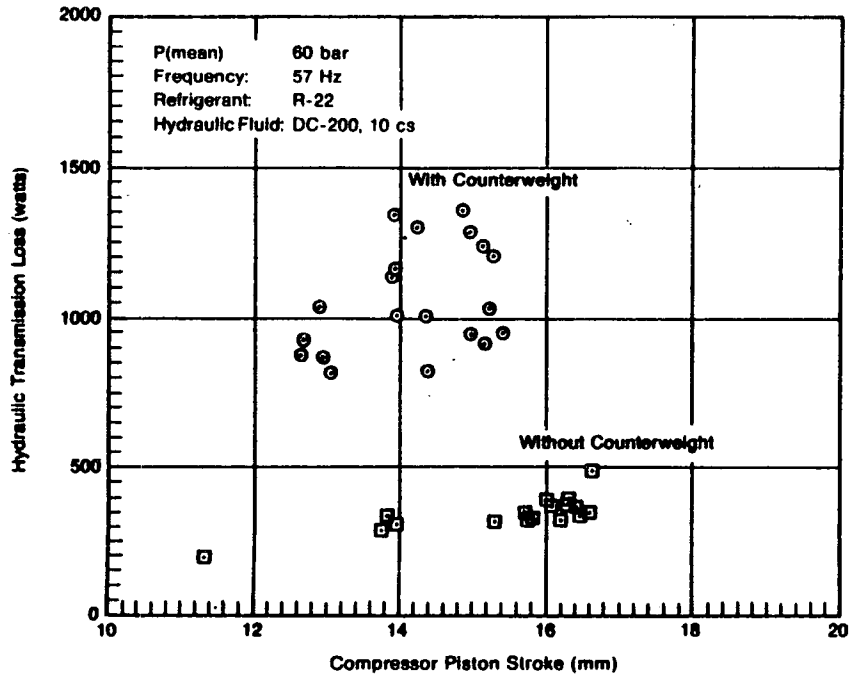

852436

Figure 2-22 HAHP Breadboard Hydraulic Transmission Loss

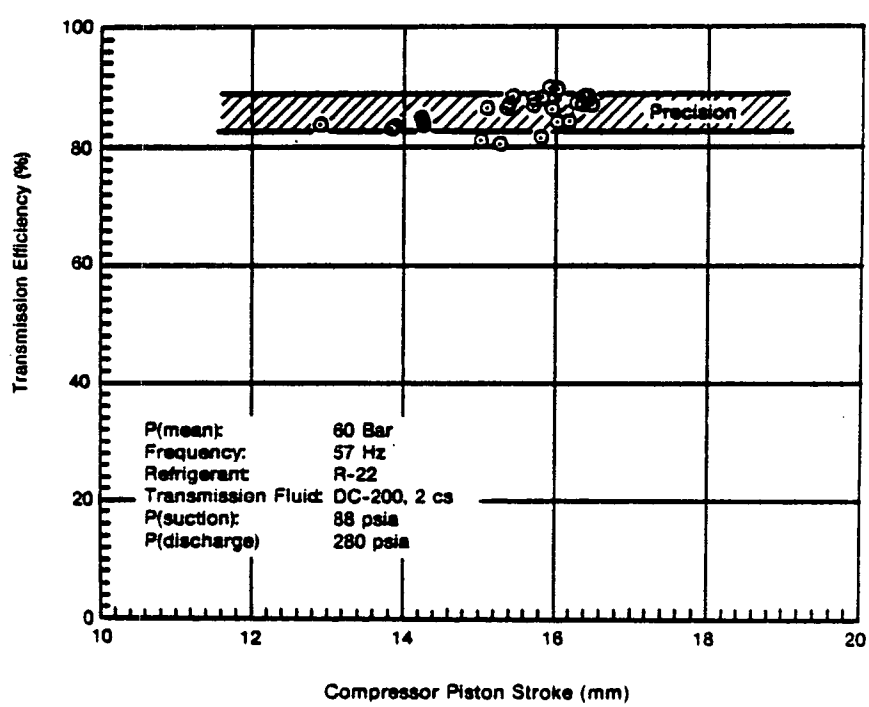

852604-1

Figure 2-23 HAHP Breadboard Hydraulic Transmission Efficiency

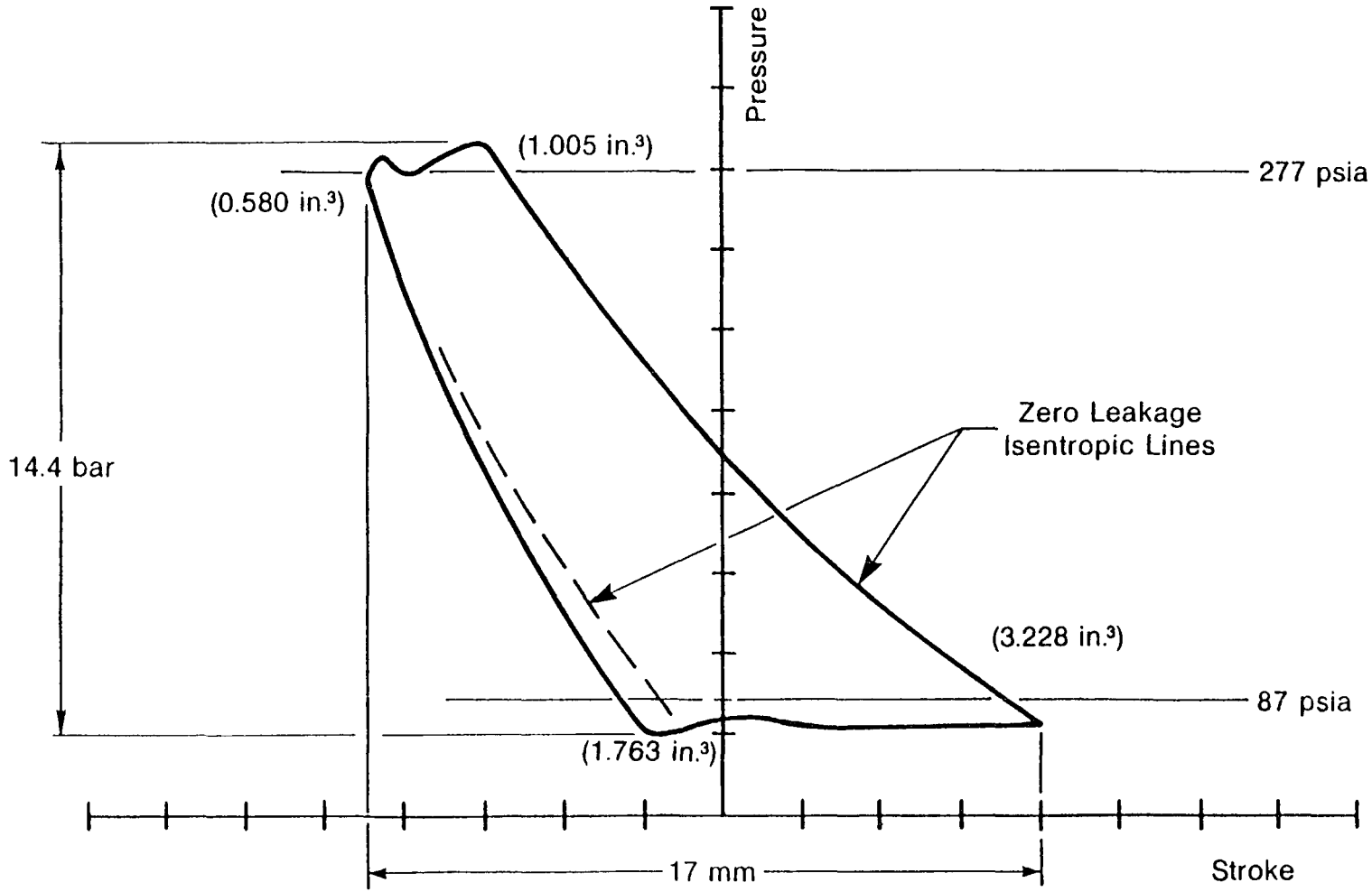

Figure 2-24 Compressor PV Diagram for R-22 Refrigerant

852438 -1

the compressor processes were nearly isentropic with only a small amount of refrigerant leakage occurring. These diagrams were repeatable and held steady over the entire time the tests were conducted.

- The reduction in hydraulic losses significantly reduced the rise in the hydraulic oil temperature, enabling better steady-state operation to be achieved. This is shown in Figures 2-25 and 2-26, which give the oil temperature rise at the 95°F ambient operating point. With the internal counterweight the temperature never reached a steady-state limit, nor did the rise show any indication of leveling off. For the direct-drive refrigerant compressor, a steady-state oil temperature was achieved after 1-1/2 hours.

The overall effect of these improvements on the performance of the breadboard system is shown in Table 2-3. The performance improvement is seen by comparing the results to those obtained with the internal counterweight. The improvement is manifested by the increase in refrigeration capacity to 29,457 Btu/hr, the increase in the hydraulic transmission efficiency to 87%, and the increase in compressor COP to 3.58.

2.3 Breadboard Heat Pump Baseline Testing

Baseline testing at nine ambient temperature conditions was conducted to establish the performance of the breadboard heat pump. The task of baseline testing consisted of writing a comprehensive test plan to organize and control the testing, a series of quality control tests to verify the accuracy of the data, and then the actual performance tests.

2.3.1 Breadboard Heat Pump Test Facility

A schematic of the test hook-up is given in Figure 2-27, showing the locations of the instruments necessary to make the performance evaluation. A description of the types of instruments used in these locations is provided in Table 2-4. Overall accuracy is defined as the sum of the measuring device, readout, and Data Acquisition System (DAS) accuracies for each parameter. The percentage value/value provided is the largest difference between the

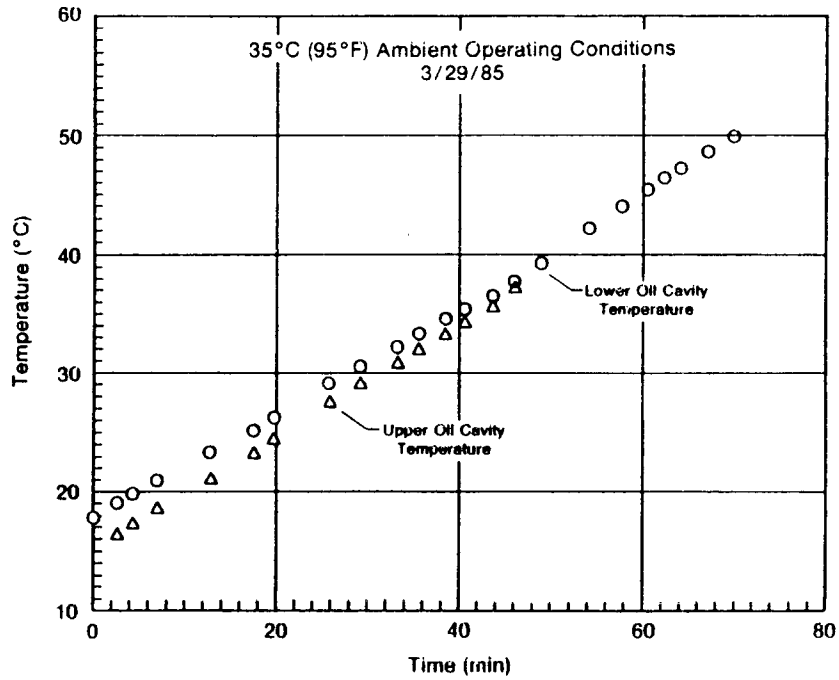

852656-1

Figure 2-25 Breadboard System Oil Cavity Temperature Rise for the Internal Counterweight Compressor

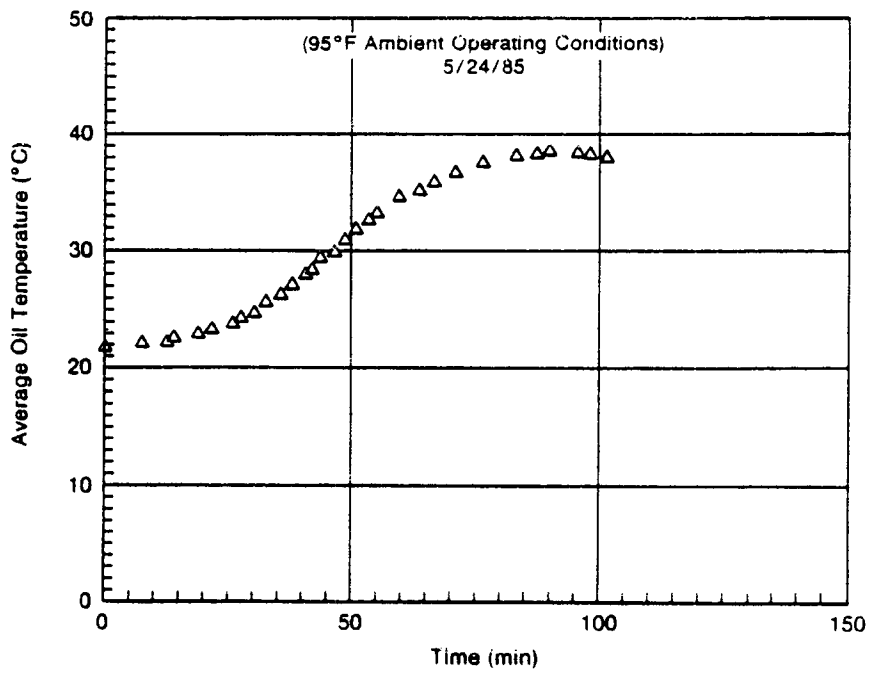

852658-1

Figure 2-26 Breadboard System Oil Cavity Temperature Rise for the Direct-Drive Compressor

Table 2-3

Comparison of HAHP Breadboard Heat Pump Module
with and without Internal Counterweight
(95°F Ambient Temperature Conditions)

Parameter	Measured Data (R-22) With Counterweight	Without Counterweight	Precision
Mean Pressure, bar	62.1	59.6	±1.0
Frequency, Hz	58.0	56.9	±0.1
Head Temperature, °C	710	715	±10.0
Counterweight Stroke, mm	15.25	N/A	--
Piston Stroke, mm	15.25	16.43	±0.20
Displacer Stroke, mm	21.73	21.71	±0.20
Suction Pressure, psia	89.6	87.3	±3.0
Discharge Pressure, psia	280.3	279.6	±5.0
Suction Temperature, °F	46.6	44.1	±1.0
Refrigerant Flow, lb_m/hr	342	439	±10.0
Refrigeration Capacity, Btu/hr	23,000	29,457	±1000.0
Counterweight Loss, W	612.3	N/A	--
Piston Power Loss, W	299.2	278	±80.0
Gas Spring Loss, W	28.7	1.8	±5.0
Engine PV Power, W	2,512	2,413	±75.0
Displacer Motor Power, W	488	504	±5.0
Overall Lower End Efficiency, %	45	68	±3.0
Hydraulic Transmission Effic., %	63	87	±3.0
Lower End COP	2.69	3.58	±0.12

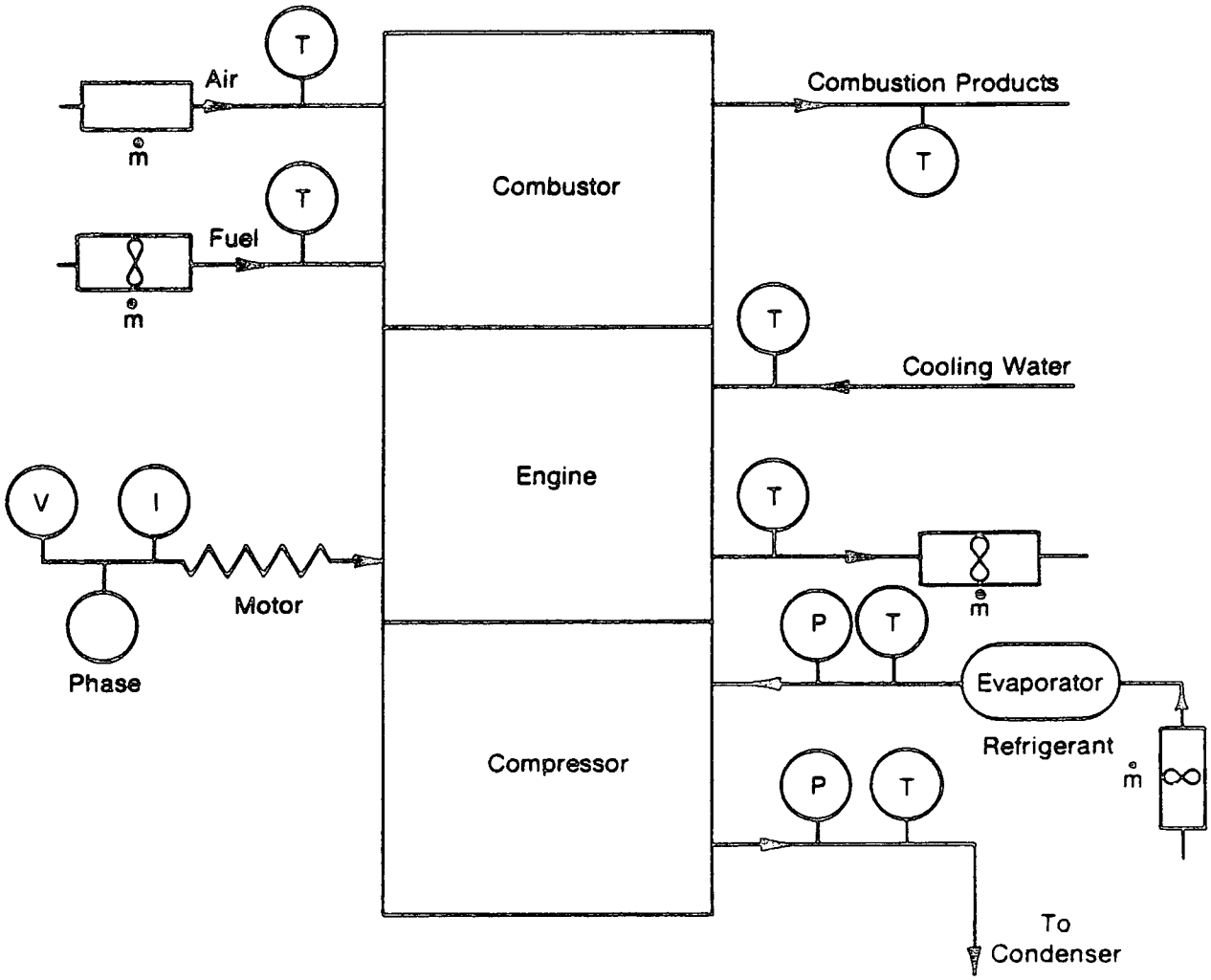

Figure 2-27 HAHP System Schematic Showing Interface Parameters

852953-1

Table 2-4

HAHP Performance Measurement Instruments

Parameter	Probe or Instrument Type	Overall Accuracy	Precision
Engine Displacer Stroke	Eddy Current/DAS*	+2%	0-22 mm
Engine Pressure Amplitude	Piezoresistive/DAS*	+1%	0-65 Bar
Engine Pressure Phase	DAS*	+0.1 Deg.	0-360 Deg.
Engine Cooling Water Inlet Temperature	RTD	+1/2%(+0.05°C max)	0-20°C
Engine Cooling Water Outlet Temperature	RTD	+1/2%(+0.05°C max)	0-20°C
Engine Displacer Motor Current	V/R (precision resistor)	+1/2%	0-13 Amps
Engine Displacer Motor Voltage	Voltage Divider	+1%	0-100 Volts
Engine Displacer Motor Phase	DAS*	+0.1 Deg.	0-360 Deg.
Engine Cooling Water Flow Rate	Bearingless Turbine	+4%	0-0.2 L/sec
Compressor Piston Stroke	Eddy Current/DAS*	+2%	0-18 mm
Compressor Cylinder Pressure Amplitude (left and right sides)	Piezoresistive/DAS*	+1-1/2%	0-300 psia
Compressor Cylinder Pressure Phase (left and right sides)	DAS*	+0.1 Deg.	0-360 Deg.
Compressor Suction Pressure	Piezoresistive	+1%	0-120 psia
Compressor Discharge Pressure	Piezoresistive	+1%	0-300 psia
Compressor Suction Temperature	Thermistor	+1% (+1°F max)	0-100°F
Compressor Discharge Temperature	Thermistor	+1-1/2%(+3°F max)	0-200°F
Compressor Refrigerant Flow Rate	Coriolis-Force Mass Flowmeter	+2%	0-900 lb/hr
Combustor Air Flow Rate	Laminar - Flow Element	+2%	0-20 scfm
Combustor Fuel Flow Rate	Positive Displacement Totalizer-Temp. Compensated	+1%	0-2 scfm
Combustor Fuel Inlet Pressure	U-Tube Manometer	+1%	0-40 in. H_2O
Combustor Air Inlet Temperature	Type-K Thermocouple	+2% (+4°F max)	70-200°F
Combustor Gas Outlet Temperature	Type-K Thermocouple	+2% (+10°F max)	70-500°F
Refrigerant Condenser Outlet Temperature	Remote Indicating Dial Thermometer	+2% (+2.5°F max)	0-120 F

*See Appendix C

parameter and its calibration reference over the entire operating range (i.e., if a displacer stroke of 18 mm is recorded, the actual value could lie between 17.64 and 18.36 mm, ±2% of recorded value). A detailed description of the Build 1 compressor configuration is given in Table 2-5.

For MTI laboratory testing, the compressor suction and discharge conditions are established by a desuperheater type of calorimeter (shown in Figure 2-28). The thermal loads at each ambient operating condition are simulated by controlling the cooling water through the desuperheater, which extracts heat from the compressor discharge gas and fixes the condenser saturation pressure. The condenser is thermally coupled to the evaporator in a shell and coil heat exchanger that transfers heat from the discharge flow to the expanded suction flow. From the condenser, the refrigerant passes through a subcooler to ensure a liquid flow through the system flowmeter. The evaporator pressure is controlled by a pressure-regulated expansion valve. The degree of superheat entering the compressor suction is controlled by passing wet refrigerant upstream of the evaporator and mixing it with the refrigerant leaving the evaporator. The refrigerant state points for the loop are shown in Figure 2-29.

The breadboard system is instrumented to provide both steady-state and dynamic measurements. The instrumentation included for the system provides energy and power measurements for each of the working volumes of the combustor, engine, hydraulic transmission, and compressor and provides quantitative data for each of the individual system components enabling a definitive evaluation of performance. The refrigerant loop and instrumentation have allowed the breadboard system to be run over a broad range of ambient conditions, as well as providing data on the system's performance at the heating and cooling rating points.

2.3.2 Breadboard Heat Pump Test Plan

2.3.2.1 Test Procedure Guidelines. The test plan provided that a performance map would be generated for the Build 1 compressor configuration by taking steady-state data at seven different ambient temperatures: 0, 17, 32, 47, 80,

Table 2-5

Compressor Description - Build 1

Parameter	Value
Weight of Piston Assembly (including 1/3 spring weight), kg	8.446
Drive Piston Seals	Dual Clearance Rings
Drive Piston - Dummy Bore Clearance, mm (in.)	0.0254 (0.001) Radial
Drive Piston Area, m^2	78.30×10^{-4}
Mechanical Springs	Centerbody Springs Only
Lower Gas Spring Volume, m^3	0.00352
Lower Gas Spring Gas	Nitrogen
Refrigerant Head Plenum Spacers Thickness, mm	25.4
Transmission Oil Type	10-cs Silicone (Dow Corning 200)
Compressor Piston Face Shims, mm (in.)	3.71 (0.146) (equivalent - equal thickness)
Compressor Cylinder Diameter, mm	55.12
Maximum Compressor Piston Stroke (Stop to Stop), mm	18.3
Compressor Cylinder Volume with Piston at Midstroke, mm^3	27,425
Compressor Cylinder Volume Not Swept (Top Dead Center Clearance Volume), mm^3	6309

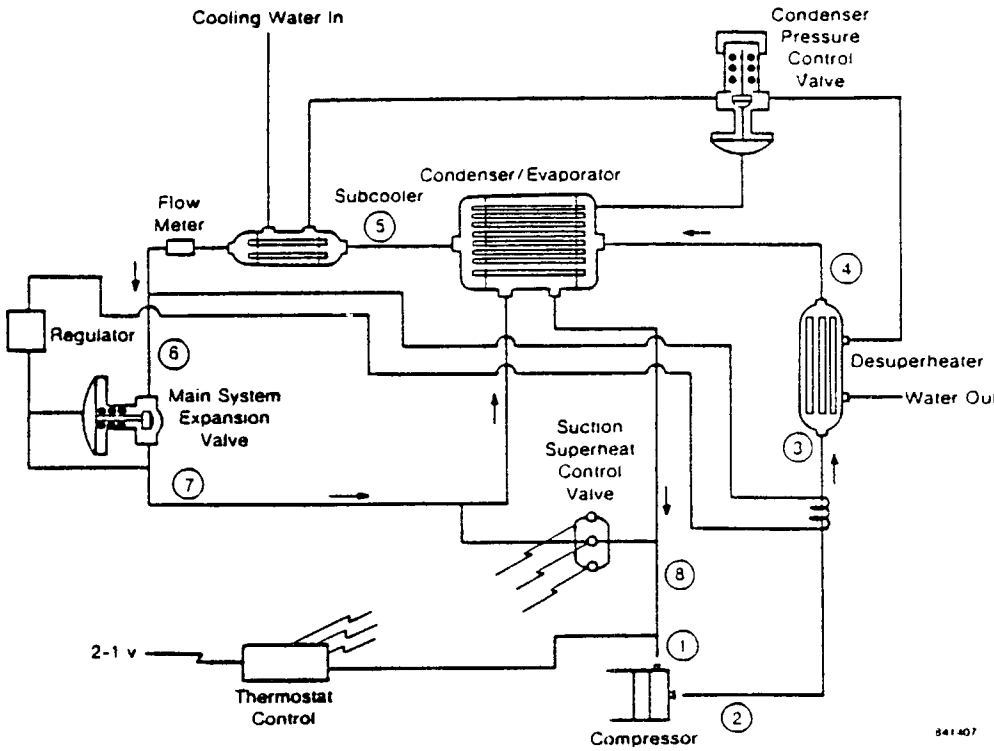

Figure 2-28 HAHP Refrigerant Calorimeter

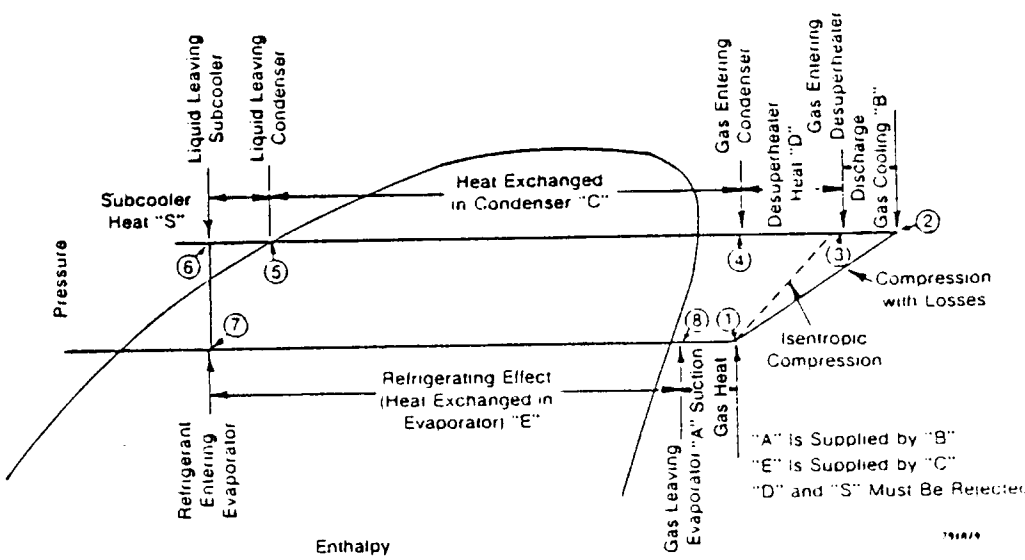

Figure 2-29 Refrigerant Test Loop State Points

87, and 95°F. The refrigerant (R-22) suction and discharge conditions for each of these ambient temperatures and two additional test points are given in Table 2-6.

For each of these ambient conditions, a series of points would be run varying the displacer stroke (X_D). A matrix for these data was completed and is provided in Table 2-7. Three data scans were taken for each point so that reliable steady-state data was assured. Steady state is defined as that point in time of system operation at which none of the performance parameters differ from scan to scan by more than 3%. The time between each scan was at least five minutes. The optimum frequency is defined as that frequency which corresponds to the largest ratio of displacer stroke to displacer motor current. For all of these points, the following parameters were constrained:

Average Heater Head Temperature	~720°C ±10°C
Engine Coolant Inlet Temperature	~0°C ±5°C
Engine Mean Pressure	~60 bar ±1/2 bar
Displacer Motor Current	≤10 amps
Compressor Piston Stroke	≤17.7 mm

It should be noted that some of the points in the matrix were not attainable due to the constraints listed above.

2.3.2.2 Breadboard Heat Pump Data Reduction and Performance Evaluation. A simplified flow schematic for the heat pump lower end is shown in Figure 2-30. The parameters that were to be measured to determine transmission and compressor performance and to allow the generation of the performance map were

- Refrigerant inlet static pressure
- Refrigerant outlet static pressure
- Refrigerant inlet temperature
- Refrigerant outlet temperature
- Refrigerant mass flow rate
- Power input (engine PV)
- Power output (compressor cylinder PV)

Table 2-6

Heat Pump Test Conditions for R-22 Refrigerant

	Cooling				Heating				
Ambient Temperature, °F	95	87	80	Test Point 2	47	32	17	0	Test Point 1
Discharge Pressure, psia	277.4	225.5	196.5	311.5	210.6	202.1	196.5	183.1	241.0
Saturation Temperature, °F	121	105	95	130	100	97	95	90	110
Suction Pressure, psia	90.7	94.7	98.7	90.7	76.2	57.7	42.9	29.8	69.6
Saturation Temperature, °F	45	47.5	50	45	35	20	5	-12	30
Suction Temperature, °F*	55	57.5	60	55	45	30	15	-2	40
Pressure Ratio	3.06	2.38	1.99	3.43	2.76	3.50	4.58	6.14	3.46

*Includes at least 10°F superheat

Table 2-7

Test Plan Matrix for Different Ambient Temperatures and Displacer Strokes

Ambient Temperature (°F)	Frequency	Displacer Stroke (XD) 16 mm	18 mm	20 mm	22 mm
0	Optimum at 22 mm XD	3 Scans*	3 Scans	3 Scans	3 Scans
17	Optimum at 22 mm XD	3 Scans	3 Scans	3 Scans	3 Scans
32	Optimum at 22 mm XD	3 Scans	3 Scans	3 Scans	3 Scans
47	Optimum at 22 mm XD	3 Scans	3 Scans	3 Scans	3 Scans
Test Point 1	Optimum at 22 mm XD	3 Scans	3 Scans	3 Scans	3 Scans
80	Optimum at 22 mm XD	3 Scans	3 Scans	3 Scans	3 Scans
87	Optimum at 22 mm XD	3 Scans	3 Scans	3 Scans	3 Scans
95	Optimum at 22 mm XD	3 Scans	3 Scans	3 Scans	3 Scans
Test Point 2	Optimum at 22 mm XD	3 Scans	3 Scans	3 Scans	3 Scans

*After steady state has been reached, three scans are taken at 5-min intervals

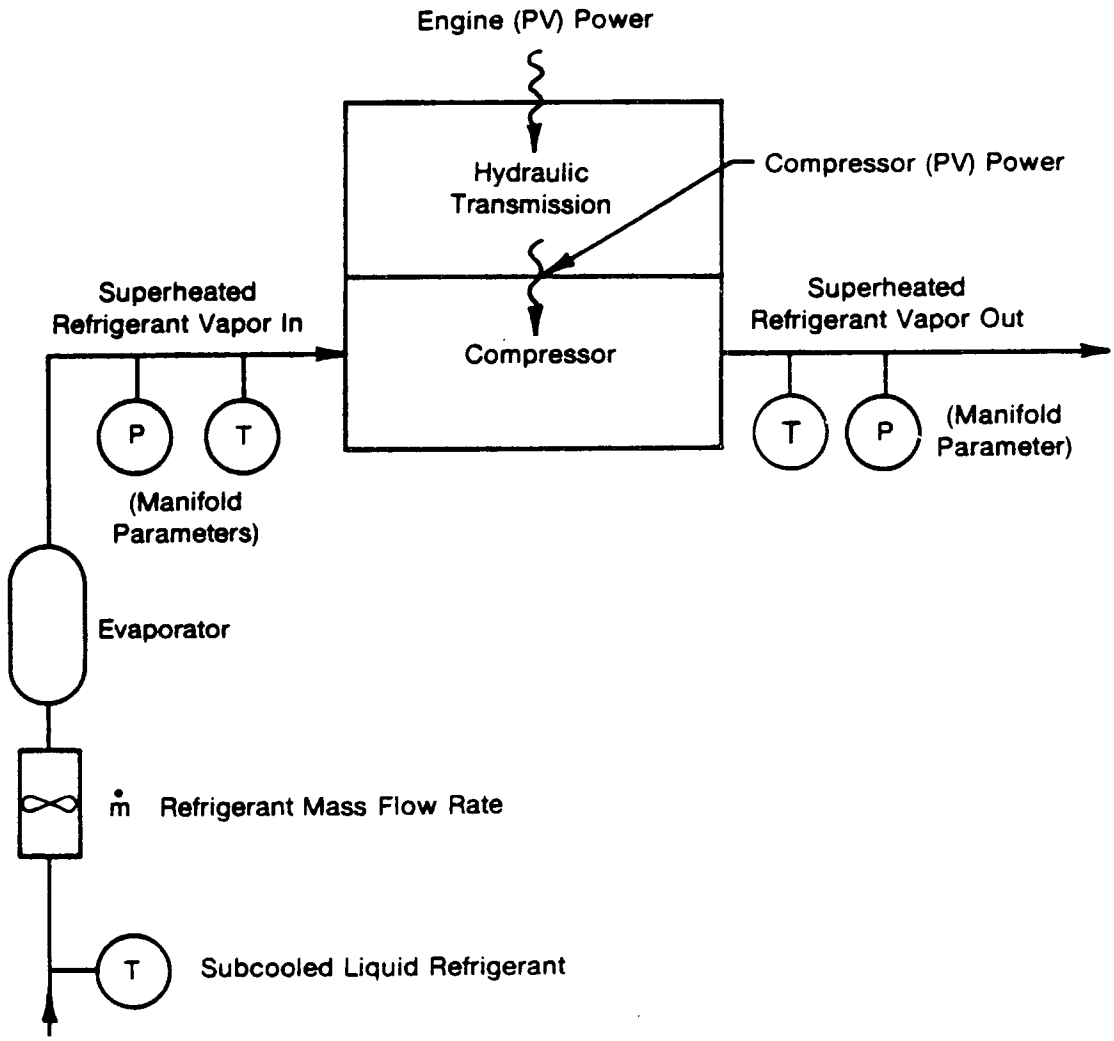

Figure 2-30 Flow Schematic for Heat Pump Lower End

852954

The following subsections define the detailed measurements and methods utilized in making the performance calculations.

Figure 2-31 provides the typical heating/cooling loads for the average home rated for 3.0 tons of cooling at a 95°F ambient temperature. The measured capacity of the heat pump using refrigerant R-22 was plotted on this graph as shown by the sample data points, and the performance of the unit was evaluated at the operating points described in Table 2-7.

Cooling Performance - The refrigeration cycle in simplified form is shown in Figure 2-32. Starting at station 1, the liquid refrigerant is evaporated at constant pressure between 1 and 2 and slightly (at least 10°F) superheated. The superheated refrigerant vapor is compressed between stations 2 and 3 and then cooled and condensed and subcooled (at least 15°F) between stations 3 and 4. Finally, the liquid is passed through an expansion valve, decreased in pressure, and partially vaporized between stations 4 and 1.

The cooling capacity and the cooling COP (assuming perfect thermal isolation from the test cell) were calculated from the following expressions:

$$\text{Cooling Capacity}_{\text{System}} = \dot{m}\,(h_2 - h_1)$$

$$\text{COP (Cooling)}_{\text{System}} = \frac{\dot{m}\,(h_2 - h_1)}{FR}$$

where: $\dot{m}$ = refrigerant mass flow rate

h_2 = enthalpy of the refrigerant vapor leaving the evaporator

h_1 = enthalpy of the refrigerant entering the evaporator. $h_1 = h_4$ where h_4 is calculated from the actual subcooling at station 4; h_4 is not corrected to a standard 15°F subcooling.

FR = firing rate of the combustor based on the higher heating value of the fuel = m_{gas} (HHV). The HHV of the natural gas is 1032 Btu/scf.

In addition, the transmission loss and the efficiencies of the hydraulic transmission and the compressor were calculated as follows:

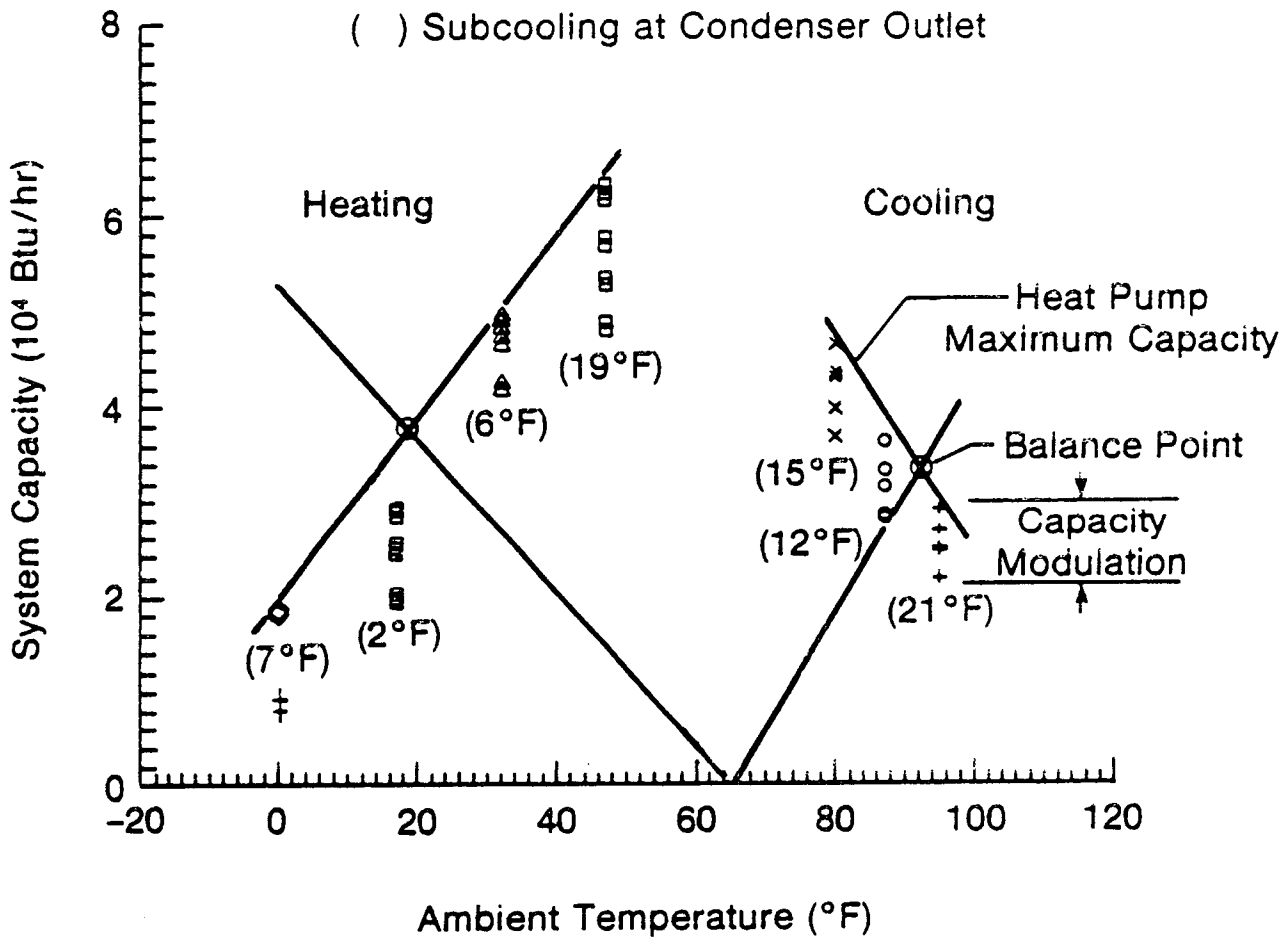

Figure 2-31 Breadboard Heating and Cooling Capacity As a Function of Ambient Temperature for a Home in the Mid-Atlantic Region, Rated at 3.0 Tons of Cooling at 95°F

86243

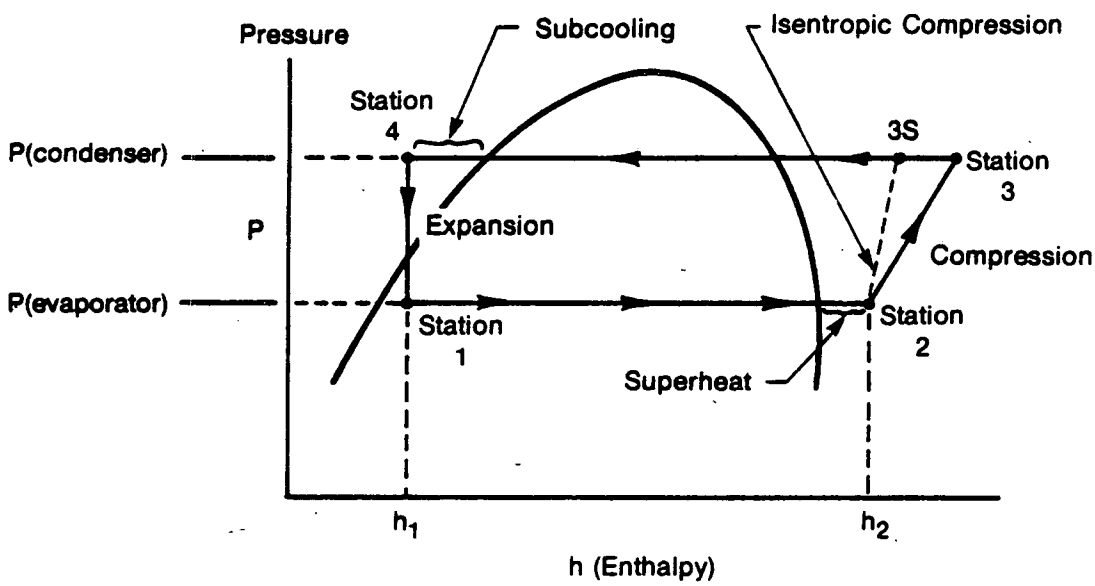

Figure 2-32 Schematic of Refrigeration Cycle

852951 -1

Transmission Loss = PV (engine) - PV (compressor)

$$\eta \text{ (Hydraulic Transmission)} = \frac{\text{PV (compressor)}}{\text{PV (engine)}}$$

$$\eta \text{ (Compressor)} = \frac{\text{Compressor Isentropic Power}}{\text{PV (compressor)}} = \frac{\dot{m}\,(h_{3s} - h_2)}{\text{PV (compressor)}}$$

where: PV (compressor) = PV work as measured by pressure transducers in the compressor cylinders and displacement probes monitoring compressor piston motion.

PV (engine) = PV work as measured by pressure transducers in the engine and displacement probes monitoring engine power piston motion. Average of PVKUL (He cavity) and PVU-OIL (upper oil cavity) work.

$\dot{m}$ = refrigerant mass flow rate

h_{3s} = isentropic enthalpy of refrigerant vapor leaving the compressor (manifold).

h_2 = enthalpy of refrigerant vapor entering the compressor (manifold).

Heating Performance - The ambient conditions (four points) below 65°F require slightly different calculations for performance evaluation. In the heating mode, performance is based on the energy exchange across the condenser rather than across the evaporator as in the cooling mode. Also included is the engine waste heat rejected to the cooling water.

The heating capacity and the heating COP are defined as:

$$\text{Heating Capacity}_{\text{System}} = \dot{m}\,(h_3 - h_4) + Qrej_{water}\,(0.85)$$

$$\text{COP (heating)}_{\text{System}} = \frac{\dot{m}\,(h_3 - h_4) + Qrej_{water}\,(0.85)}{FR}$$

where: $\dot{m}$ = refrigerant mass flow rate

h_3 = enthalpy of refrigerant vapor leaving the compressor (manifold)

h_4 = enthalpy of refrigerant liquid leaving the condenser; h_4 is calculated from the actual subcooling at station 4

$Qrej_{water}$ = rejected engine heat = $\dot{m}_{water}$ (Cp)(ΔT)

FR = firing rate of the combustor based on the higher heating value of the fuel = $\dot{m}_{gas}$ (HHV) (the HHV is assumed to be 1032 Btu/scf)

0.85 = standard accepted efficiency of conventional heat exchangers

The calculations for the efficiency of the hydraulic transmission and the compressor are made in the same manner as those in the cooling mode.

Energy Balance - An energy balance for the engine at each data point was to be made and is given in the following expression (see Figure 3-33):

$$E_{in} = E_{out}$$

$$Q_{air} + FR + P_{motor} = Qrej_{air} + Qrej_{water} + PV\ (engine)$$

Where: Q_{air} = energy content of the combustor inlet air

FR = firing rate of the combustor based on the lower heating value of the fuel = $\dot{m}_{gas}$ (LHV) (the LHV for natural gas is 929 Btu/scf

$Qrej_{air}$ = energy content of the combustor exhaust gases

$Qrej_{water}$ = rejected engine heat = $\dot{m}_{water}$ $(Cp)_{water}(\Delta T)_{water}$

P_{motor} = electric power input to the engine displacer motor

PV(engine)= PV work as measured by pressure transducers in the engine and displacement probes monitoring engine power piston motion. Average of PVKUL (He cavity) and PVU-OIL (upper oil cavity) work.

Finally, an energy balance confidence value can be calculated from

$$\text{Confidence Value} = E_{out}/E_{in}$$

The closer this confidence value is to unity, the greater the accuracy and reliability of the data collected. This value will never be consistently 1.0,

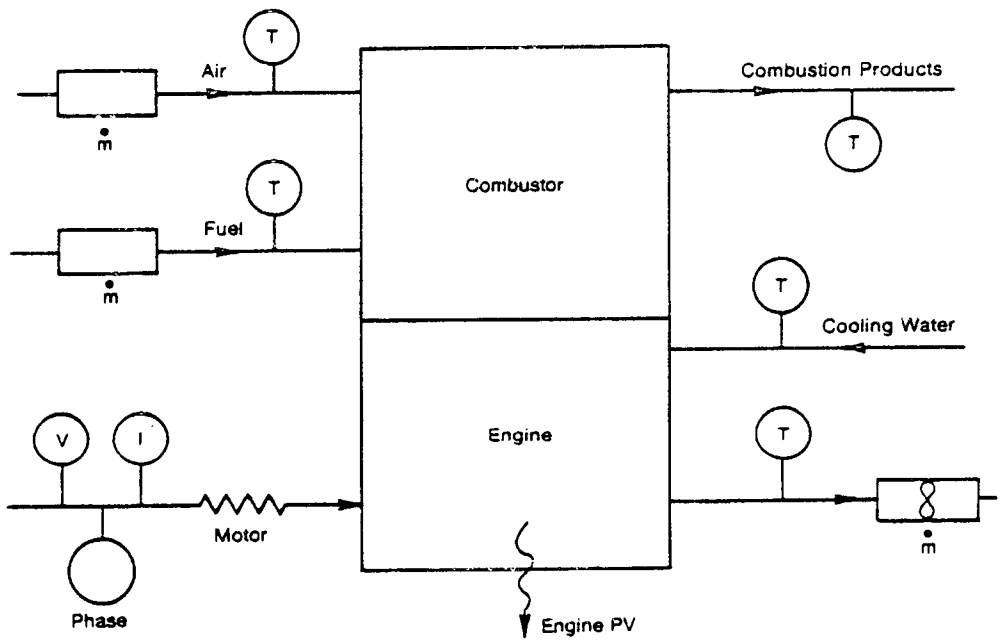

Figure 2-33 HAHP Engine Schematic Showing Parameters for Engine Energy Balance

853488

since some lesser order energy terms (such as thermal losses to the test cell) are omitted, actual heating value of the gas fuel is not determined, and because of the compound effect of instrument and data acquisition system inaccuracies. It is generally felt that values above 0.85 represent acceptable data, values above 0.90 are consistent with good data, and values above 0.95 represent exceptional data.

2.3.2.3 Transmission Efficiency As a Function of Transmission Fluid Viscosity. An investigation of the effect of the transmission fluid viscosity on the transmission efficiency was to be made using four distinct viscosity oils. Silicone oil with 2 and 10 cs viscosity and the conventional mineral-based refrigeration oil with 10 and 33 cs viscosity were tested at the 95°F ambient condiitons. Plots of hydraulic transmission efficiency versus compressor piston stroke and compressor efficiency versus compressor piston stroke were generated for each of the oils. Also, a plot of oil temperature versus time was made for each oil.

2.3.3 Performance Data Presentation

This test program was the basis for evaluation of the breadboard system's performance relative to the heating and cooling requirements shown in Figure 2-31. Much of the data is presented in graphical form including the following:

- Capacity versus ambient temperature and compressor piston stroke
- Coefficient of performance versus ambient temperature
- Coefficient of performance versus compressor piston stroke at 47 and 80°F
- Compressor efficiency versus compressor piston stroke
- Transmission efficiency versus compressor piston stroke
- Engine PV versus compressor piston stroke for each ambient.

The following sections provide a graphical presentation of the important performance parameters as a function of compressor stroke and ambient temperatures. These graphs provide a useful format for evaluating the breadboard heat pump's performance. A more detailed compilation of the data is presented

in Appendix B, and a description of the data reduction parameters recorded during a test is given in Appendix C.

2.3.4 Energy Balance Results

Definition - A proper performance evaluation of the heat pump system requires reliable data. One of the best ways to assure the collection of such data is to perform an energy balance of the system being evaluated. The system boundary is established, and the parameters are identified in order to determine all of the energy flows entering and leaving this boundary. It is important to point out that there are some lesser order energy terms, such as thermal radiation and flow leakage, that are usually omitted from the energy balance. However, before a term can be omitted, an approximation of its energy content must be made either experimentally or analytically. If the term's contribution to the total energy in or out is less than 5%, it is usually omitted. In addition, in most instances the summation of the second-order terms does not exceed 10% of the total energy in or out. Finally, the actual energy balance is made by summing all of the major terms of system energy output and dividing that by the summation of all major system energy input terms. This quotient, usually referred to as the Confidence Value, will never be consistently 1.0, since some lesser order terms are omitted and because of instrument inaccuracies.

Imbalance Resolution - Prior to conducting the performance tests on the heat pump system, a decision was made to use a factory-calibrated, temperature-compensated, positive-displacement fuel gas flowmeter. Previous energy balances on FPSEs had required such a device for accurate flow measurements of the fuel gas. Accuracy is extremely important since the fuel energy is the largest single energy term. The cooling water temperature in and out RTDs were calibrated, and the specific heat (Cp) was determined for the cooling water/ethylene glycol mixture. In addition, a calibration was made on the cooling water flowmeter. Next, lesser order energy terms, such as combustor can radiation and combustor air leakage, were investigated. These terms were considered to be second order and could be neglected.

The performance testing was begun, and energy balances for the entire engine/compressor assembly were found to be out of acceptable tolerance. Figure 2-34 depicts a typical system energy balance yielding a confidence value of only 0.73. A new energy balance boundary was established, cutting the lower end out of system. This provided a more straight-forward approach by eliminating the unknown lower end second-order terms (losses). The energy balance, as shown in Figure 2-35, increased from 0.73 to 0.80. This slight change in tactics had a significant impact on the energy balance but did not yield a confidence value within the acceptable range.

A long and tedious series of investigations followed, in order to determine the source(s) of the energy imbalance. The following steps were taken:

- Checked calibration of fuel gas flowmeter with two other positive displacement meters.
- Recalibrated cooling water RTDs
- Checked and recalculated specific heat for the cooling water mixture
- Recalibrated cooling water flowmeter
- Performed energy balance check on cooling water circuit
- Measured combustor can OD temperature and calculated radiation losses
- Analyzed exhaust gas for unburned hydrocarbons
- Recalibrated combustor air inlet flowmeter
- Located and sealed combustor air leaks
- Measured combustor leakage via exhaust gas flowmeter.

More than half of the 6-week investigation period was occupied by checks on the second-order terms in the upper end. The investigation showed that combustor can radiation and combustor gas leakage are second order but do make a difference in the energy balance. After all the steps were completed, performance tests were resumed and the energy balance had improved as shown in Figure 2-36. The confidence value had been improved to the acceptable level of 0.85 (without consideration of second-order terms) and 0.93 including combustor radiation and leakage losses. The source of the imbalance was determined to be widespread; almost every major energy term contributed a share, owing to inaccurate calibrations and data acquisition methods. The

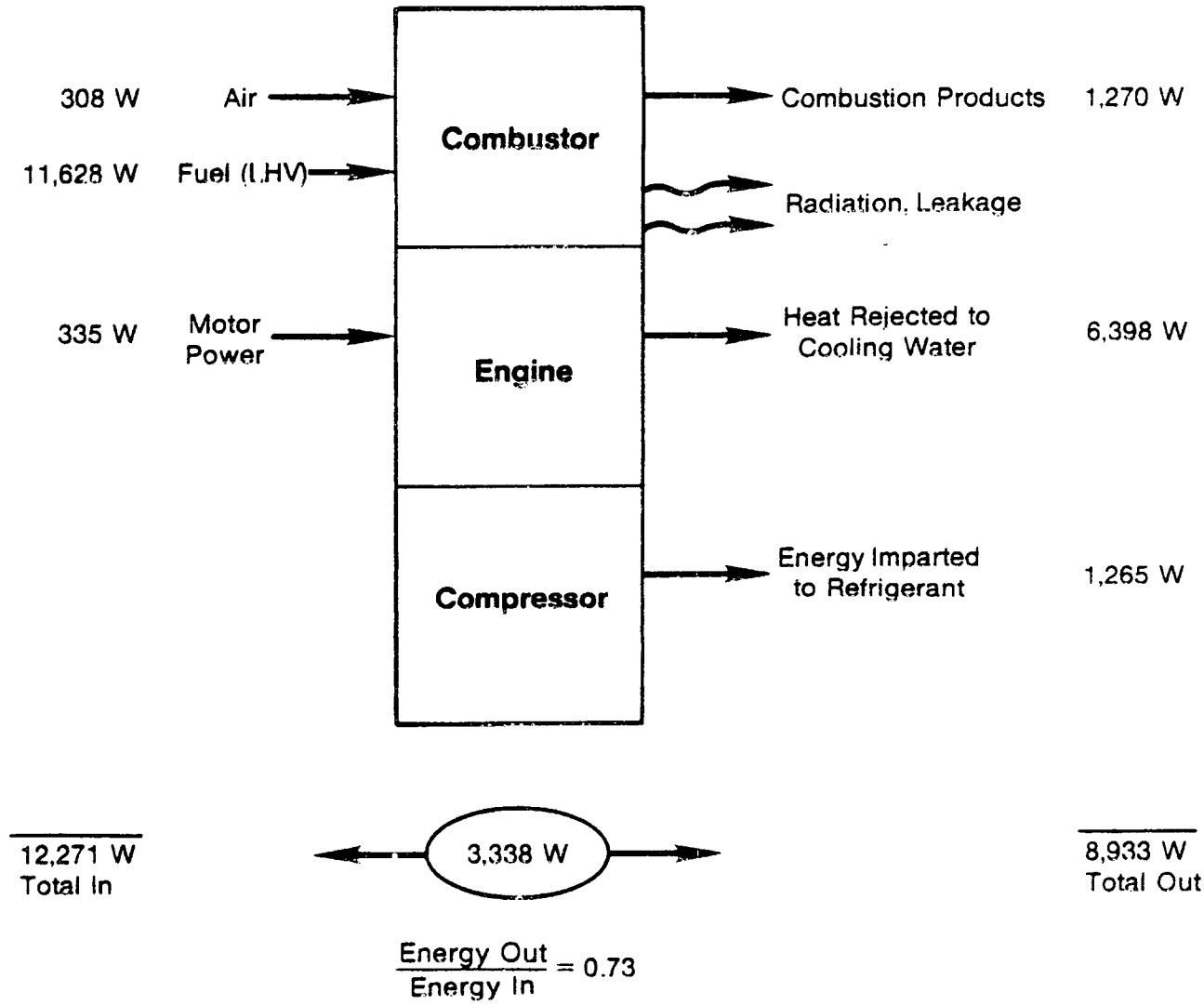

Figure 2-34 Entire System Energy Balance (8/15/85 Scan No. 8)

86905

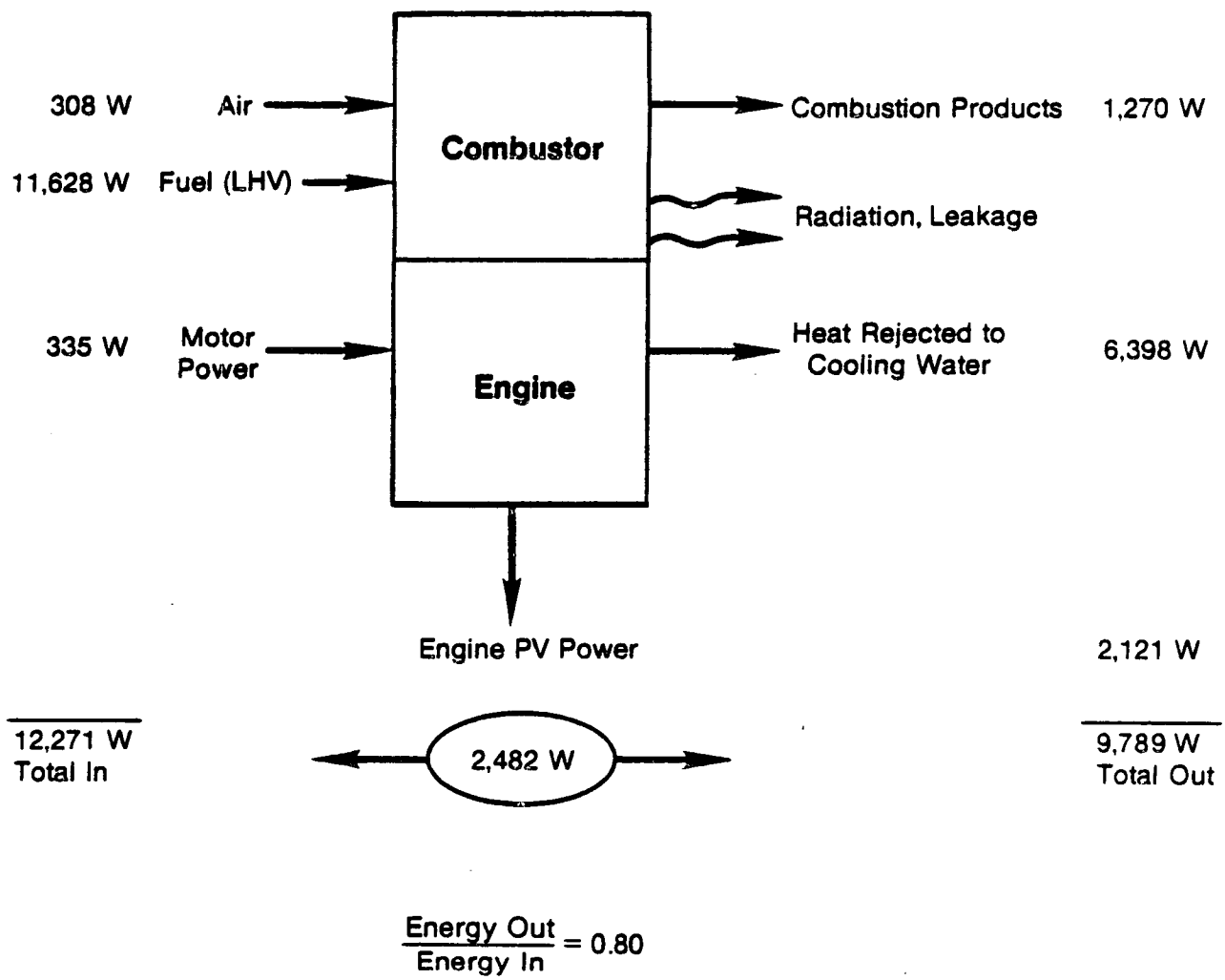

Figure 2-35 Upper End Energy Balance
(8/15/85 Scan No. 8)

86906

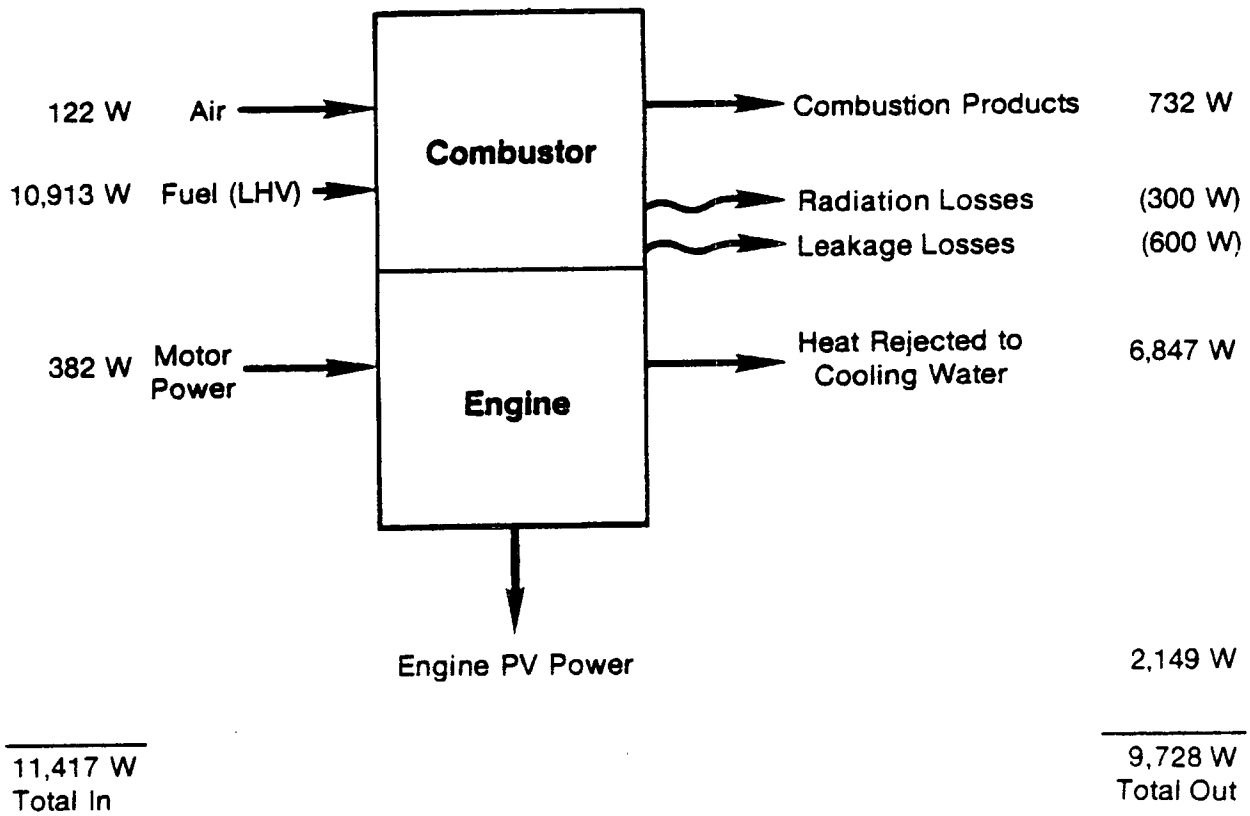

Without Losses $\frac{\text{Energy Out}}{\text{Energy In}} = 0.85$ (Δ = 1,689 W)

With Losses $\frac{\text{Energy Out}}{\text{Energy In}} = 0.93$ (Δ = 789 W)

Figure 2-36 Upper End Energy Balance After Instrumentation Calibration (9/25/85 Scan No. 20)

853405 -1

actual task of taking performance data on the heat pump system could now proceed with some degree of confidence.

2.3.5 Performance Test Results

The test plan specified that the performance of the heat pump system should be measured at steady-state conditions. Prior to running these performance tests, the time required for the machine to reach steady-state conditions for good performance data acquisition was unknown. A transient test was made where the system was started up cold, and data were taken every 5 minutes. These data were then plotted in order to determine a time after which steady-state conditions were assured. As shown on Figures 2-37 and 2-38 the refrigerant flow rate and compressor stroke were very steady over the entire time period that the oil was heating. A plot of drive piston loss versus time showing that this parameter does not increase with time is provided in Figure 2-39. The compressor suction and discharge gas properties were also found to be constant over this period. It could therefore be concluded that steady-state data could be assumed after a relatively short period of warm-up time and that the key performance parameters do not depend upon transmission oil temperature.

Subsequent to the resolution of the energy balance problem, data were taken for many of the ambient conditions specified in the test plan, and cursory evaluations were made. Results showed that the compressor data were not repeatable and that the refrigerant mass flow rates, especially in the heating mode conditions, could not be substantiated by comparing with flow rates calculated from the compressor cylinder PV diagrams. In addition, the compressor discharge gas temperature was suppressed well below the level corresponding to 75 to 80% compressor efficiency. The discrepancies between calculated and measured refrigerant flow rates and between calculated and measured compressor discharge temperatures are given in Table 2-8. After a short period of investigation, the refrigerant calorimeter loop was found to be the source of the aforementioned anomalies. Oil leaks past the chevron seals from the transmission to the compressor and enters the calorimeter loop along with the refrigerant gas that is discharged from the compressor. Even though the amount of oil transmitted to the loop during each run is small, the

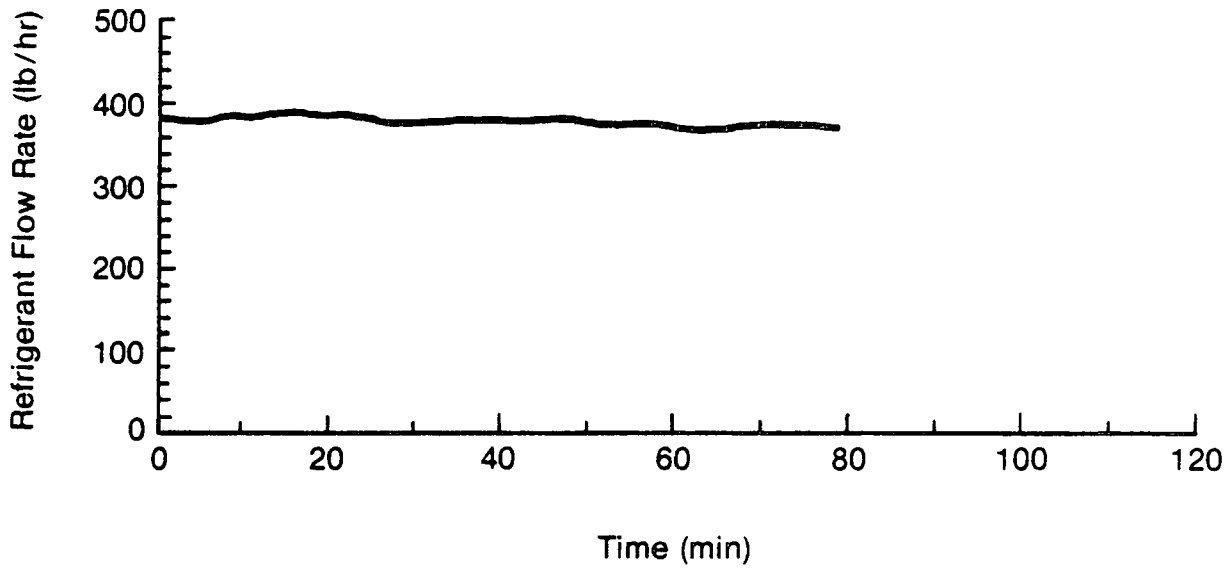

Ambient Temperature: 95°F
10-cs Silicone Oil

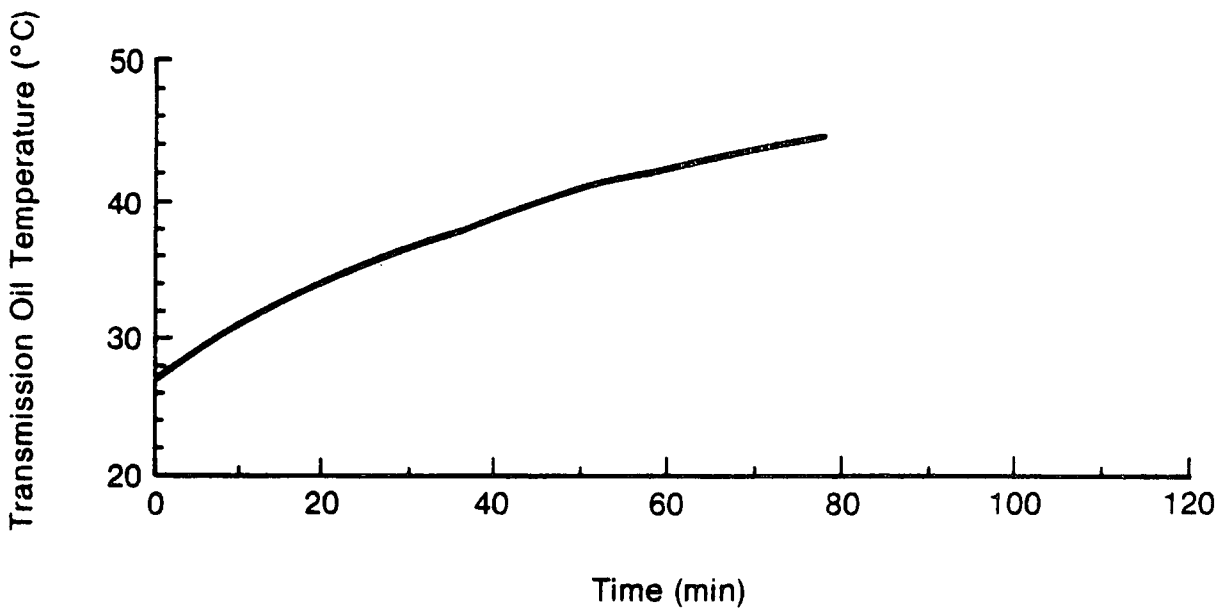

Figure 2-37 Heat Pump Mapping of Refrigerant Flow As a Function of Time

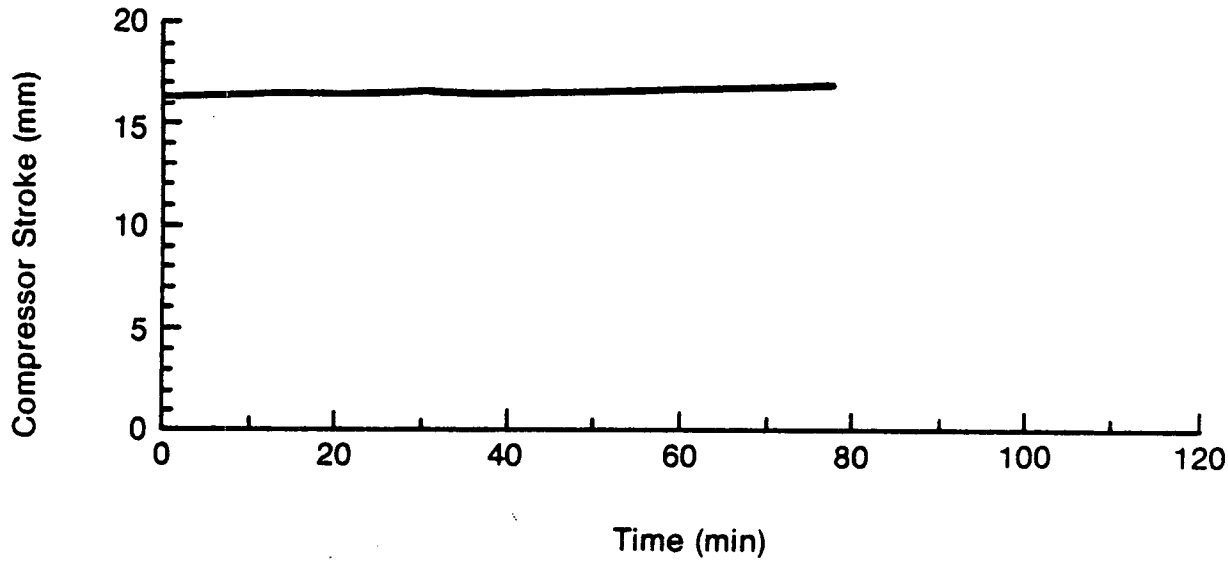

Ambient Temperature: 95°F
10-cs Silicone Oil

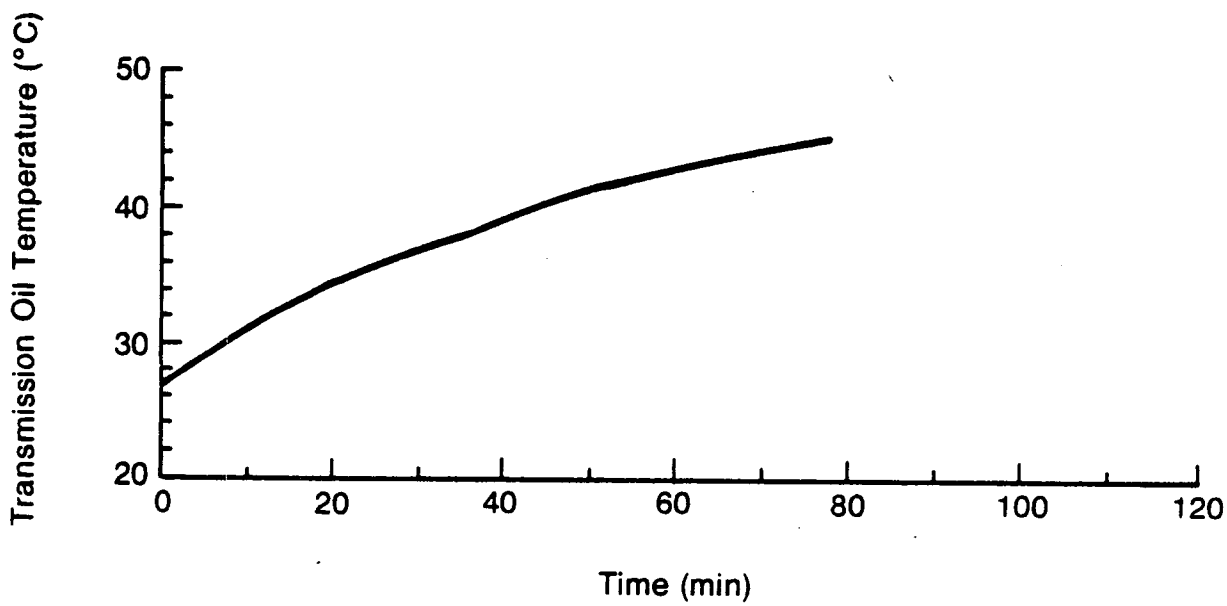

Figure 2-38 Heat Pump Mapping of Compressor Stroke As a Function of Time

861349

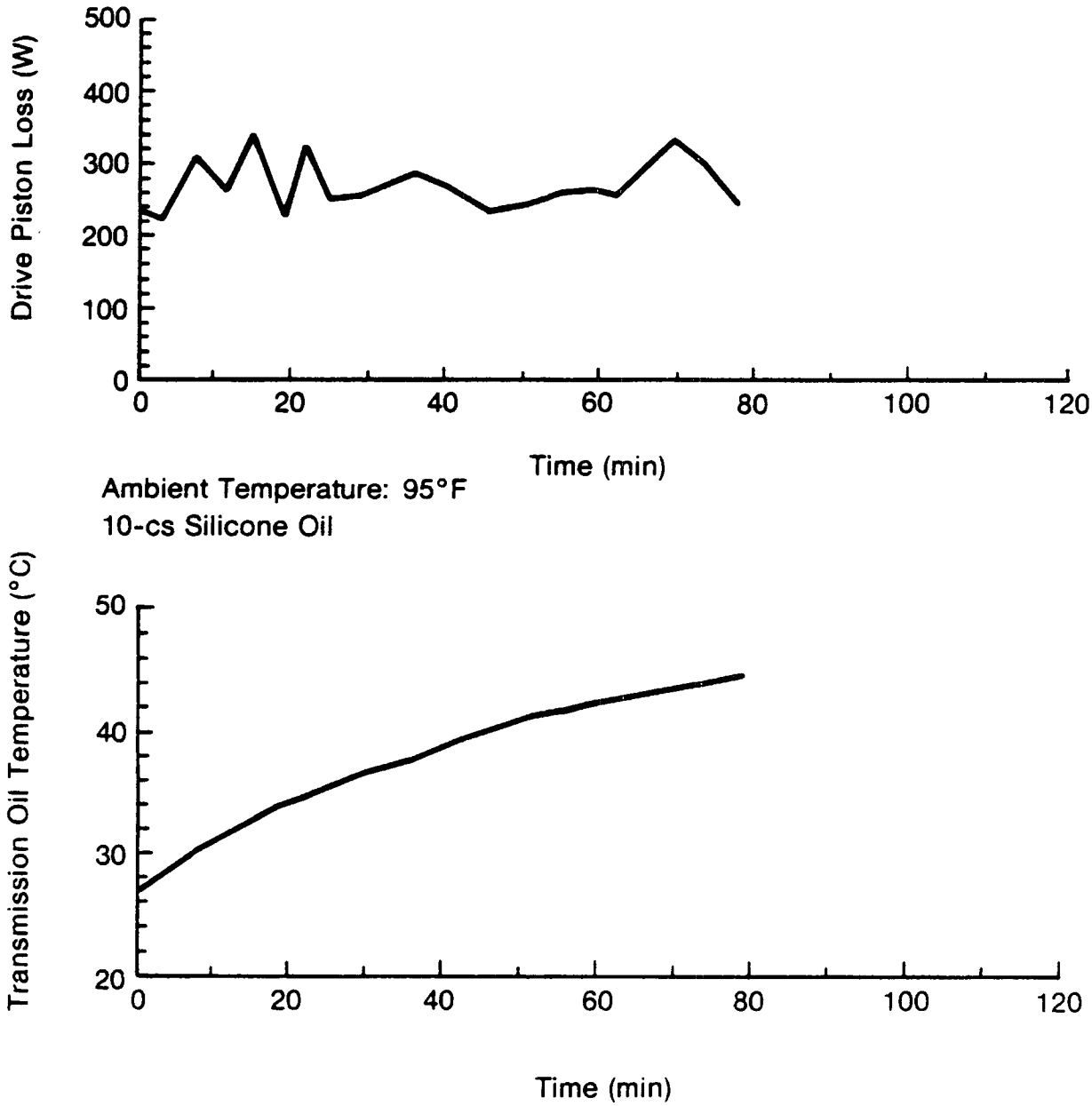

Figure 2-39 Heat Pump Mapping of Drive Piston Loss As a Function of Time

861346

Table 2-8

Key Parameter Comparisons for Tests Conducted with the Oil Accumulation in the Refrigerant Loop

Calculated and Measured Refrigerant Flow Rates

Condition (°F)	Caluculated Flow (lb/hr)	Measured Flow (lb/hr)
95	417	420
87	526	553
47	433	478
32	358	395
17	224	322

Calculated and Measured Compressor Discharge Temperatures

Condition (°F)	Calculated Discharge Temperature (°F)	Measured Discharge Temperature (°F)
95	189	148 → 158
47	160	123
32	168	121
17	212	130

amount accumulated over several weeks is very significant. The loop was harboring oil in the condenser/evaporator, and when it was "blown down," these areas were not being purged of oil.

Large quantities of oil circulating in the liquid regions of the calorimeter loop were not apparent until the measured refrigerant flow rate was compared to the flow rate calculated from the compressor cylinder pressure/volume data. The discrepancy between the two values was extremely pronounced at the 17°F ambient conditions. Also, large quantities of oil droplets entrained in the refrigerant gas leaving the calorimeter loop (entering the compressor-suction) were causing a suppression of the discharge gas temperature. Again, this effect was more profound at the 17°F ambient conditions. The oil accumulation problem was corrected by installing drains in the calorimeter loop that would allow a complete evacuation of the unit including all the oil that had accumulated. A decision was made to blowdown and completely drain the loop before running each new test condition and to take a liquid sample from the loop near the end of each test condition. In this manner, the behavior of the refrigerant system could be closely monitored and valid performance evaluations assured.

Starting with the 95°F ambient condition, steady-state ambient data were retaken with close monitoring of the system energy balance, the oil in the refrigerant system, and the parameters to be held constant for each ambient condition. Prior to conducting the performance tests, it was determined that the compressor piston stroke would be limited to ∿18 mm. This limit on compressor piston stroke governs the diaphragm excursions to about 4.3 cubic inches of volumetric amplitude (1/2 volumetric stroke), which in turn correlates to ∿46,000 psi effective stress. This will yield a minimum fatigue life of about ∿1000 hours. A graphical representation of compressor piston stroke versus diaphragm fatigue life is shown in Figure 2-40.

The test plan called for four displacer strokes at each ambient temperature condition; however, due to the above mentioned diaphragm limitation, some of the points listed could not be run (see Table 2-9). Since the stroke ratio between the engine displacer and the compressor piston could not be accurately predetermined for all test conditions, the point at which the displacer stroke

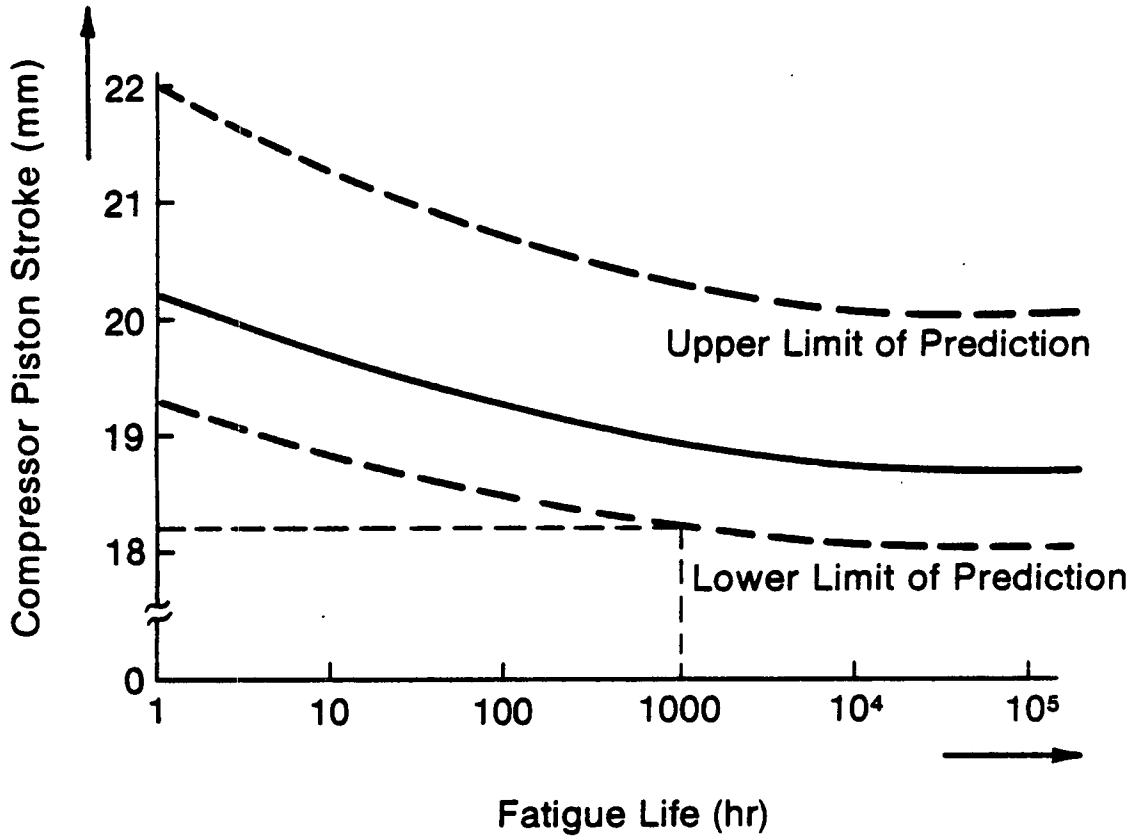

Assumptions:

Material: Vacuum Melted AMS4340 Steel Heat Treated and Tempered to Rc 38

Minimum Ultimate Stress:	170 ksi
Minimum Yield Stress:	155 ksi
Material Endurance (Infinite Life):	67 ksi

- Mean Stress Equals Zero (Good Diaphragm Centering)
- Reliability Factor Equals 0.895 (90% Survival Rate)
- Surface Factor Equals 0.95 (Pseudo-polished)
- Stress Concentration Factor equals 1.135 (at Outer Fillet)
- Lower Limit of Prediction Based on Surface Factor Equals 0.89 (Ground)
- Upper Limit of Prediction Based on Surface Factor Equals 0.98 and Deletion of Stress Concentration Factor

Figure 2-40 Diaphragm Life Prediction

86242

Table 2-9

Actual Matrix of Test Data for Different Ambient Temperatures and Displacer Strokes

Ambient Temperature (°F)	Frequency	Displacer Stroke (X_D) 16 mm	18 mm	20 mm	22 mm
0	Optimum at 9 mm XD	3 Scans* (9 mm)	---	---	---
17	Optimum at 13 mm XD	3 Scans (9 mm)	3 Scans (11 mm)	3 Scans (13 mm)	---
32	Optimum at 20 mm XD	3 Scans	3 Scans	3 Scans	---
47	Optimum at 22 mm XD	3 Scans	3 Scans	3 Scans	3 Scans
Test Point 1	Optimum at 22 mm XD	3 Scans	3 Scans	3 Scans	3 Scans
80	Optimum at 22 mm XD	3 Scans	3 Scans	3 Scans	3 Scans
87	Optimum at 22 mm XD	3 Scans	3 Scans	3 Scans	3 Scans
95	Optimum at 22 mm XD	3 Scans	3 Scans	3 Scans	3 Scans
Test Point 2	Optimum at 22 mm XD	3 Scans	3 Scans	3 Scans	3 Scans

*After steady state has been reached, 3 scans are taken at 5-min intervals

level would correspond with the maximum compressor piston stroke level was unknown. This information was revealed as the test program was run. The three lowest ambient test conditions (32, 17, and 0°F) were compressor piston stroke limited as opposed to the others being engine displacer stroke limited. This occurs at lower ambient temperatures because the compressor must stroke out more to achieve the refrigerant flow due to the higher pressure ratios and the lower density of the suction gas that occurs at these conditions. In fact, at the 0°F ambient condition, the displacer stroke was ~9 mm at the point where the compressor piston stroke (~18 mm) was limiting the capacity of the machine.

2.3.5.1 Steady-State Ambient Temperature Tests. Steady-state data were taken at seven different ambient temperatures: 95, 87, 80, 47, 32, 17 and 0°F. The oil used in the compressor transmission housing was 10-cs silicone (Dow Corning 200). Engine displacer stroke was varied at each ambient condition as shown in Table 2-9. The test plan provided compressor capacity turndown data due to simple modulation of the engine displacer.

Capacity - A plot of system capacity versus ambient temperature for a home in the mid-Atlantic region, rated at 3.0 tons of cooling at 95°F, is given in Figure 2-41. The heating mode data appear on the left side of the plot and the cooling mode data on the right, along with the amount of subcooling that occurred in the refrigerant calorimeter loop at each ambient condition. The amount of liquid subcooling that occurs in the loop between the outlet of the condenser and the inlet to the expansion valve cannot be independently controlled in the MTI calorimeter loop. The subcooling depends upon several factors including the ambient conditions set and the calorimeter cooling water temperature. Note that the capacity of the machine at the 95°F ambient condition is very near 30,000 Btu/hr (2-1/2 tons).

Figure 2-42a show capacity as a function of compressor piston stroke for the cooling mode points (80, 87, 95°F). Because the pressure ratio is lowest and the suction gas density is highest for the 80°F ambient condition, the compressor doesn't have to stroke out as far (as for the 87 or 95°F conditions) to load up the engine; Therefore, the 80°F ambient condition has the lowest compressor piston strokes, point for point. Figure 2-42b is a plot of

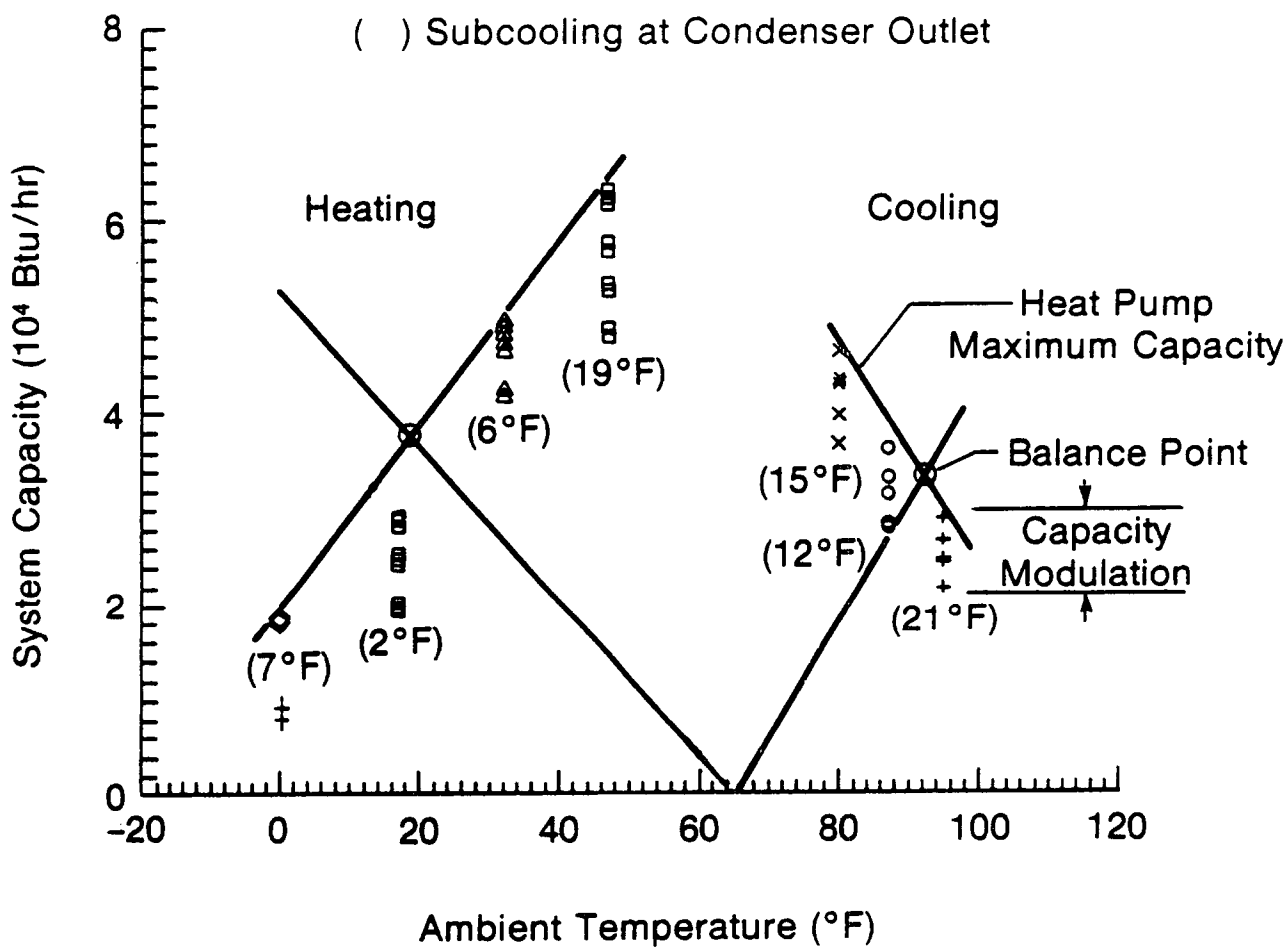

Figure 2-41 Breadboard Heating and Cooling Capacity As a Function of Ambient Temperature for a Home in the Mid-Atlantic Region, Rated at 3.0 Tons of Cooling at 95°F

86243

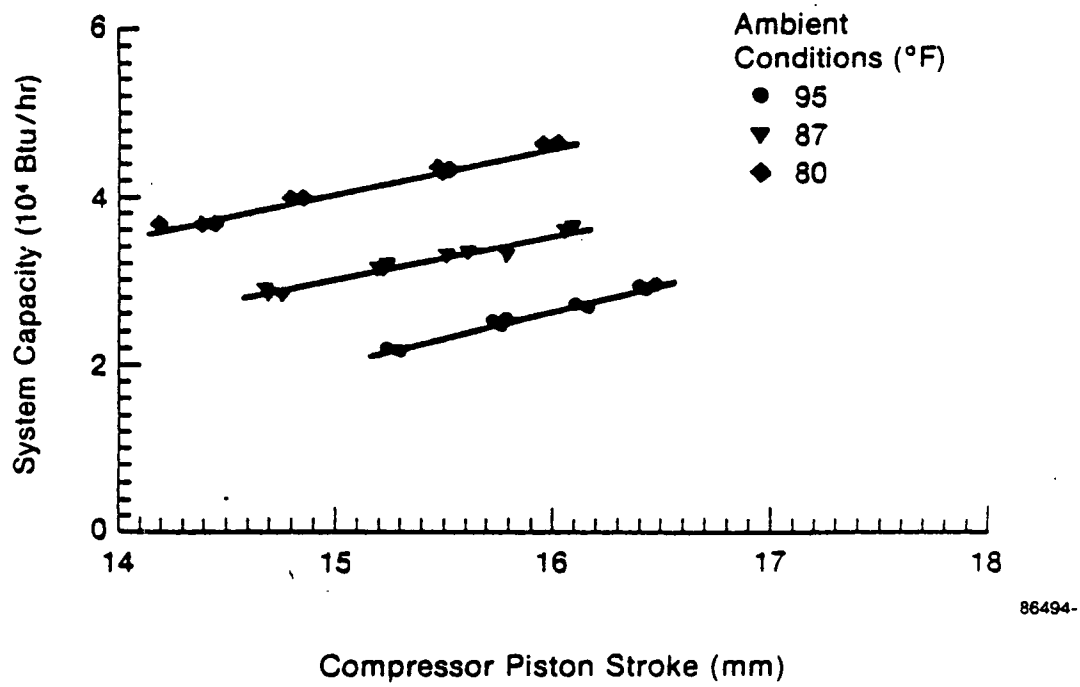

Figure 42a Breadboard Heat Pump Cooling Capacity As a Function of Compressor Piston Stroke and Ambient Temperature

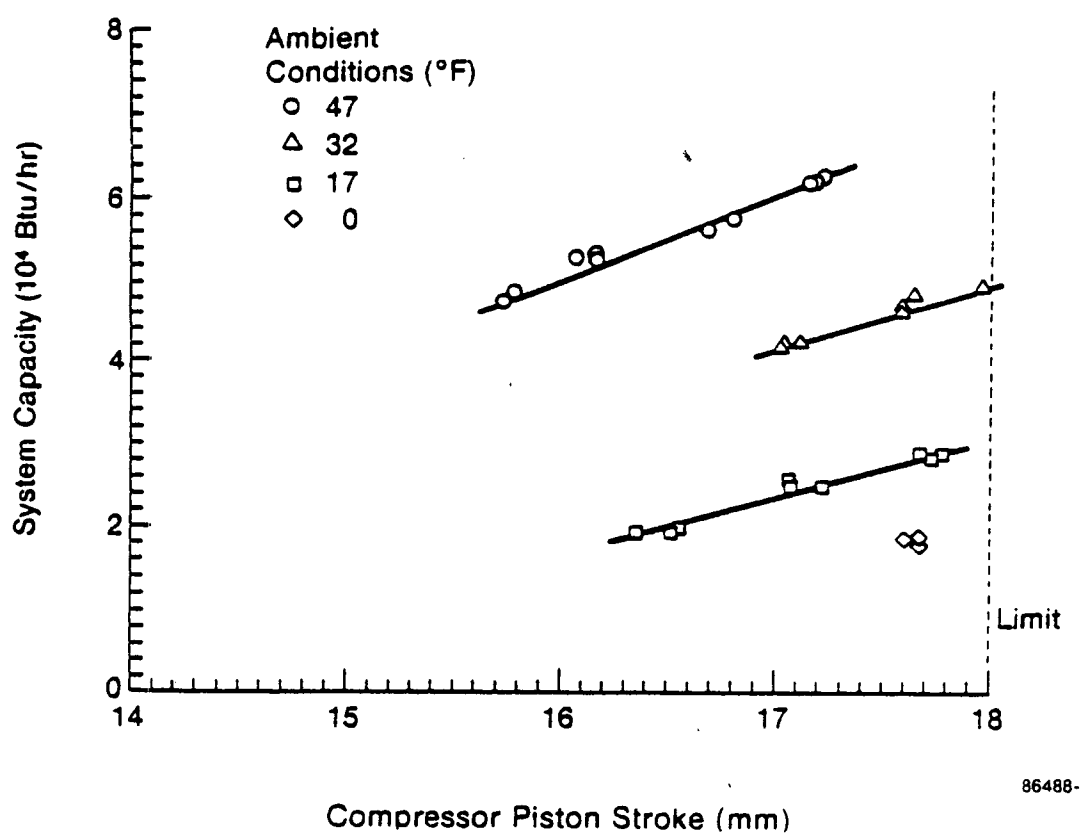

Figure 42b Breadboard Heat Pump Heating Capacity As a Function of Compressor Piston Stroke and Ambient Temperature

capacity versus compressor piston stroke for the heating mode points (0, 17, 32, 47°F). Note that the three lowest points (0, 17 and 32°F) were limited by compressor piston stroke. The 22-mm X_D point could not be run for the 32°F ambient condition, and none of the established displacer stroke points could be run at the 0 and 17°F ambient conditions due to the compressor piston stroke limit. Only one point (3 data scans) was run at the 0°F ambient condition since the displacer stroke was only 9 mm at the compressor piston stroke limit.

System Coefficient of Performance - A plot of system coefficient of performance (COP) is given in Figure 2-43. The COP drops off dramatically as the demand for either cooling or heating increases. The variation in COP for each different ambient condition is due to two factors: data scatter and variation with respect to capacity modulation. There is a slight tendency for the system COP to decrease with increasing capacity at a fixed ambient temperature. This is evidenced by the plots of COP versus compressor piston stroke for the 80°F ambient condition and the 47°F ambient condition in Figure 2-44. This observation is easily made since capacity is a direct function of compressor piston stroke, which is the parameter on the abscissa of each of these plots. This small decrease in system COP at high compressor piston strokes can probably be attributed to the increase in lower end losses at high stroke levels.

Compressor Efficiency - Figure 2-45 depicts the compressor efficiency as a function of compressor stroke. The mean efficiency for ambient temperature conditions from 32 to 95°F is between 74 and 76%. All but one of the data points for the 0 and 17°F ambient conditions falls below the mean line, some quite a bit below. The decrease in compressor efficiency at these low ambient conditions may be explained by the fact that the ratio between stroke and compressor PV power is quite large. However, the decrease in efficiency may not be real, owing to an acute sensitivity to parameters in the calculation. Recall that the calculation of compressor efficiency is made by dividing the product of the refrigerant mass flow rate and the "ideal enthalpy" by the compressor PV power. For a particular ambient condition, the ideal enthalpy is basically a fixed parameter, so the efficiency is dictated by the quotient of the mass flow rate and compressor PV power. The compressor efficiency is

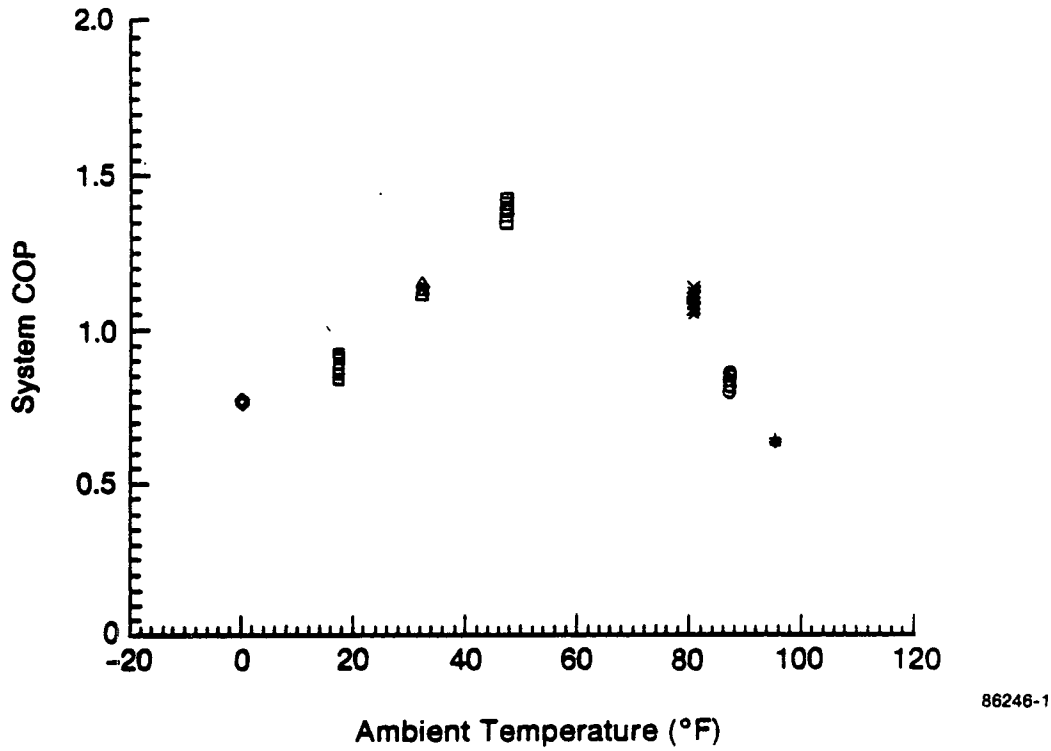

Figure 2-43 Breadboard Heat Pump System Coefficient of Performance As a Function of Ambient Temperature

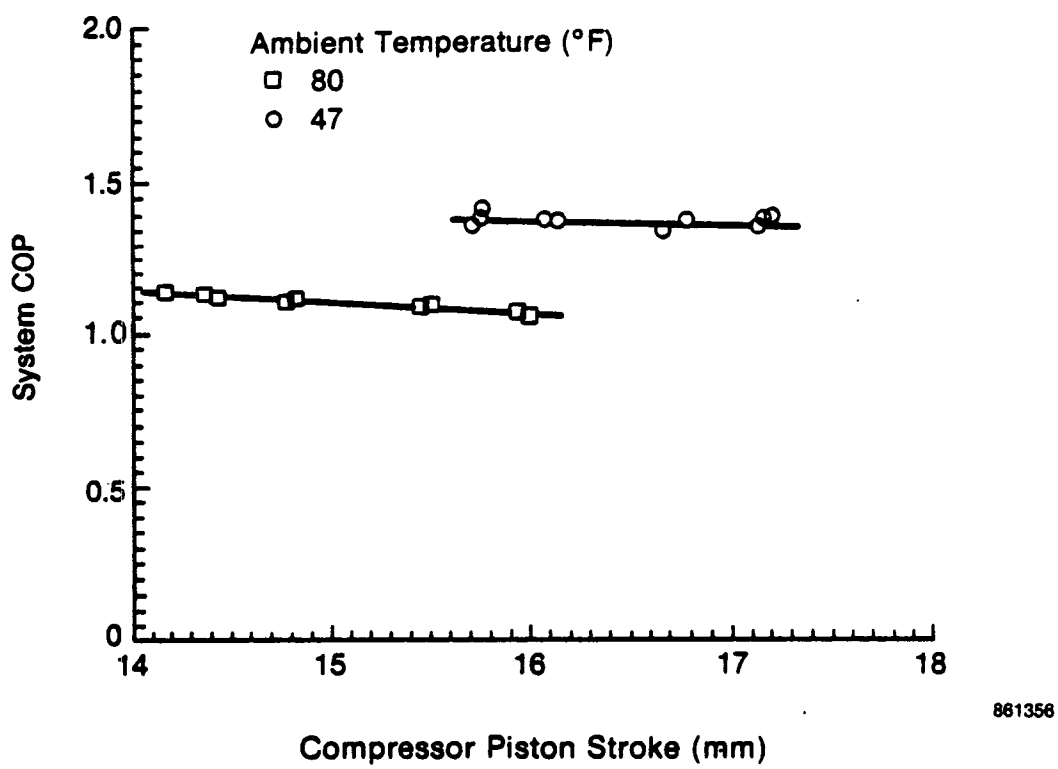

Figure 2-44 Breadboard Heat Pump System Coefficient of Performance As a Function of Compressor Piston Stroke

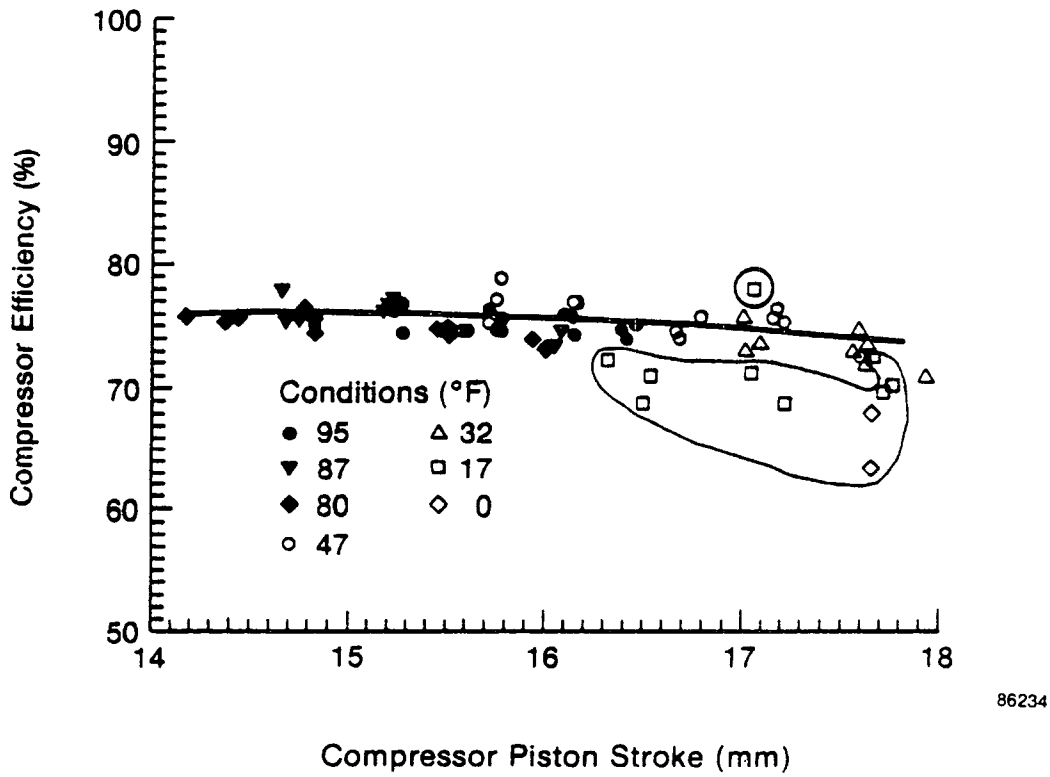

Figure 2-45 Composite of Compressor Efficiency As a Function of Compressor Piston Stroke at All Ambient Temperatures

very sensitive to small variations in the refrigerant mass flow rate at the low compressor PV power points encountered at the 17 and 0°F ambient conditions. In fact, the variation in efficiency is six times greater at the 0°F ambient condition than at the 95°F ambient condition. Another revealing plot of compressor efficiency is that given in Figure 2-46 where efficiency is plotted against ambient temperature. Data scatter is an important factor at the 0°F ambient condition since the three values plotted are from the same set point. Also, the high efficiency (~78%) value plotted at the 17°F ambient condition is probably from a bad data scan.

Piston Power Loss and Transmission Efficiency - Figure 2-47 provides a plot of piston power loss as a function of compressor piston stroke for all of the ambient conditions tested. Despite the fact that there is a fair amount of scatter in these data, there is a definite trend of increasing loss with increasing stroke. The slope of this band of data is ~50 W/mm and the bandwidth is ~135 W. The large variation (bandwidth) is understandable since many parameters are involved in the computation. Piston power loss is defined as the resultant of a power balance on the compressor spool, as shown in Figure 2-48. Specifically, this loss is the sum of the difference in upper and lower oil cavity PV powers and the compressor piston PV power. Piston power may be expressed as follows:

Piston Power Loss = PVU-OIL + PVL-OIL + PLHVP + PRHVP

where, as shown in Figure 2-49,

PVU-OIL = PV power upper oil cavity
PVL-OIL = PV power lower oil cavity
PLHVP = PV power refrigerant compressor - left piston; and the sign convention used is that power entering the piston is positive and power leaving the piston is negative
PRHVP = PV power refrigerant compressor - right piston

This loss can also be expressed in a slightly different way. Referring to Figure 2-48, the piston power loss can be defined as the loss associated with the power transfer within the compressor housing itself, i.e.,

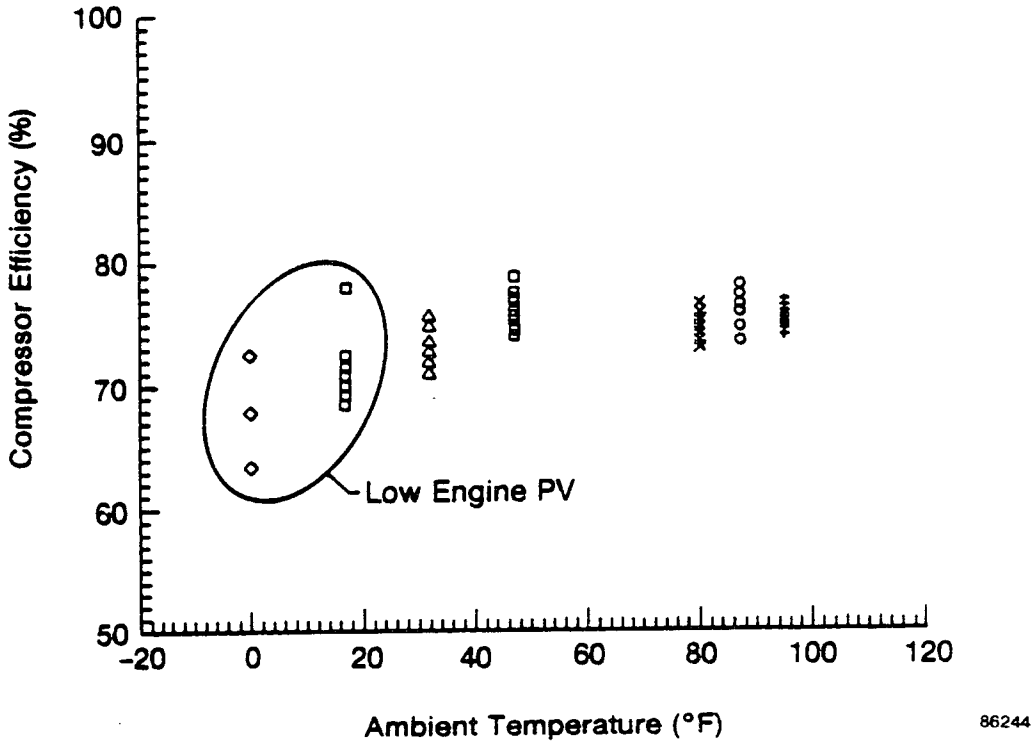

Figure 2-46 Breadboard Heat Pump Compressor Efficiency As a Function of Ambient Temperature

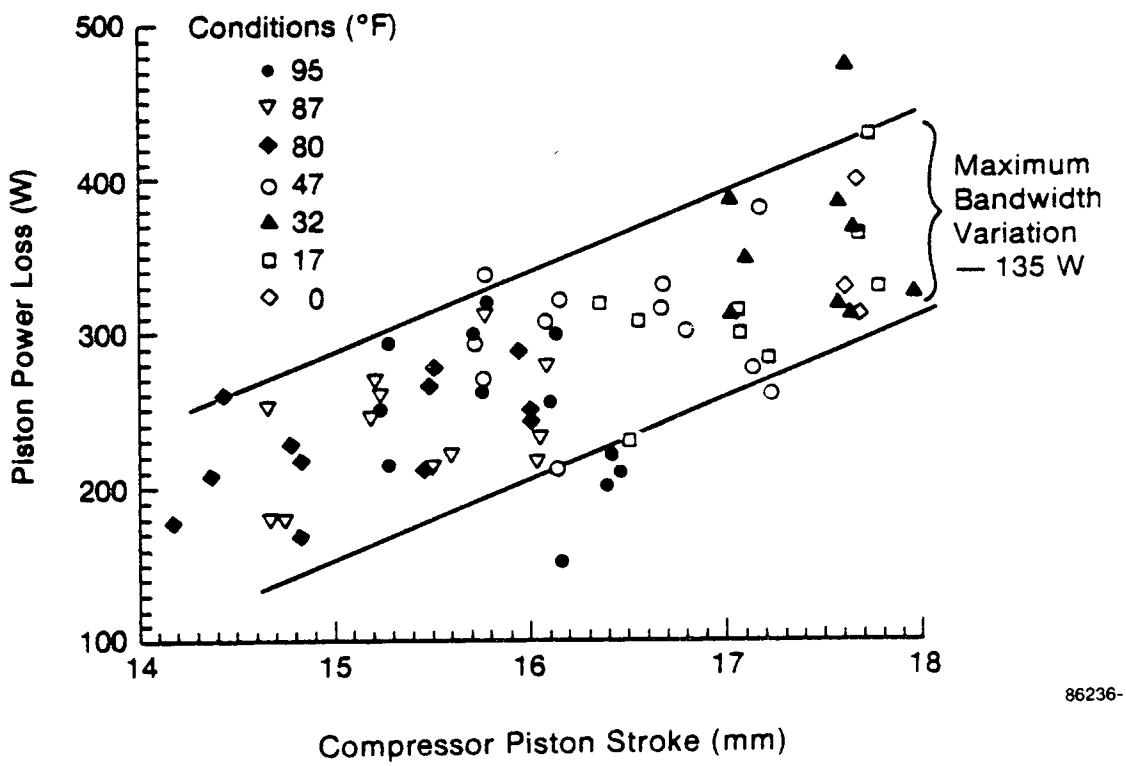

Figure 2-47 Hydraulic Transmission Power Loss As a Function of Compressor Piston Stroke

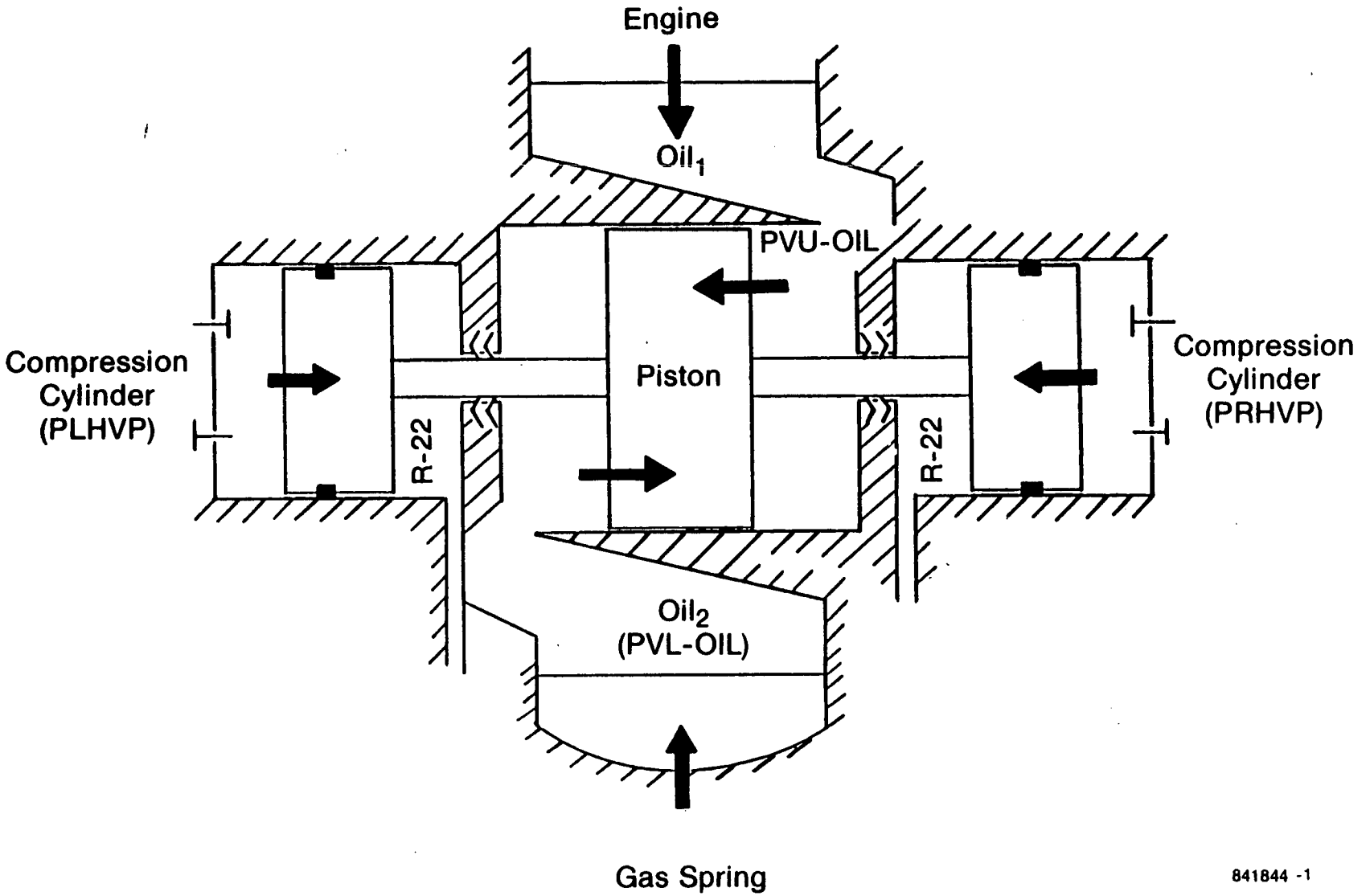

Figure 2-48 Compressor Measured Energy Flow

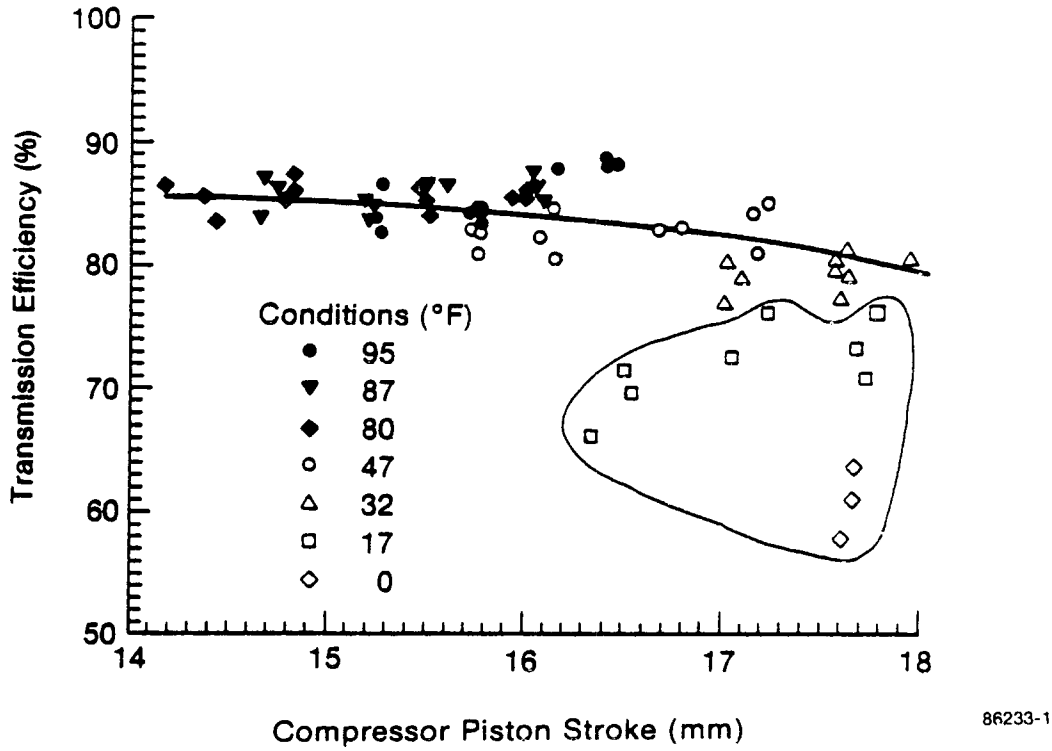

Figure 2-49 Hydraulic Transmission Efficiency As a Function of Compressor Piston Stroke

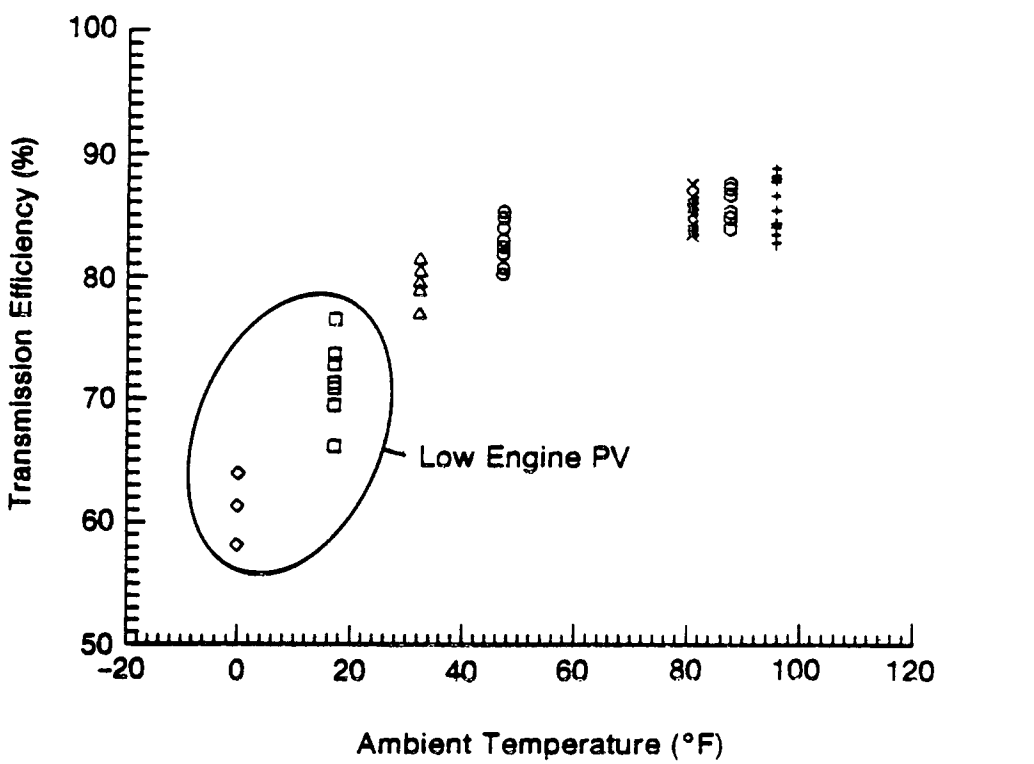

Figure 2-50 Hydraulic Transmission Efficiency As a Function of Ambient Temperature

Piston Power Loss = PV (engine) - PV (compressor) - PV (lower gas spring)

where:

PV (compressor) = PLHVP + PRHVP

PV (lower gas spring) = power designated in the lower gas spring.

Figure 2-49 depicts the transmission efficiency as a function of compressor piston stroke. The mean efficiency for ambient temperature conditions from 32 to 95°F appears to be between 80 and 86%. The efficiencies for the 0 and 17°F ambient conditions fall well below the mean line. At these conditions the transmission loss is higher and the engine power levels are lower. Both trends contribute to the lower transmission efficiencies at the low ambient conditions. Figure 2-50 relates transmission efficiency to ambient temperature conditions.

Engine PV Power - Figures 2-51a and 2-51b provide a plot of engine PV power versus compressor piston stroke and ambient temperature. All of these data are very well behaved in that all of the points lie very close to their mean line. No mean line can be drawn for the 0°F ambient condition since only one set of points was generated. The figure defines the range of engine power output that is required to drive the transmission and compressor. In the EM FPSE, the power output at a particular compressor piston stroke is modulated by controlling the displacer stroke with the displacer motor.

Refrigerant Flow Rate - Another interesting plot of the performance data is given in Figure 2-52, showing refrigerant mass flow rate versus compressor piston stroke for the seven ambient temperature conditions. Note that the slope of the mean lines for the cooling mode conditions is somewhat steeper than those for the heating mode. This is again due to the difference in suction gas densities. At high suction gas density conditions, a small change in stroke produces a dramatic change in refrigerant mass flow rate.

Summary of Conditions Run with 10-cs Silicone Oil - The primary steady-state performance parameters for all of the different test conditions are given in

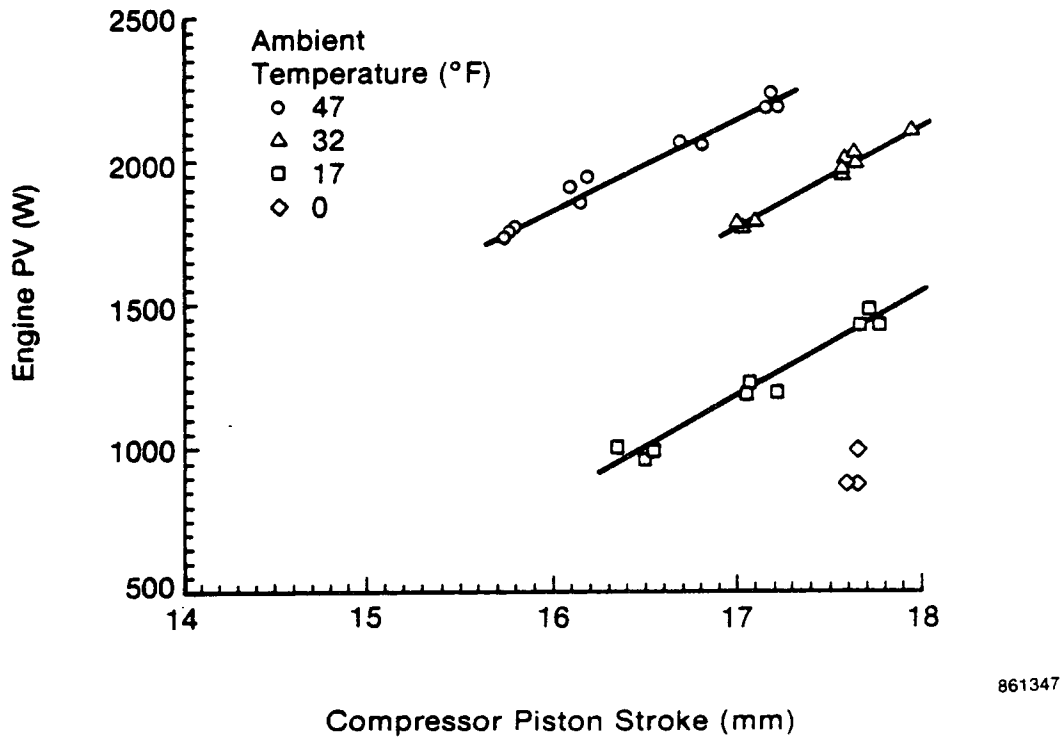

Figure 2-51a Breadboard Heat Pump Engine PV Power As a Function of Compressor Piston Stroke for the Heating Ambient Temperatures

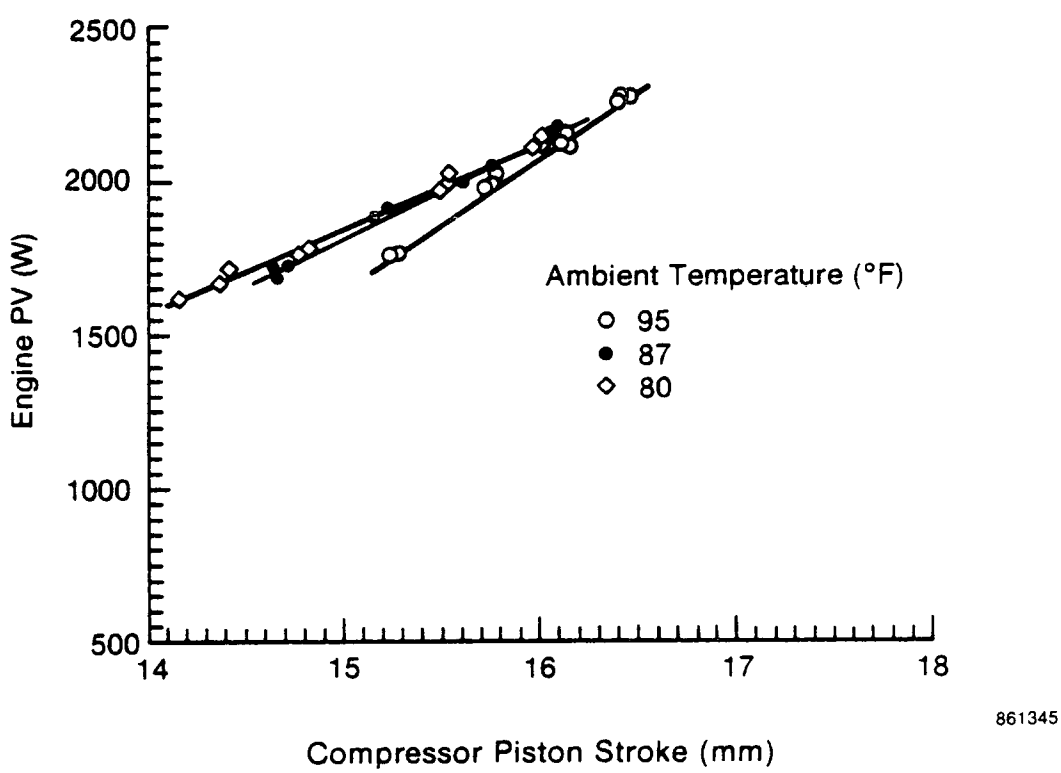

Figure 2-51b Breadboard Heat Pump Engine PV Power As a Function of Compressor Piston Stroke for the Cooling Ambient Temperatures

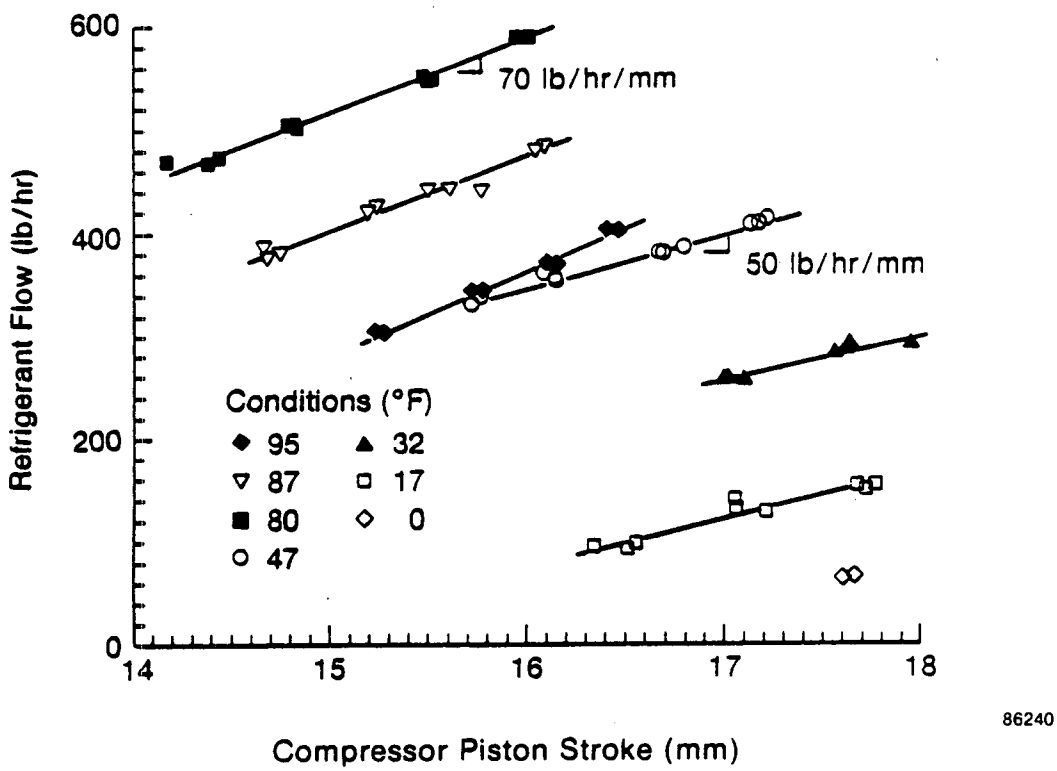

Figure 2-52 Breadboard Heat Pump Refrigerant (R-22) Flow Rate As a Function of Compressor Piston Stroke and Ambient Temperature

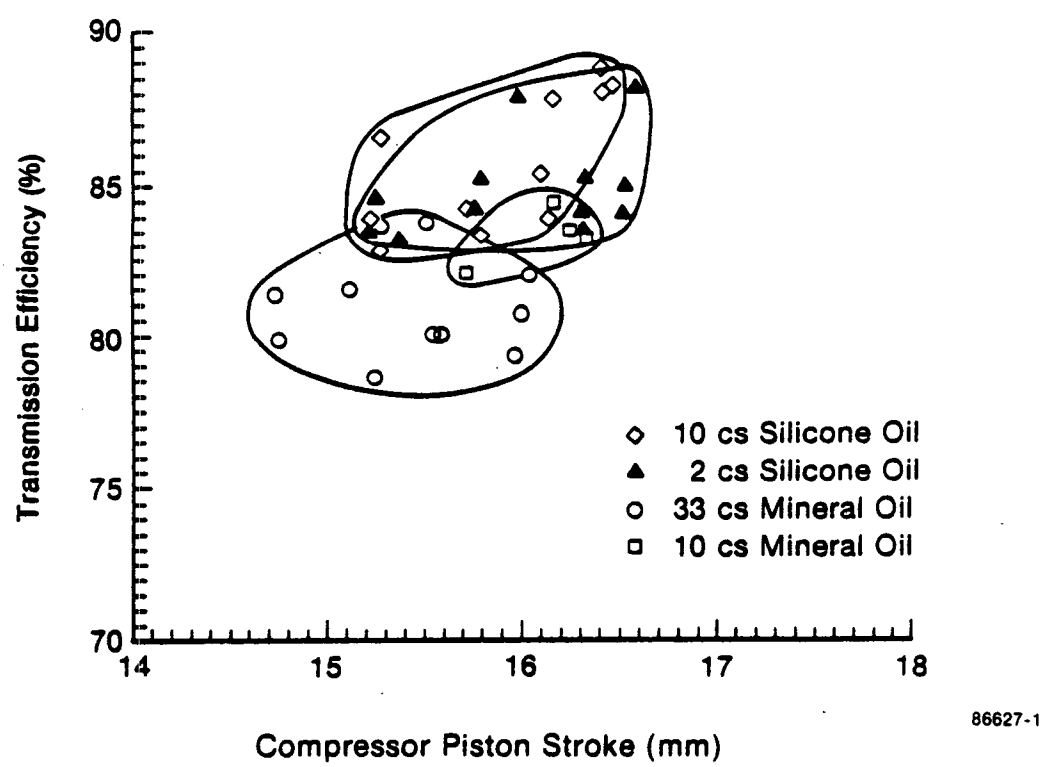

Figure 2-53 Breadboard Heat Pump Hydraulic Transmission Efficiency As a Function of Compressor Piston Stroke and Hydraulic Fluid Viscosity

Table 2-10

Heat Pump Mapping for Steady-State Performance Parameters
(for 10-cs Silicon Oil)

Ambient Temperature (°F)	Maximum Average Refrigerant Flow Rate (lb/hr)	Maximum Average System Capacity (Btu/hr)	Maximum Average System COP	Average Subcooling (°F)	Optimum Freqeuncy at 22 mm X_D (Hz)
95	402	28,950	0.635	21	56.4
87	480	35,939	0.828	12	55.3
80	587	46,285	1.068	15	54.7
Cooling Test Point	340	23,404	0.522	18	56.9
47	408	62,342	1.388	19	54.9
32	290	48,919	1.140	6	(54.6)*
17	150	28,696	0.888	2	(54.3)
0	64	18,450	0.765	7	(53.8)
Heating Test Point	337	54,483	1.182	4	55.6

*Limited by compressor stroke ( ) - may not be optimum at 22-mm X_D.

Table 2-10. All of these conditions were run using the Dow Corning 200 silicone oil having 10-cs viscosity. As pointed out previously, the 32, 17, and 0°F ambient conditions were compressor piston stroke limited. Also note that subcooling is a dependent rather than an independent parameter in MTI's refrigerant calorimeter test loop. This means that the operator does not have direct control over this parameter. The maximum average of several parameters is defined as the average of the parameter corresponding to the highest (maximum) displacer strokes run at a particular test condition. For most conditions, this corresponds to the 22-mm displacer stroke points. Included in Table 2-10 are the optimum frequencies that were empirically determined during these performance tests. For most test conditions, they correspond to the frequency at which the displacer motor current is minimum at 22-mm displacer stroke points. However, the optimum frequencies for the 32, 17, and 0°F test conditions correspond to the minimum motor current at the maximum displacer stroke run.

Excluding the two special test conditions, the optimum frequency variation is greater than 2.5 Hz, the difference between 56.4 Hz at the 95°F ambient condition and 53.8 Hz at the 0°F ambient condition. The effect on heat pump performance due to operating at off-optimum frequency was not investigated in these tests.

2.3.5.2 Transmission Oil Viscosity Tests. During the last phase of performance testing, the effect of the transmission fluid (oil) viscosity on the compressor performance was investigated. Four different oils were run in the compressor, as described in Table 2-11. The compressor was operated at the 95°F ambient condition using each of the oils as the transmission fluid.

Transmission Efficiency and Compressor Piston Loss Versus Oil Viscosity - Figure 2-53 shows the effect of oil viscosity on transmission efficiency. There is some scatter in these data, but the general trends are quite clear. The transmission efficiencies for the 2-cs and 10-cs viscosity silicone oils and the 10-cs mineral-based oil are close to each other and average ~84%. The efficiency for the 33-cs mineral-based oil is definitely lower than the others and averages ~81%. Therefore, the lower clearance seal leakage obtained with the 33-cs oil is overpowered by the higher viscous drag losses imposed on the

Table 2-11

Heat Pump Mapping for Compressor Transmission Oil Properties

Oil Name	Oil Type	Specific Gravity @ 75°F	Viscosity @ 75°F (cs)	Viscosity @ 100°F (cs)
Dow Corning 200 - 10 cs	Silicone Base	0.935	10	8.0*
Dow Corning 200 - 2 cs	Silicone Base	0.872	2	1.9*
Suniso 3GS	Mineral Base - Refrigeration	0.916	70	33.0
Texaco Code 600	Mineral Base - Transformer	0.89	NA	8.8

*Estimated from limited data.

oil flowing in the transmission. Note that the data for the 10-cs mineral oil is limited to five data scans, three at the 22-mm X_D point and two at the 20-mm X_D point.

Figure 2-54 shows piston power loss versus compressor piston stroke for the four oils. Again the data for the 2-cs and 10-cs silicone oils and the 10-cs mineral oil are grouped close together, and the 33-cs oil data are set apart from the others. These losses are somewhat higher for the highest viscosity oil; the average loss for the 33-cs oil is ~320 W whereas the average loss for the other three oils is ~250 W. However, the interesting or most significant characteristic of the data is the slope of a mean lines drawn through the set of points for the 33-cs and for the 10-cs and 2-cs oils. The slope of such a line is much greater for the 33-cs oil and predicts high power piston losses out in the 20-22 mm compressor stroke range.

Compressor Efficiency Versus Oil Viscosity - Figure 2-55 depicts the compressor efficiency versus compressor piston stroke for the four oils tested. The marked superiority of the 33-cs mineral oil and inferiority of the 2-cs silicone oil is erroneous in this graph. There is, however, a significant difference between the measured and calculated compressor piston strokes for these two oils. The compressor piston strokes calculated from the lower end gas spring pressure amplitude for the 33-cs mineral oil are higher than the measured strokes, and by correcting the denominator of the compressor efficiency calculation:

$$\eta_{comp} = \frac{\dot{m}_{Refrig} \, (\Delta H)_{Ideal}}{\text{Compressor PV}}$$

the corrected efficiency can be computed,

$$\eta_{comp} = \frac{\dot{m}_{Refrig} \, (\Delta H)_{Ideal}}{\text{Compressor PV} \left(\frac{X_{p\,Cal}}{X_p}\right)}$$

yielding lower compressor efficiencies. Just the opposite is the case for the 2-cs silicone oil: the calculated strokes are lower than the measured strokes and will therefore yield higher compressor efficiencies.

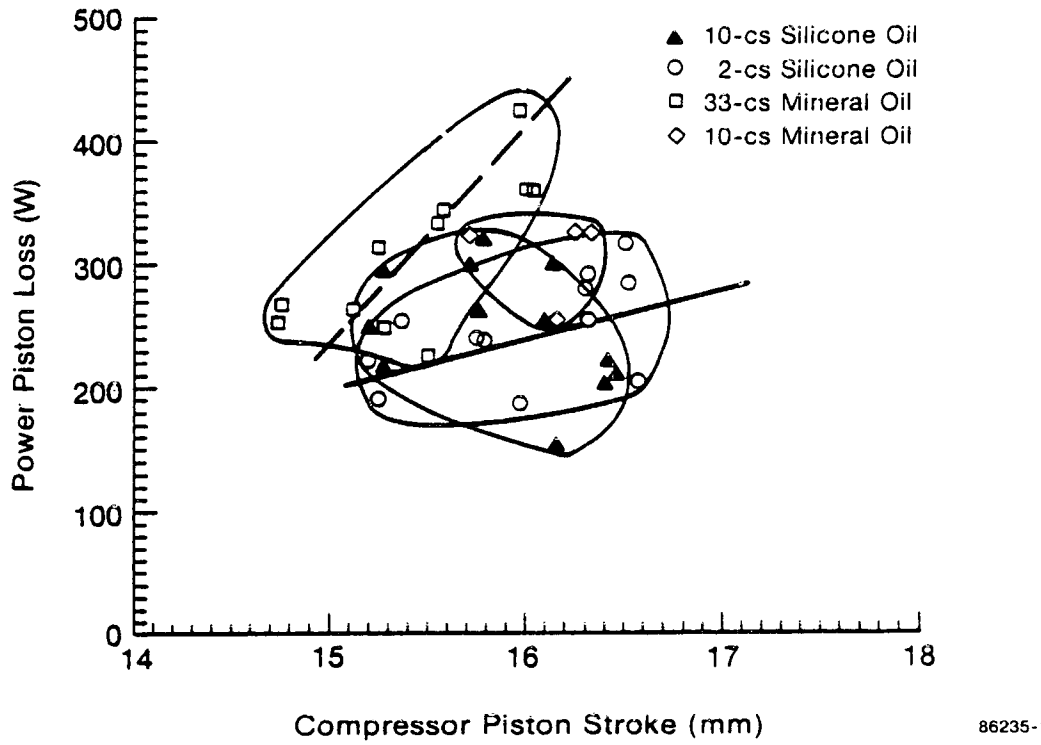

Figure 2-54 Transmission Power Loss As a Function of Compressor Piston Stroke and Hydraulic Fluid Viscosity

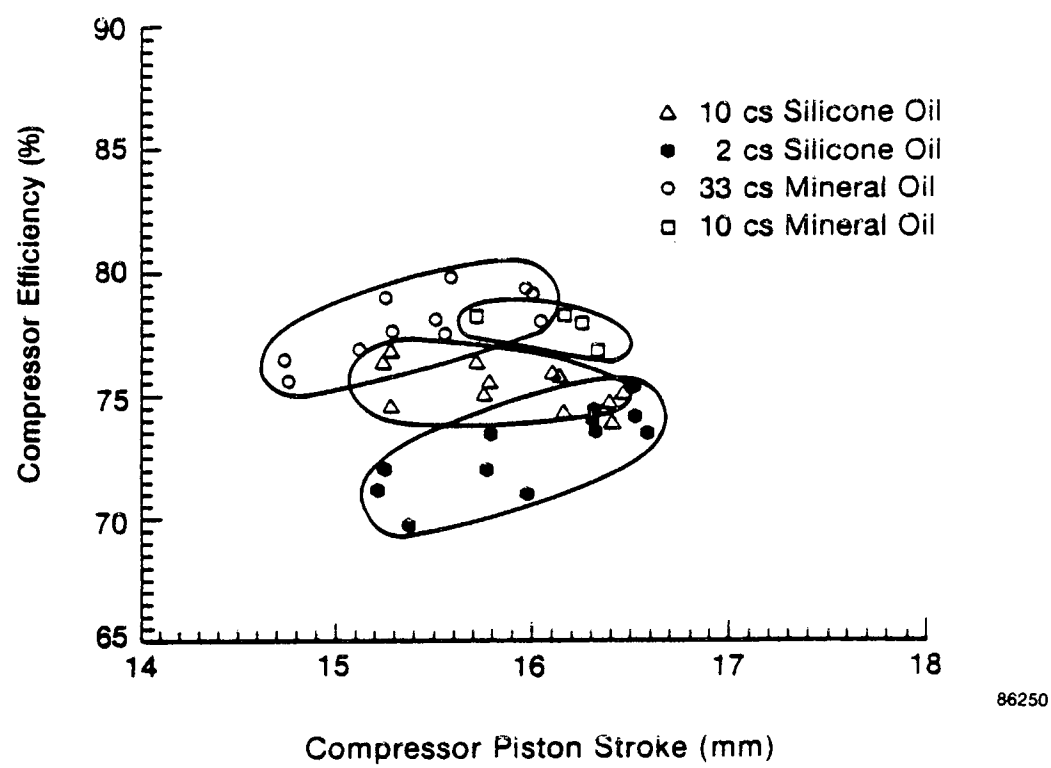

Figure 2-55 Breadboard Heat Pump Compressor Efficiency As a Function of Compressor Piston Stroke and Hydraulic Fluid Viscosity

Figure 2-56 provides a much different picture of the relationship between compressor efficiency and compressor piston stroke. The data points in this graph are much more compact, and it is very difficult to discern distinct groups as in the previous curve (Figure 2-55). Figure 2-56 shows a 6 to 7% total scatter in efficiency, which is expected due to the large number of instruments and parameters involved in the computation; there appears to be no change in efficiency with respect to compressor piston stroke. A mean level of compressor efficiency, falling between 75 and 76%, for all oil test data can be obtained from this graph.

Oil Temperature Versus Oil Viscosity - Per the test plan, a graph of transmission oil temperature versus time was made for each of the four oils tested. These graphs are provided in Figure 2-57 and represent initial (transient) periods of heat pump operation prior to the acquisition of steady-state data. The compressor in each case was operated steadily at the power level corresponding to the highest engine displacer stroke of 22 mm and data taken approximately every five minutes. Near the end of this transient run, steady-state data are taken for the 22-mm X_D point, and then the engine power is cut back to the 20-mm X_D point. As pointed out in section 2.3.5 of this report, the performance of the heat pump is not effected by increasing oil temperatures subsequent to the first 15 to 20 minutes of operation.

A superposition of each of the oil temperature curves reveals that there is no significant difference in oil temperature rate of increase for each of the four oils tested. The maximum temperature that would be obtained by continued running at the 22-mm X_D point was not investigated, but can be estimated from the transient run graphs to be 50-60°C (125-140°F).

Oil Leakage Versus Oil Viscosity - Oil leakage past the transmission chevron seals was a parameter investigated during the oil viscosity tests. The oil leakage rate for each of the four oils tested is given in Table 2-12. The 2-cs silicone oil exhibited the lowest leakage rate, and the 10-cs silicone oil had the highest leakage rate. Thus, the oil with the lowest viscosity leaked the least. A possible explanation for this may be a result of the improved wiping action of the chevron seals with an oil having a thinner film. In conjunction with the oil leakage investigation, a close watch was made on the oil

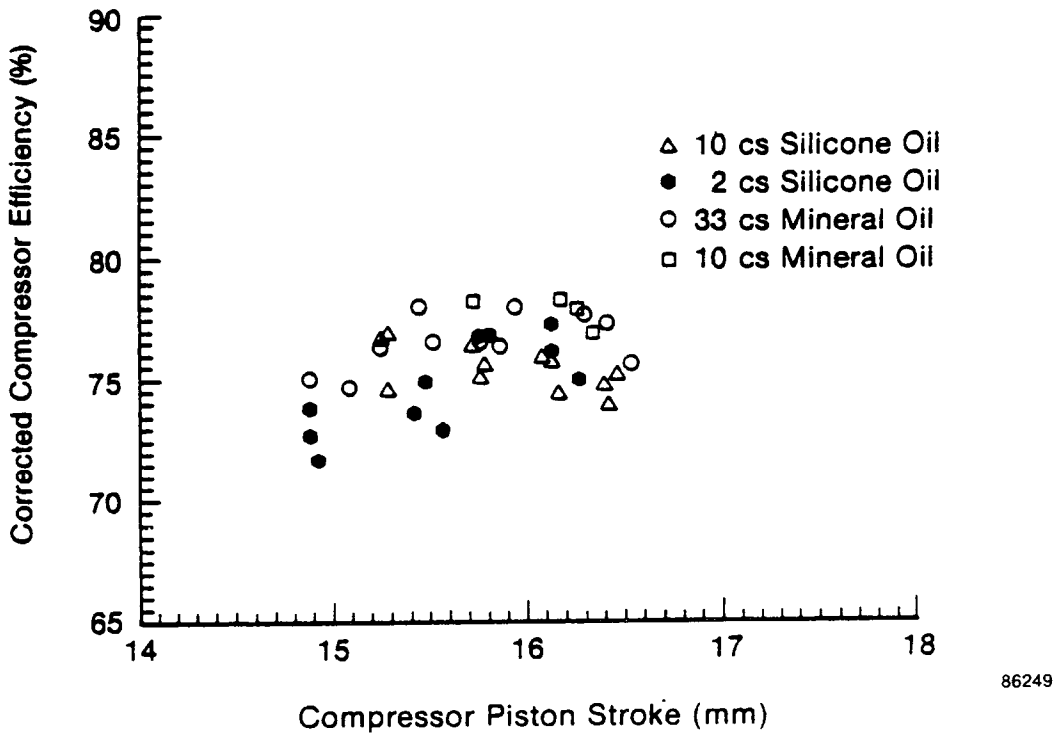

Figure 2-56 Corrected Compressor Efficiency As a Function of Compressor Piston Stroke and Hydraulic Fluid Viscosity

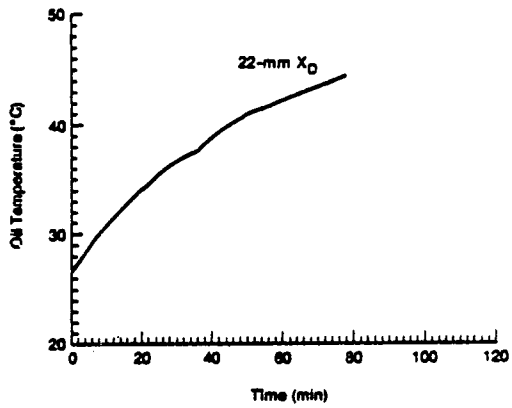

a) 2-cs Silicone Oil

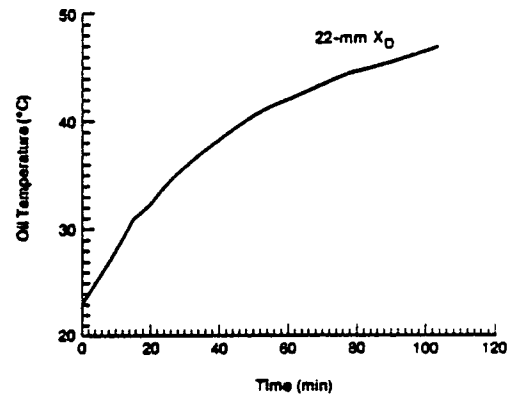

b) 10-cs Silicone Oil

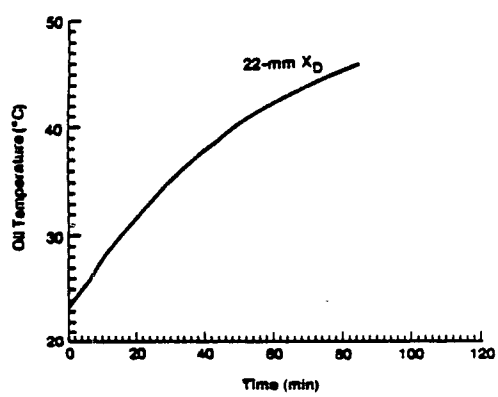

c) 33-cs Mineral Oil

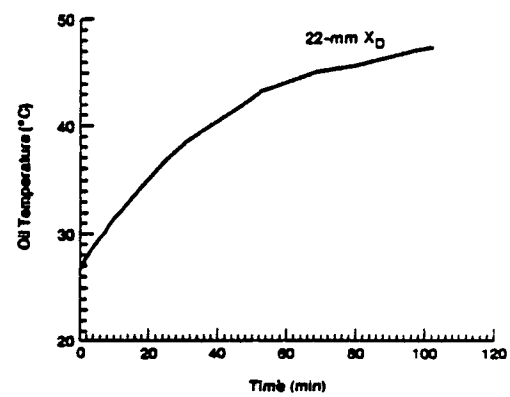

d) 10-cs Mineral Oil

Figure 2-57 Hydraulic Fluid Temperature Rise with Time for a 22-mm Displacer Stroke

86228-1

Table 2-12

Heat Pump Mapping for Compressor Chevron Seal Leakage from Oil Viscosity Tests

Oil Type	Oil Leakage Rate mL/hr	Oil Entrained in Refrigerant at End of test (%)
10-cs Silicone	172	4.8
2-cs Silicone	102	2.2
33-cs Mineral	137	3.3
10-cs Mineral	114	NA

circulation in the refrigerant calorimeter loop. Near the end of each test, which usually lasted about 4 hours, a sample of liquid refrigerant was taken from the loop. The amount of oil in each sample was measured and a percentage was calculated. These percentages are also given in Table 2-12. The percentage of oil measured in the loop for each of the oils (no data available for the 10-cs mineral oil) correlates well with the chevron seal leakage rate.

2.3.6 Conclusions and Recommendations

The heat pump system, including the Build 1 externally balanced direct-acting reasonant compressor, was operated for a period of approximately 5 months without a major rebuild. A posttest inspection of the transmission and compressor after 176 hours of operation revealed no detectable wear on any of the component parts.

The chevron oil seals were in good condition and were functioning properly at the end of the test program. The system was found to be stable; and repeatable, reliable data were taken throughout the entire set of test conditions.

Summarizing, the following conclusions can be made from the performance test data evaluation of the Build 1 compressor.

- The cooling capacity of the compressor at the 95°F ambient condition is near the 2.5-ton goal.
- The range of optimum frequencies is ~2-1/2 Hz between the 95 and 0°F ambient conditions.
- The average compressor efficiency for 14 to 18 mm compressor piston strokes and ambient temperature conditions between 32 and 95°F is ~75 to 76%.
- The average transmission efficiency for 14 to 18 mm compressor piston strokes and ambient temperature conditions between 32 and 95°F is ~84%.
- The transmission efficiency and transmission losses for the 33-cs mineral base oil are significantly higher than for the other transmission oils tested.

- There is little or no difference in performance between the 2-cs silicone and 10-cs silicone oils.
- Compressor efficiency is not a function of the viscosity or type of oil utilized in the transmission.
- Transmission and compressor performance are not a function of the temperature of the transmission oil.
- At the 32, 17, and 0°F ambient conditions the compressor piston stroke limit (17.7 mm) was reached prior to attaining the engine displacer stroke limit (22 mm). This compressor piston stroke limits the heating capacity of the machine, especially at the 17 and 0°F ambient conditions.
- The engine displacer stroke limit (22 mm) restricts the cooling capacity of the heat pump system, especially at the 95°F ambient conditions.
- Transmission oil seal (chevron) leakage was greatest for the 10-cs silicone oil and lowest for the 2-cs silicone oil.

During execution of the performance test plan, several concepts surfaced that should be investigated. The following actions are recommended:

- The low ambient temperature conditions, i.e., 17 and 0°F, should be run at larger compressor piston strokes, which will necessitate acquisition of diaphragms with greater excursion capability. This will enable performance characterization at higher compressor piston strokes (> 18 mm).
- The compressor should be tested at higher (95 to 115°F) ambient temperature conditions.
- The effect of frequency variation on performance should be investigated to determine the need for frequency control devices in future systems.
- A more detailed evaluation of the 10-cs mineral-based oil should be made because its cost is much less than the silicon-based fluids.
- The goals for system COP have not been achieved yet. Since the results of Phase IC have shown that the performance of the hydraulic transmission and compressor is now very good, future development efforts should concentrate on improving the efficiencies of the engine and combustor.

APPENDIX A

DESCRIPTION OF A FPSE HEAT PUMP

Figure A-1 is a layout drawing of the FPSE/HP and compressor assembly. The power unit, located above the engine diaphragm, is based on the Mark I FPSE being developed at MTI under the GRI-sponsored "Residential FPSE Development Program" for use as a general-purpose Stirling-engine driver for electric generator and heat pump systems. The Mark I engine consists of

- A natural-gas combustor
- A displacer drive subsystem
- A heater head and thermal regenerator
- A cooler.

The lower end of the unit consists of a hydraulic transmission that efficiently transfers engine power to the refrigerant compressor. These subassemblies, along with the gas springs in the power module, form a coupled resonant system that effectively functions with the Stirling engine. In the engine, the displacer shuttles the engine working fluid (Helium) between the hot and cold spaces, generating the driving pressure wave for the system. The pistons (refrigerant compressor) extract work from the gas to power the load (refrigerant circuit); hence, in this system, power is extracted from the engine and delivered to the compressor through the hydraulic fluid, providing a force/displacement transfer path between the engine and compressor. This coupling also applies the proper dynamics to the engine, providing resonant characteristics and volumetric phase relationships.

Hermetic separation between the engine working fluid and refrigerant is achieved by employing a flexible metal diaphragm between the engine and hydraulic system. Engine power is transferred to the compressor through the volumetric displacements of the diaphragm, and corresponding displacement of oil in the hydraulic transmission induced by the pressure wave in the engine. Benefits to be derived from this HAHP system as compared to an inertially driven compressor are:

- The use of the power-transfer diaphgram reduces the system from a three-degree-of-freedom to a two-degree-of-freedom resonant system, improving its operating control and stability.

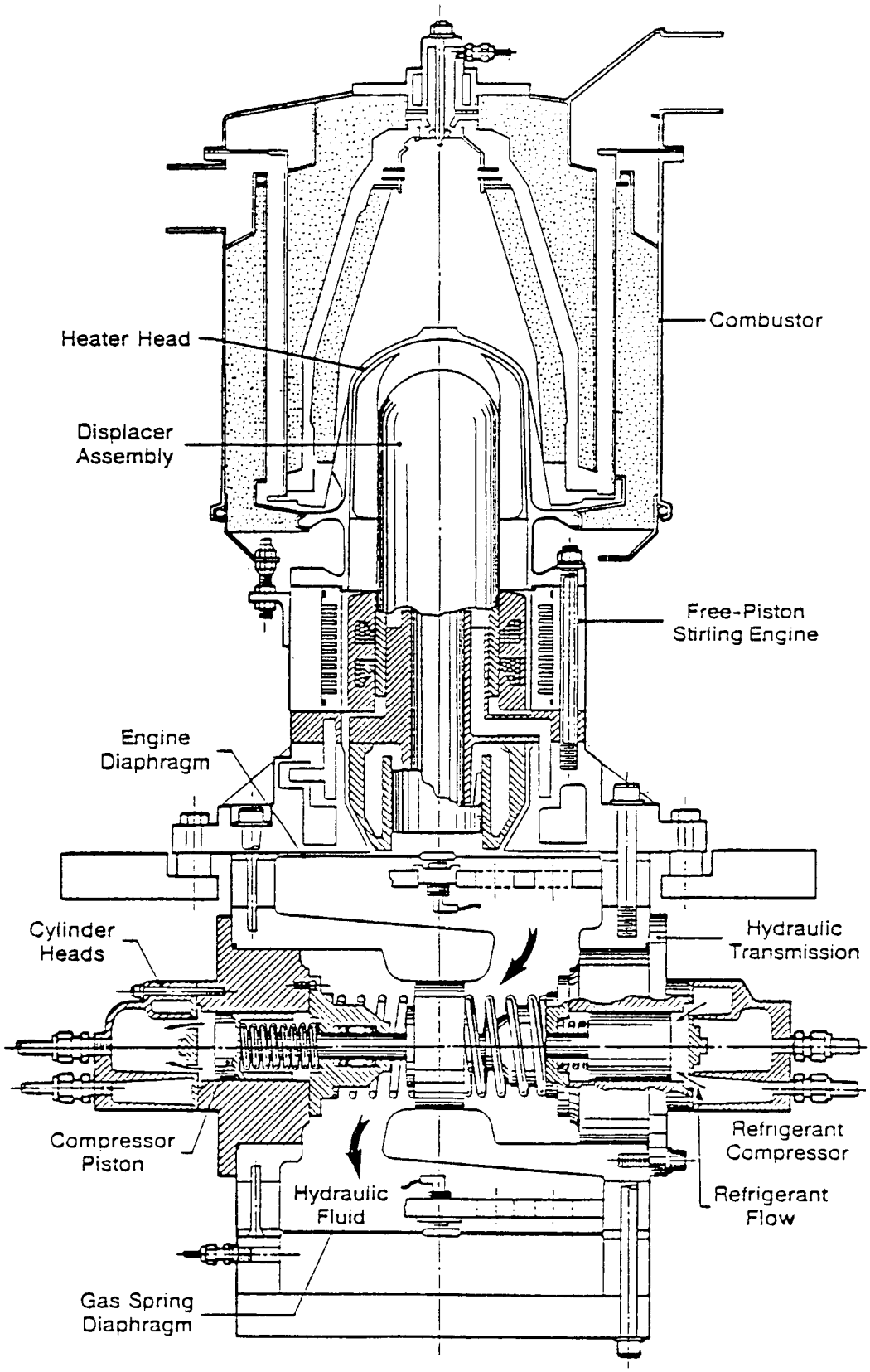

Figure A-1 Mark I Free-Piston Stirling Engine-Driven Heat Pump (Mark I engine configuration shown is similar to EM No. 4 FPSE)

853393

- Hermetic separation of the working fluids thermally isolates the refrigerant suction flow into the compressor, minimizing the super-heating of the suction vapor and the associated penalties in compressor performance

- The compressor closely resembles a conventional heat pump refrigerant compressor, allowing for the design and use of some standard heat pump compressor parts.

A.1 Component Description

This section describes the individual components of the breadboard power module.

A.1.1 Engine Components

A.1.1.1 Combustor - The combustor consists of a natural-gas turbulent burner and a preheater. Figure A-2 is a schematic diagram of the combustor shown in Figure A-1. During operation at the 95°F ambient operating point, air enters the preheater at 95°F and is warmed to 1467°F by the exhaust gases. The preheated air is mixed with fuel in the burner and ignited, raising its temperature to 3550°F. The hot gas is then passed over the heater head, providing heat input to the engine. The gas from the head enters the preheater at 1550°F and is further cooled by transferring heat to the air intake stream. Combustor efficiency is predicted at 82% for the 95°F operating point, based on the higher heating value for natural gas. Initial rig testing of the combustor has indicated that the combustor will achieve this efficiency.

A drawing of the FPSE External Heat System, consisting of the combustor and heater head, is shown in Figure A-3.

A.1.1.2 Displacer Drive System - The displacer drive system consists of the displacer, displacer rod, gas bearing support, gas spring pistons and cylinders, and displacer control. The dynamic arrangement for the displacer drive system is shown in Figure A-4. As depicted, the displacer is a free member

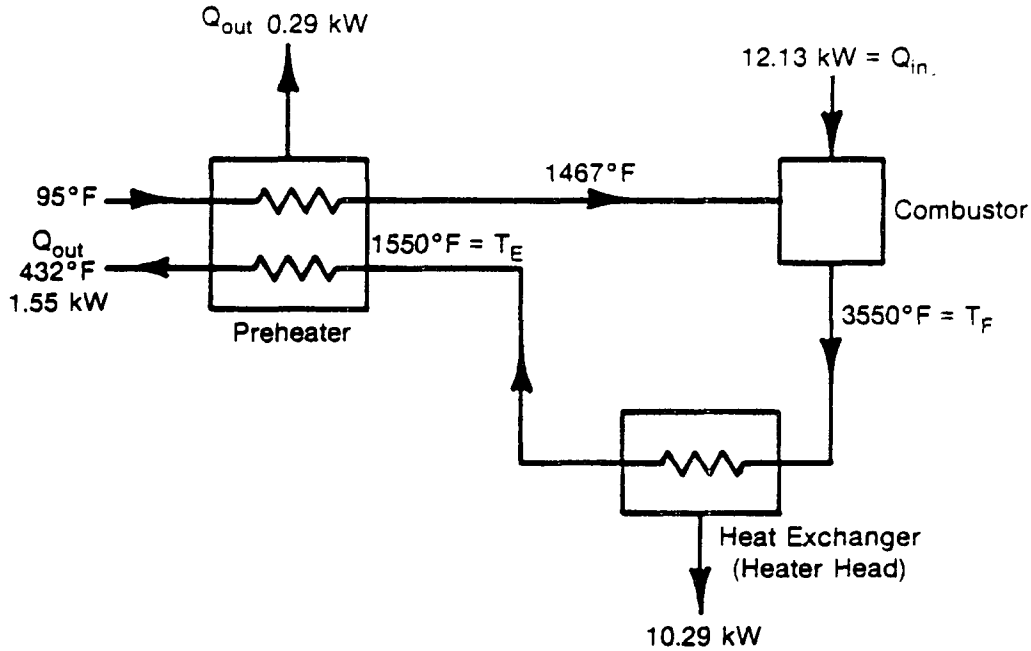

Predicted Efficiency Preheater:	≈0.94
Predicted Efficiency Combustion:	≈1.00
Predicted Efficiency Combustor:	≈0.82 (HHV)
Combustion Temperature:	3550°F
Air Preheater Temperature:	1467°F
A/F:	16.18
QA:	623 $SCFH_{32}$
QF:	38.5 $SCFH_{32}$
Radiation Losses:	2.4%
Heater Head Efficiency:	$0.93 = \frac{T_F - T_E}{T_F - T_H} = \frac{3550 - 1555}{3550 - 1400}$

$$\frac{Q_{in} - Q_{out}}{Q_{in}} = \frac{Q_{heat}}{Q_{in}}$$

Nomenclature:

T_H = Heater Head Temperature
Q_{in} = Heat into the System from Fuel
Q_{out} = Heat Lost from the Preheater
A/F = Air/Fuel Ratio
QA = Airflow
QF = Fuel Flow

Figure A-2 Free-Piston Stirling Engine Combustor Schematic

842133-1

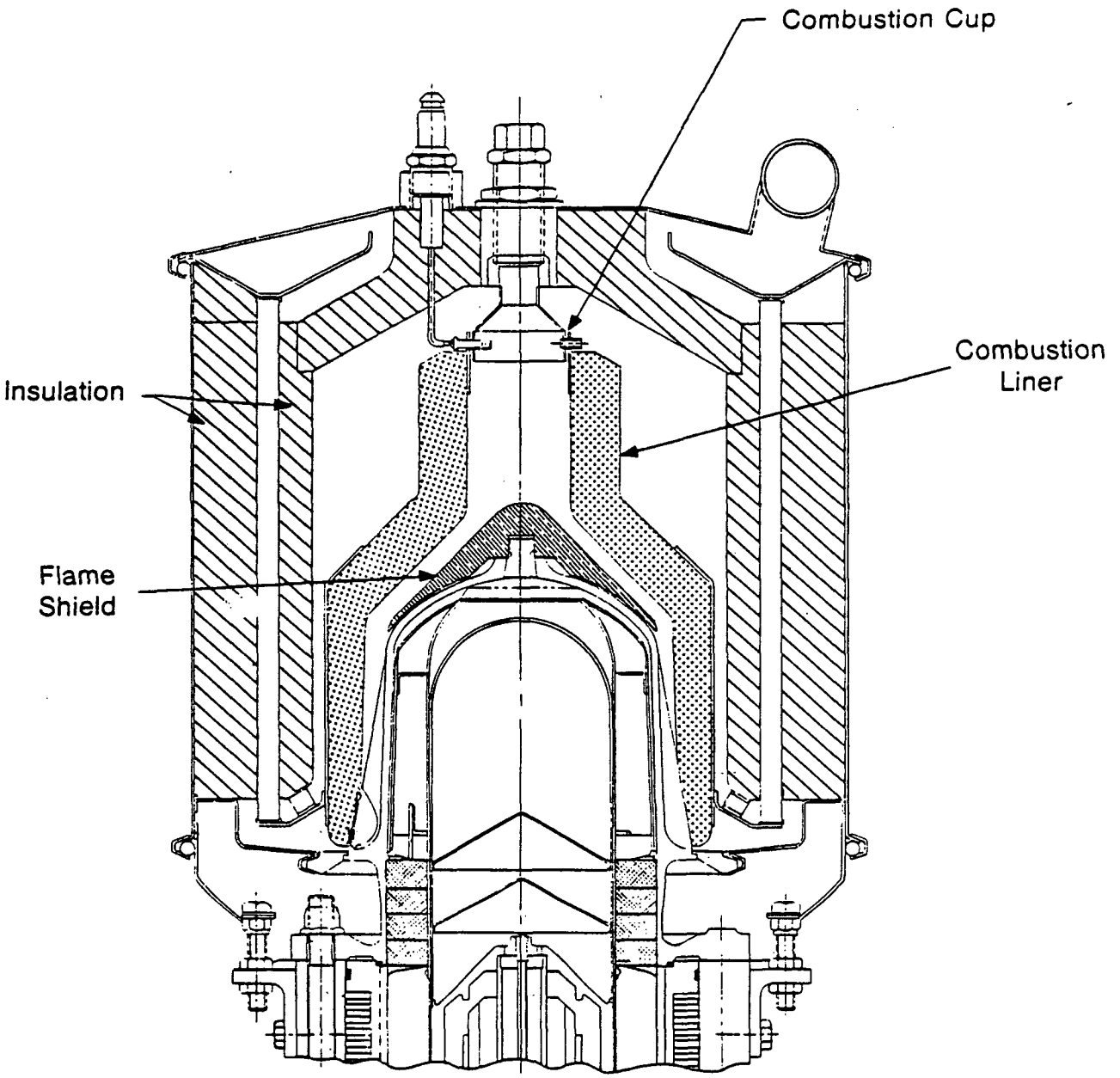

Figure A-3 Free-Piston Stirling Engine External Heat System

822159

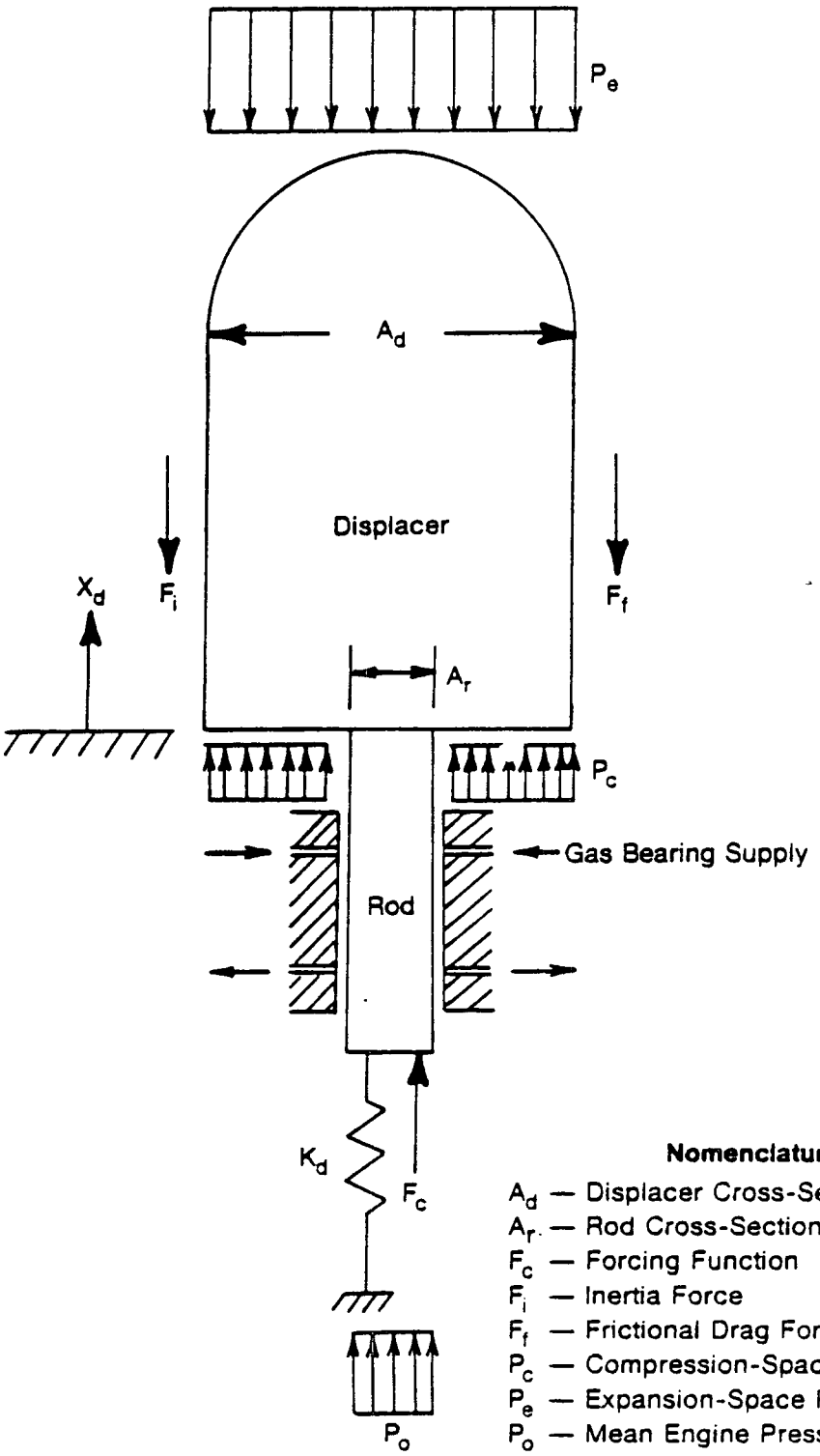

Nomenclature

A_d — Displacer Cross-Sectional Area
A_r — Rod Cross-Sectional Area
F_c — Forcing Function
F_i — Inertia Force
F_f — Frictional Drag Force
P_c — Compression-Space Pressure
P_e — Expansion-Space Pressure
P_o — Mean Engine Pressure
X_d — Displacer Motion
K_d — Gas Spring Stiffness

Figure A-4 Displacer Rod Dynamics

841831

radially supported by gas bearings on the rod and axially balanced by the dynamic forces. The function of each component in this system is as follows:

Displacer - The displacer is used to shuttle the engine working fluid through the heat exchanger components in the engine to the hot expansion and cool compression volumes.

Displacer Rod - The displacer rod serves two functions: 1) it transmits radial support for the displacer; and, 2) it provides the thermodynamic power required to move the displacer against the losses from the heat exchanger pressure drop, gas spring thermal hysteresis, and gas spring leakage pumping loss.

Gas Bearing Support - Hydrostatic gas bearings are used to provide radial support for the displacer. The gas bearings are located along the displacer rod and are designed to be internally fed by bleeding gas out of the working volumes (compression space) during the high-pressure portion of the cycle.

Gas Spring Piston and Cylinders - Gas springs are employed to provide a restoring force to the displacer, providing its resonant characteristics. As shown in Figure A-5, the displacer gas springs are the heater-side gas spring located in the bottom end (cool end) of the displacer and the load-side gas spring located at the base of the displacer rod.

Displacer Control - The displacer control is a linear electric motor that allows external control of the displacer for startup and stroke modulation, providing primary engine control to the system for load matching at different ambient operating conditions. Displacer control is achieved by applying a forcing function, F_c (Figure A-4), to the displacer to control stroke.

A.1.1.3 Heater Head and Thermal Regenerator - The heater head design for the engine is based on a monolithic heater head concept that has been under development for the past several years. The monolithic heater head design has the potential of being more reliable and less costly because it eliminates the fitting and brazing of the tubes required in a tubular design. The concept of the head is to use a one-piece head construction with fins on the inner and outer sides of the head to transfer the heat from the combusted gases in the

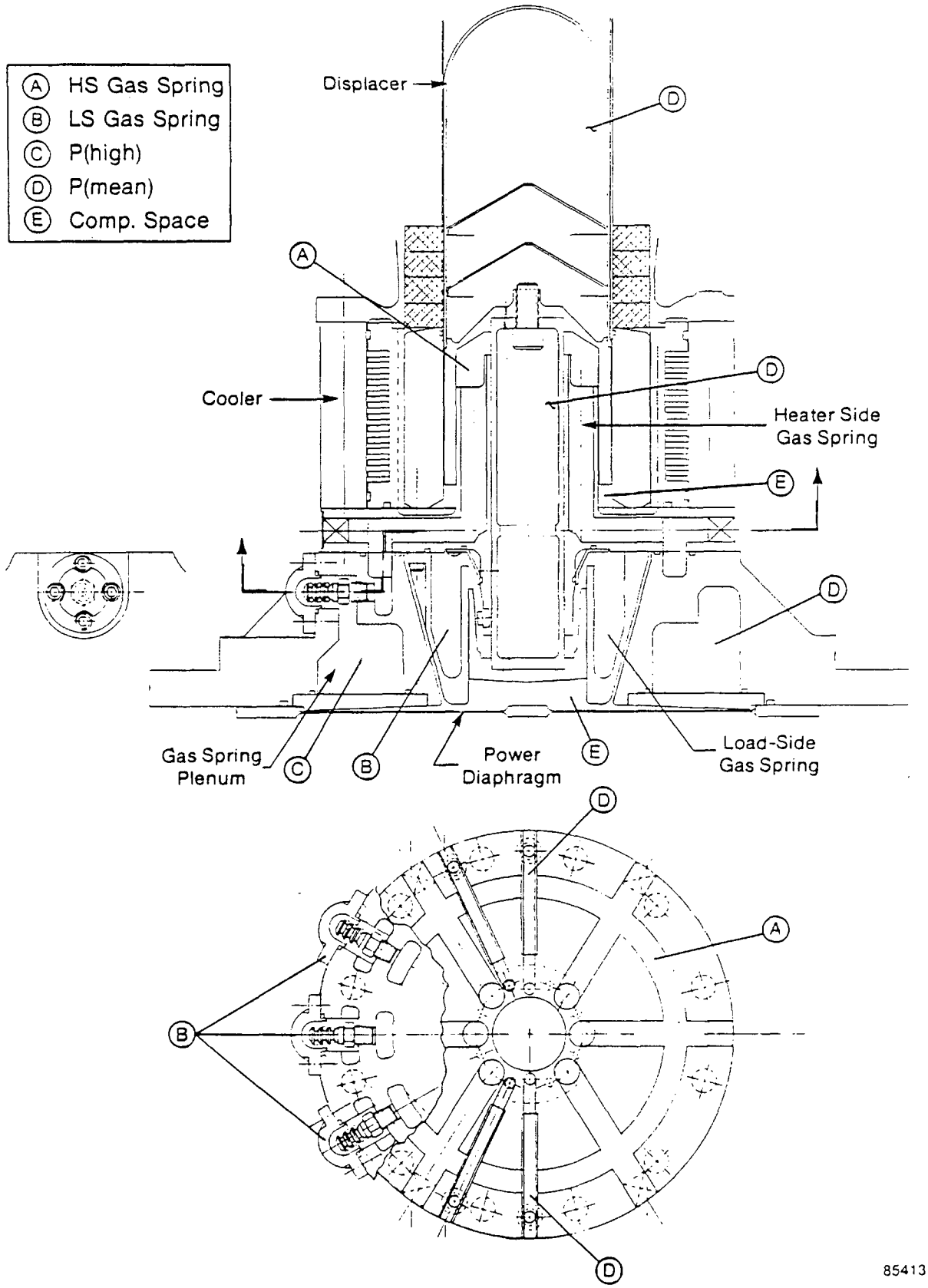

Figure A-5 Free-Piston Stirling Engine Displacer Gas Spring Design (Mark I engine configuration shown is similar to EM No. 4 FPSE)

combustor to the working fluid of the engine. The monolithic head configuration with external fins is shown in Figure A-6. The lower portion of the head houses an annular thermal regenerator. The regenerator serves to periodically exchange heat in the gas streams being shuttled between the cooler and heater head. This heat exchanger provides the internal storage of heat necessary to approach the ideal potential of Carnot efficiency. Standard, fine wire-mesh materials are used in the regenerator.

A.1.1.4 Cooler - The cooler is designed for water cooling with internal and external fins to enhance its heat transfer characteristics. The function of the cooler is to reject heat from the working fluid.

A.1.2 Rankine Refrigerant Compressor

The heat pump compressor is a resonant-piston compressor sinusoidally driven by the pressure wave in the engine. In the design for the compressor and hydraulic coupling (shown in Figure A-1), the compressor was positioned horizontally in order to allow the use of pistons, piston cylinders, cylinder heads, and valve assemblies similar to those commonly used in electrically driven, residential-size heat pump compressors. The operation of the compressor, closely linked to the operation of the hydraulic transmission, will be described in the following section.

A.1.3 Hydraulic Coupling (Transmission)

The hydraulic transmission (provides the force displacement link between the engine and compressor), which consists of the engine power diaphragm, gas spring diaphragm, hydraulic oil, and compressor gas spring, transfers power from the engine to the compressor through deflections of the engine power diaphragm, creating a force unbalance across the compressor drive piston (Figure A-1), forcing it to move. Compression spaces on either side of the piston compress the refrigerant. The lower gas spring diaphragm and compressor gas spring provide the restoring force for the compressor piston. Descriptively, the compressor operation can be seen more clearly in Figure A-7, which defines each of the oil volumes and the interaction between the oil and compressor piston. Starting with motion of the engine diaphragm down, the pressure increases in volume A, producing movement of the drive piston to the left.

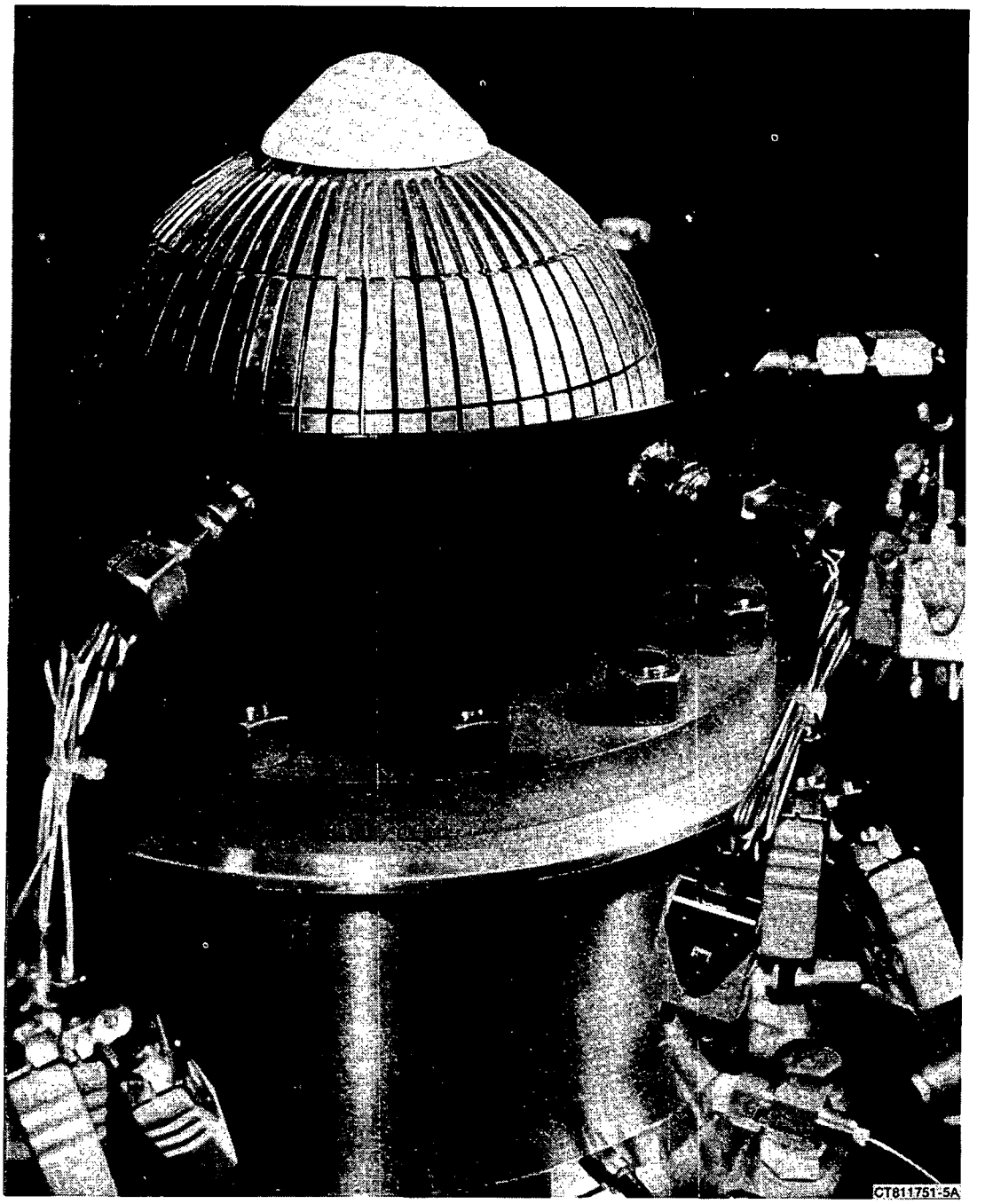

Figure A-6 Monolithic Heater Head Configuration for Engineering Model Engine

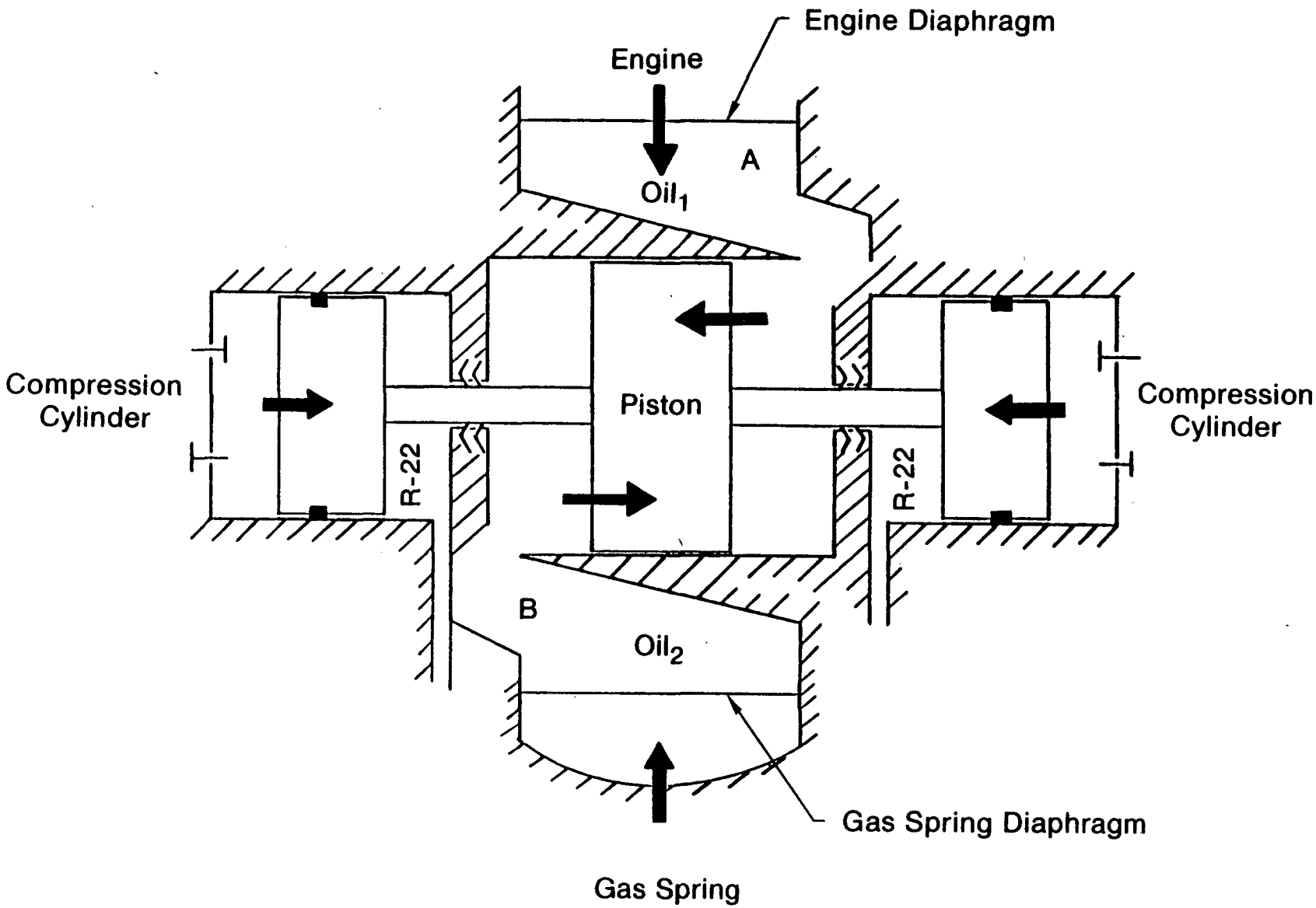

Figure A-7 Hydraulic Transmission and Compressor Schematic

841844

This motion produces two resultant effects: 1) the oil in volume B acts on the compressor gas spring diaphragm (located at the bottom) causing it to deflect down, thus creating a restoring force on the drive piston; and, 2) the movement of the compressor piston to the left produces the compression stroke in the left compression volume and the intake stroke in the right compression volume.

The compressor and hydraulic transmission designs were selected for the following important features:

- Engine/compressor fluids are hermetically sealed from one another

- The horizontal design makes the compressor cylinder heads accessible from outside the machine; thus, repairs can be easily made to the compressor valve assemblies without having to disassemble the entire machine, and the suction manifolds can be insulated to minimize superheating of the suction refrigerant vapor

- The diaphragms allow the Stirling engine power piston and compressor piston to be combined into a single mass, reducing the system from a three-degree to a two-degree-of-freedom system, thus improving the system's operating control.

The hardware for the hydrauic transmission housing and refrigerant compression cylinders is shown in Figure A-8.

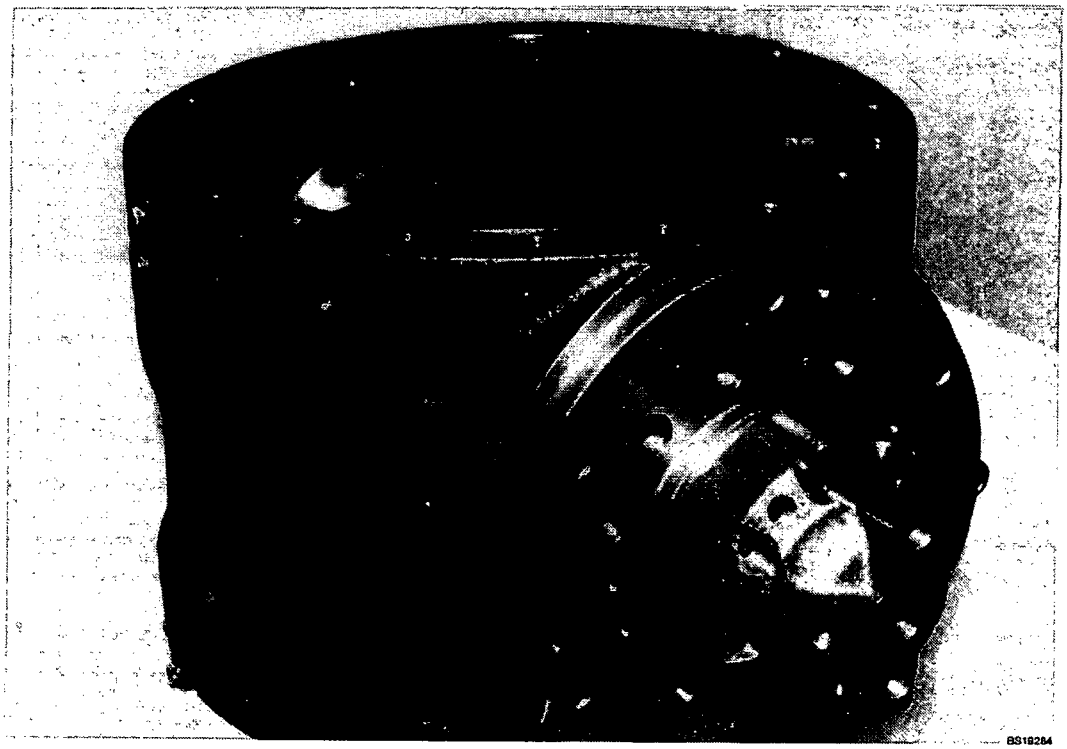

Side View

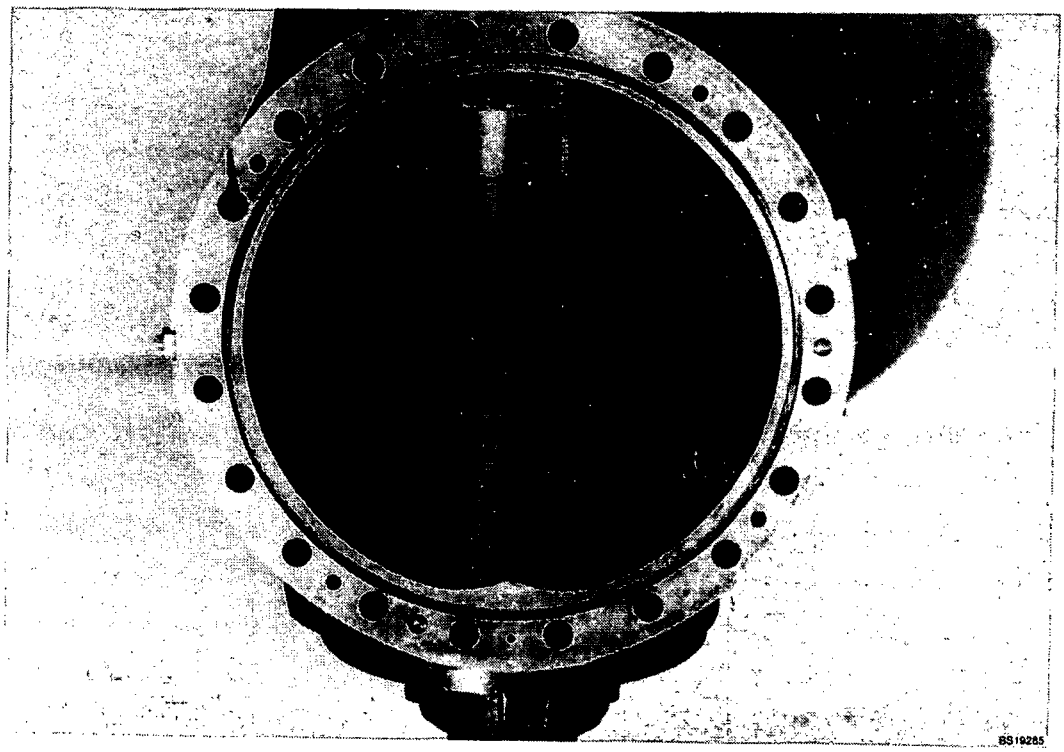

Top View

Figure A-8 Compressor Housing

V5-82

APPENDIX B

HEAT PUMP PERFORMANCE DATA

Appendix B is a summary of the Breadboard Heat Pump test data. Tests were performed at each of nine different ambient temperature conditions with 10-cs silicone oil in the transmission and three tests at 95°F ambient temperature conditions with different viscosity grade oils. The twelve data sheets present the data at different piston strokes (power levels) as described in Section 2.3.2, "Breadboard Heat Pump Test Plan," and oil viscosities as described in Section 2.3.2.3, "Transmission Efficiency As a Function of Transmission Fluid Viscosity." Each entry in the data sheet is an average of that parameter for the three data scans taken at each level after it was clearly established that steady-state operation existed.

All of the parameters in the data tables are either self-explanatory or have been defined in the text with the exception of the lower end COP. The lower end COP may be defined as:

$$\text{Lower End COP} = \frac{\text{Compressor Capacity}}{\text{Engine PV Power}}$$

where compressor capacity, as defined in Section 2.3.2, is the heating and cooling capacity produced in the refrigerant, which does not include the engine rejected heat in the heating mode.

HEAT PUMP MAPPING

AVERAGE DATA SUMMARY

TEST POINT #2

97 DAY CONDITION

DATE: NOV 12, 1985

10 CS SILICONE OIL

REFRIGERANT 22

Displacer Stroke(MM)	21.89	20.05	18.02	15.96
Compressor Stroke (MM)	16.81	16.38	16.01	15.40
Frequency - avg (Hz)	56.85	56.96	56.94	56.85
Heater Head Temp - avg (Deg C)	716.6	711.5	717.7	707.8
Eng. Cooling Water In Temp (Deg C)	-1.108	-1.613	-2.571	-4.450
Mean Engine Pressure (BAR)	59.84	59.91	59.82	59.97
Combustor Exhaust Temp (Deg C)	129.3	131.8	131.7	130.4
Combustor LHV Firing Rate (KW)	11.86	10.90	9.925	8.798
Engine Cooling Water Heat (KW)	8.423	7.955	7.061	6.234
Displacer Phase Angle (Deg)	90.80	88.28	84.84	79.36
Displacer Motor Power (Watts)	624.8	349.4	127.2	-11.53
Engine PV Power - avg (Watts)	2287.	2142.	1921.	1656.
Piston Power Loss (Watts)	296.6	337.2	283.6	362.2
Oil Temperature - avg (Deg C)	42.48	47.60	46.34	43.13
Compressor PV Power (Watts)	1939.	1753.	1591.	1323.
Compressor Suction Pressure (Psia)	89.48	89.74	90.16	91.05
Compressor Suction Temp (Deg F)	63.53	62.09	60.29	59.37
Compressor Discharge Press. (Psia)	310.2	309.6	309.0	308.3
Compressor Discharge Temp. (Deg F)	205.1	203.3	199.2	196.1
Subcooled Refrigerant Temp. (Deg F)	111.8	111.6	111.9	112.0
Refrigerant Mass Flowrate (Lb/Hr)	339.9	308.9	281.1	237.8
Transmission Efficiency (%)	84.83	81.86	82.84	80.57
Compressor Isentropic Power (Watts)	1421.	1280.	1151.	958.8
Compressor Efficiency (%)	73.26	73.01	72.33	73.12
Lower End COP	3.000	2.902	2.926	2.871
System Capacity (BTU/Hr)	23404.	21205.	19175.	16165.
System COP - HHV	.5204	.5129	.5096	.4846
Energy Balance Confidence Value	.9146	.9569	.9541	.9605

HEAT PUMP MAPPING

AVERAGE DATA SUMMARY

95 DAY CONDITION
DATE: NOV 11, 1985

10 CS SILICONE OIL
REFRIGERANT 22

Displacer Stroke(MM)	21.88	20.20	18.08	16.08
Compressor Stroke (MM)	16.42	16.13	15.75	15.26
Frequency - avg (Hz)	56.36	56.29	56.34	56.30
Heater Head Temp - avg (Deg C)	721.9	717.6	721.5	720.2
Eng. Cooling Water In Temp (Deg C)	-1.113	-1.505	-3.312	-5.473
Mean Engine Pressure (BAR)	59.97	59.72	59.86	60.00
Combustor Exhaust Temp (Deg C)	121.5	131.8	131.5	131.1
Combustor LHV Firing Rate (KW)	12.02	11.04	10.15	9.044
Engine Cooling Water Heat (KW)	8.658	8.011	6.988	6.216
Displacer Phase Angle (Deg)	97.65	95.93	92.67	88.22
Displacer Motor Power (Watts)	696.8	402.7	122.0	-18.52
Engine PV Power - avg (Watts)	2265.	2125.	1995.	1767.
Piston Power Loss (Watts)	210.7	235.3	293.2	252.5
Oil Temperature - avg (Deg C)	36.82	41.45	41.63	39.36
Compressor PV Power (Watts)	2001.	1820.	1676.	1492.
Compressor Suction Pressure (Psia)	89.50	90.21	90.34	89.88
Compressor Suction Temp (Deg F)	58.02	60.13	60.50	60.08
Compressor Discharge Press. (Psia)	277.0	276.9	276.4	276.9
Compressor Discharge Temp. (Deg F)	184.0	185.3	182.7	181.7
Subcooled Refrigerant Temp. (Deg F)	98.57	98.87	98.50	101.5
Refrigerant Mass Flowrate (Lb/Hr)	401.2	369.7	342.4	304.0
Transmission Efficiency (%)	88.33	85.68	83.99	84.43
Compressor Isentropic Power (Watts)	1492.	1372.	1268.	1132.
Compressor Efficiency (%)	74.57	75.35	75.64	75.91
Lower End COP	3.746	3.692	3.650	3.609
System Capacity (BTU/Hr)	28950.	26766.	24850.	21756.
System COP - HHV	.6353	.6397	.6460	.6345
Energy Balance Confidence Value	.9078	.9443	.9322	.9431

HEAT PUMP MAPPING

AVERAGE DATA SUMMARY

87 DAY CONDITION
DATE: NOV 14, 1985

10 CS SILICONE OIL
REFRIGERANT 22

Displacer Stroke(MM)	22.03	20.05	18.10	16.13
Compressor Stroke (MM)	16.05	15.62	15.21	14.69
Frequency - avg (Hz)	55.25	55.34	55.34	55.36
Heater Head Temp - avg (Deg C)	711.3	719.8	718.0	717.0
Eng. Cooling Water In Temp (Deg C)	.4885	.2762	-.8472	-2.687
Mean Engine Pressure (BAR)	60.09	59.79	59.97	59.96
Combustor Exhaust Temp (Deg C)	126.9	130.6	130.3	129.7
Combustor LHV Firing Rate (KW)	11.45	10.85	9.790	8.894
Engine Cooling Water Heat (KW)	8.531	7.688	6.954	6.122
Displacer Phase Angle (Deg)	108.3	106.9	103.8	101.7
Displacer Motor Power (Watts)	927.7	539.6	232.1	61.09
Engine PV Power - avg (Watts)	2136.	2001.	1890.	1701.
Piston Power Loss (Watts)	243.5	249.1	258.8	204.1
Oil Temperature - avg (Deg C)	39.44	42.08	41.23	38.94
Compressor PV Power (Watts)	1845.	1718.	1598.	1459.
Compressor Suction Pressure (Psia)	94.67	93.07	93.56	93.40
Compressor Suction Temp (Deg F)	64.23	63.27	63.62	65.43
Compressor Discharge Press. (Psia)	225.0	225.3	226.4	225.7
Compressor Discharge Temp. (Deg F)	164.5	164.1	162.4	163.1
Subcooled Refrigerant Temp. (Deg F)	92.67	92.30	93.13	94.53
Refrigerant Mass Flowrate (Lb/Hr)	480.3	442.1	422.5	382.4
Transmission Efficiency (%)	86.38	85.90	84.59	85.75
Compressor Isentropic Power (Watts)	1363.	1284.	1226.	1114.
Compressor Efficiency (%)	73.88	74.71	76.70	76.39
Lower End COP	4.931	4.849	4.891	4.910
System Capacity (BTU/Hr)	35939.	33094.	31533.	28500.
System COP - HHV	.8281	.8044	.8496	.8453
Energy Balance Confidence Value	.9164	.9080	.9413	.9311

HEAT PUMP MAPPING

AVERAGE DATA SUMMARY

80 DAY CONDITION
DATE: NOV 15, 1985

10 CS SILICONE OIL
REFRIGERANT 22

Displacer Stroke(MM)	22.01	20.10	17.86	15.96
Compressor Stroke (MM)	15.98	15.49	14.81	14.33
Frequency - avg (Hz)	54.66	54.64	54.66	54.68
Heater Head Temp - avg (Deg C)	720.5	717.2	715.5	710.8
Eng. Cooling Water In Temp (Deg C)	-.7260	-.5632	-1.595	-3.127
Mean Engine Pressure (BAR)	60.04	59.85	59.91	60.03
Combustor Exhaust Temp (Deg C)	125.5	130.2	129.7	128.9
Combustor LHV Firing Rate (KW)	11.43	10.43	9.387	8.577
Engine Cooling Water Heat (KW)	8.467	7.817	6.793	5.970
Displacer Phase Angle (Deg)	114.7	113.1	111.8	108.9
Displacer Motor Power (Watts)	1012.	598.5	312.1	107.4
Engine PV Power - avg (Watts)	2106.	1963.	1765.	1656.
Piston Power Loss (Watts)	260.2	251.2	205.0	214.6
Oil Temperature - avg (Deg C)	35.58	38.78	38.20	36.10
Compressor PV Power (Watts)	1808.	1672.	1521.	1411.
Compressor Suction Pressure (Psia)	98.02	97.76	97.70	98.04
Compressor Suction Temp (Deg F)	63.08	65.19	66.50	65.87
Compressor Discharge Press. (Psia)	198.7	198.3	197.5	198.1
Compressor Discharge Temp. (Deg F)	141.3	143.1	143.2	142.4
Subcooled Refrigerant Temp. (Deg F)	77.87	78.70	80.00	81.67
Refrigerant Mass Flowrate (Lb/Hr)	586.6	546.9	503.0	469.4
Transmission Efficiency (%)	85.83	85.16	86.19	85.24
Compressor Isentropic Power (Watts)	1328.	1249.	1148.	1067.
Compressor Efficiency (%)	73.48	74.69	75.46	75.61
Lower End COP	6.441	6.454	6.592	6.507
System Capacity (BTU/Hr)	46285.	43231.	39691.	36742.
System COP - HHV	1.068	1.093	1.115	1.130
Energy Balance Confidence Value	.9005	.9415	.9382	.9354

HEAT PUMP MAPPING

AVERAGE DATA SUMMARY

47 DAY CONDITION
DATE: NOV 18, 1985

10 CS SILICONE OIL
REFRIGERANT 22

Displacer Stroke(MM)	22.04	20.13	18.09	16.04
Compressor Stroke (MM)	17.17	16.71	16.12	15.75
Frequency - avg (Hz)	54.93	54.96	54.96	54.92
Heater Head Temp - avg (Deg C)	721.3	715.8	712.0	712.7
Eng. Cooling Water In Temp (Deg C)	-.3276	.3849	-.1298	-1.662
Mean Engine Pressure (BAR)	60.01	59.93	59.87	59.86
Combustor Exhaust Temp (Deg C)	133.8	133.8	132.5	131.1
Combustor LHV Firing Rate (KW)	11.85	11.04	10.07	9.122
Engine Cooling Water Heat (KW)	8.738	7.793	7.135	6.393
Displacer Phase Angle (Deg)	110.0	108.1	106.5	103.5
Displacer Motor Power (Watts)	769.5	411.8	167.9	-11.01
Engine PV Power - avg (Watts)	2203.	2063.	1893.	1756.
Piston Power Loss (Watts)	306.0	314.8	279.7	299.3
Oil Temperature - avg (Deg C)	41.34	43.33	42.47	40.04
Compressor PV Power (Watts)	1837.	1710.	1558.	1442.
Compressor Suction Pressure (Psia)	74.67	75.31	75.79	76.03
Compressor Suction Temp (Deg F)	51.49	50.83	52.38	51.91
Compressor Discharge Press. (Psia)	210.4	209.6	209.9	209.6
Compressor Discharge Temp. (Deg F)	166.0	163.4	163.6	161.6
Subcooled Refrigerant Temp. (Deg F)	80.30	80.83	81.97	83.73
Refrigerant Mass Flowrate (Lb/Hr)	407.6	380.5	358.9	334.3
Transmission Efficiency (%)	83.42	82.90	82.35	82.14
Compressor Isentropic Power (Watts)	1389.	1277.	1202.	1113.
Compressor Efficiency (%)	75.58	74.65	77.16	77.16
Lower End COP	4.923	4.872	4.992	4.957
System Capacity (BTU/Hr)	62342.	56888.	52923.	48242.
System COP - HHV	1.388	1.359	1.387	1.395
Energy Balance Confidence Value	.9242	.9187	.9411	.9546

HEAT PUMP MAPPING

AVERAGE DATA SUMMARY

TEST POINT #1
45 DAY CONDITION
DATE NOV 19, 1985

10 CS SILICONE OIL
REFRIGERANT 22

Displacer Stroke(MM)	21.86	20.01	18.03	16.24
Compressor Stroke (MM)	17.50	17.20	16.86	16.45
Frequency - avg (Hz)	55.59	55.64	55.66	55.61
Heater Head Temp - avg (Deg C)	721.7	713.6	719.8	711.9
Eng. Cooling Water In Temp (Deg C)	.8218	1.121	.6910	-.9556
Mean Engine Pressure (BAR)	59.81	60.06	60.26	59.83
Combustor Exhaust Temp (Deg C)	130.7	130.2	129.5	127.5
Combustor LHV Firing Rate (KW)	12.16	11.32	10.47	9.514
Engine Cooling Water Heat (KW)	8.786	8.132	7.329	6.566
Displacer Phase Angle (Deg)	103.0	100.8	100.0	97.44
Displacer Motor Power (Watts)	631.1	303.8	85.91	-50.08
Engine PV Power - avg (Watts)	2282.	2127.	1948.	1729.
Piston Power Loss (Watts)	378.7	363.9	333.1	306.7
Oil Temperature - avg (Deg C)	45.25	47.52	46.71	43.40
Compressor PV Power (Watts)	1859.	1718.	1566.	1410.
Compressor Suction Pressure (Psia)	70.74	71.05	71.05	70.98
Compressor Suction Temp (Deg F)	47.32	46.93	44.19	44.91
Compressor Discharge Press. (Psia)	240.6	240.6	240.6	240.8
Compressor Discharge Temp. (Deg F)	187.4	186.4	185.3	184.8
Subcooled Refrigerant Temp. (Deg F)	104.9	105.6	106.5	107.2
Refrigerant Mass Flowrate (Lb/Hr)	336.9	310.7	281.4	247.4
Transmission Efficiency (%)	81.49	80.79	80.38	81.63
Compressor Isentropic Power (Watts)	1362.	1249.	1122.	990.3
Compressor Efficiency (%)	73.29	72.71	71.67	70.25
Lower End COP	3.725	3.655	3.572	3.520
System Capacity (BTU/Hr)	54483.	50112.	45004.	39806.
System COP - HHV	1.182	1.168	1.134	1.104
Energy Balance Confidence Value	.9226	.9421	.9399	.9346

HEAT PUMP MAPPING

AVERAGE DATA SUMMARY

32 DAY CONDITION
DATE: NOV 20, 1985

10 CS SILICONE OIL
REFRIGERANT 22

Displacer Stroke(MM)	19.32	18.11	15.99
Compressor Stroke (MM)	17.73	17.58	17.04
Frequency - avg (Hz)	54.64	54.62	54.67
Heater Head Temp - avg (Deg C)	713.8	718.5	702.1
Eng. Cooling Water In Temp (Deg C)	.3243	-.1550	-2.040
Mean Engine Pressure (BAR)	59.33	59.94	60.25
Combustor Exhaust Temp (Deg C)	126.6	128.6	128.5
Combustor LHV Firing Rate (KW)	11.33	10.83	9.653
Engine Cooling Water Heat (KW)	7.893	7.384	6.700
Displacer Phase Angle (Deg)	106.4	103.3	103.2
Displacer Motor Power (Watts)	179.3	48.84	-82.50
Engine PV Power - avg (Watts)	2050.	1995.	1779.
Piston Power Loss (Watts)	334.2	391.5	348.5
Oil Temperature - avg (Deg C)	39.73	41.64	40.59
Compressor PV Power (Watts)	1648.	1578.	1402.
Compressor Suction Pressure (Psia)	58.01	58.33	58.95
Compressor Suction Temp (Deg F)	37.03	37.98	38.45
Compressor Discharge Press. (Psia)	202.2	202.8	202.3
Compressor Discharge Temp. (Deg F)	177.5	178.1	176.8
Subcooled Refrigerant Temp. (Deg F)	90.70	91.53	91.93
Refrigerant Mass Flowrate (Lb/Hr)	289.5	282.6	255.8
Transmission Efficiency (%)	80.41	79.11	78.81
Compressor Isentropic Power (Watts)	1189.	1160.	1039.
Compressor Efficiency (%)	72.15	73.56	74.14
Lower End COP	3.722	3.716	3.748
System Capacity (BTU/Hr)	48919.	46702.	42178.
System COP - HHV	1.139	1.138	1.153
Energy Balance Confidence Value	.9220	.9223	.9462

HEAT PUMP MAPPING

AVERAGE DATA SUMMARY

17 DAY CONDITION
DATE: NOV 25, 1985

10 CS SILICONE OIL
REFRIGERANT 22

Displacer Stroke(MM)	12.70	10.90	9.054
Compressor Stroke (MM)	17.72	17.11	16.47
Frequency - avg (Hz)	54.28	54.33	54.29
Heater Head Temp - avg (Deg C)	701.0	702.6	702.2
Eng. Cooling Water In Temp (Deg C)	-4.005	-5.457	-7.174
Mean Engine Pressure (BAR)	59.71	59.64	59.57
Combustor Exhaust Temp (Deg C)	116.3	126.7	126.7
Combustor LHV Firing Rate (KW)	8.524	7.380	6.111
Engine Cooling Water Heat (KW)	5.185	4.538	3.881
Displacer Phase Angle (Deg)	102.6	101.5	96.26
Displacer Motor Power (Watts)	-166.1	-137.0	-87.82
Engine PV Power - avg (Watts)	1445.	1203.	986.4
Piston Power Loss (Watts)	372.7	298.0	284.1
Oil Temperature - avg (Deg C)	31.34	33.38	32.22
Compressor PV Power (Watts)	1066.	892.9	680.3
Compressor Suction Pressure (Psia)	43.43	43.54	42.63
Compressor Suction Temp (Deg F)	20.10	17.34	20.39
Compressor Discharge Press. (Psia)	197.0	195.3	197.2
Compressor Discharge Temp. (Deg F)	193.9	191.5	189.4
Subcooled Refrigerant Temp. (Deg F)	92.83	92.47	93.20
Refrigerant Mass Flowrate (Lb/Hr)	150.2	131.4	94.28
Transmission Efficiency (%)	73.77	74.22	69.00
Compressor Isentropic Power (Watts)	752.6	648.4	480.6
Compressor Efficiency (%)	70.63	72.70	70.67
Lower End COP	2.772	2.902	2.513
System Capacity (BTU/Hr)	28696.	25070.	19714.
System COP - HHV	.8881	.8962	.8509
Energy Balance Confidence Value	.8435	.8488	.8665

HEAT PUMP MAPPING

AVERAGE DATA SUMMARY

0 DAY CONDITION
DATE: DEC 2, 1985

10 CS SILICONE OIL
REFRIGERANT 22

Displacer Stroke(MM)	8.794
Compressor Stroke (MM)	17.64
Frequency - avg (Hz)	53.77
Heater Head Temp - avg (Deg C)	686.8
Eng. Cooling Water In Temp (Deg C)	-8.564
Mean Engine Pressure (BAR)	59.85
Combustor Exhaust Temp (Deg C)	103.9
Combustor LHV Firing Rate (KW)	6.365
Engine Cooling Water Heat (KW)	4.283
Displacer Phase Angle (Deg)	100.9
Displacer Motor Power (Watts)	-50.02
Engine PV Power - avg (Watts)	923.4
Piston Power Loss (Watts)	345.7
Oil Temperature - avg (Deg C)	30.66
Compressor PV Power (Watts)	564.2
Compressor Suction Pressure (Psia)	31.09
Compressor Suction Temp (Deg F)	1.757
Compressor Discharge Press. (Psia)	186.0
Compressor Discharge Temp. (Deg F)	192.6
Subcooled Refrigerant Temp. (Deg F)	82.47
Refrigerant Mass Flowrate (Lb/Hr)	64.49
Transmission Efficiency (%)	61.10
Compressor Isentropic Power (Watts)	381.5
Compressor Efficiency (%)	67.88
Lower End COP	1.918
System Capacity (BTU/Hr)	18450.
System COP - HHV	.7647
Energy Balance Confidence Value	.8671

HEAT PUMP MAPPING

AVERAGE DATA SUMMARY

95 DAY CONDITION
DATE: DEC 5, 1985

2 CS SILICONE OIL
REFRIGERANT 22

Displacer Stroke(MM)	21.92	19.99	18.10	16.04
Compressor Stroke (MM)	16.53	16.31	15.84	15.27
Frequency - avg (Hz)	56.35	56.36	56.30	56.26
Heater Head Temp - avg (Deg C)	710.2	708.5	713.6	714.7
Eng. Cooling Water In Temp (Deg C)	.7829	-.5225	-2.387	-4.421
Mean Engine Pressure (BAR)	59.99	60.03	60.07	60.36
Combustor Exhaust Temp (Deg C)	130.3	130.1	128.7	127.8
Combustor LHV Firing Rate (KW)	11.91	11.13	10.14	8.967
Engine Cooling Water Heat (KW)	8.117	7.409	6.665	5.543
Displacer Phase Angle (Deg)	96.84	92.55	90.04	84.85
Displacer Motor Power (Watts)	692.0	364.9	143.7	46.95
Engine PV Power - avg (Watts)	2289.	2139.	1940.	1709.
Piston Power Loss (Watts)	268.7	275.0	221.7	222.0
Oil Temperature - avg (Deg C)	44.19	46.58	45.20	42.05
Compressor PV Power (Watts)	1960.	1803.	1663.	1432.
Compressor Suction Pressure (Psia)	91.31	90.79	90.08	91.50
Compressor Suction Temp (Deg F)	62.10	58.33	56.92	55.84
Compressor Discharge Press. (Psia)	276.4	277.2	277.6	277.7
Compressor Discharge Temp. (Deg F)	188.8	187.9	188.2	183.9
Subcooled Refrigerant Temp. (Deg F)	107.2	109.4	111.7	111.6
Refrigerant Mass Flowrate (Lb/Hr)	396.6	364.1	325.5	281.4
Transmission Efficiency (%)	85.66	84.29	85.75	83.77
Compressor Isentropic Power (Watts)	1457.	1334.	1200.	1016.
Compressor Efficiency (%)	74.35	74.01	72.15	70.97
Lower End COP	3.555	3.424	3.329	3.256
System Capacity (BTU/Hr)	27759.	24988.	22030.	18983.
System COP - HHV	.6150	.5925	.5729	.5585
Energy Balance Confidence Value	.8797	.8866	.8926	.8616

HEAT PUMP MAPPING

AVERAGE DATA SUMMARY

95 DAY CONDITION
DATE: JAN 7, 1986

33 CS MINERAL BASE
REFRIGERANT 22

Displacer Stroke(MM)	21.99	19.97	17.96	16.01
Compressor Stroke (MM)	16.00	15.55	15.21	14.74
Frequency - avg (Hz)	56.67	56.59	56.69	56.67
Heater Head Temp - avg (Deg C)	709.9	708.1	710.3	707.7
Eng. Cooling Water In Temp (Deg C)	-2.498	-2.594	-3.565	-4.845
Mean Engine Pressure (BAR)	60.26	60.12	60.17	59.61
Combustor Exhaust Temp (Deg C)	128.6	128.4	126.4	125.4
Combustor LHV Firing Rate (KW)	12.22	11.17	10.26	9.039
Engine Cooling Water Heat (KW)	8.526	7.693	6.743	5.987
Displacer Phase Angle (Deg)	94.80	92.35	88.67	85.30
Displacer Motor Power (Watts)	739.9	380.9	141.5	7.608
Engine PV Power - avg (Watts)	2228.	2004.	1836.	1645.
Piston Power Loss (Watts)	381.2	300.3	275.0	259.9
Oil Temperature - avg (Deg C)	43.75	47.26	47.54	46.60
Compressor PV Power (Watts)	1797.	1628.	1491.	1325.
Compressor Suction Pressure (Psia)	90.37	91.39	91.92	91.75
Compressor Suction Temp (Deg F)	58.05	61.05	62.09	58.82
Compressor Discharge Press. (Psia)	278.1	277.0	277.6	277.1
Compressor Discharge Temp. (Deg F)	186.9	188.9	190.3	187.1
Subcooled Refrigerant Temp. (Deg F)	97.00	100.7	103.4	106.2
Refrigerant Mass Flowrate (Lb/Hr)	383.4	348.3	316.8	277.8
Transmission Efficiency (%)	80.65	81.29	81.23	80.56
Compressor Isentropic Power (Watts)	1416.	1277.	1160.	1007.
Compressor Efficiency (%)	78.81	78.43	77.79	76.00
Lower End COP	3.663	3.664	3.601	3.450
System Capacity (BTU/Hr)	27841.	25041.	22552.	19359.
System COP - HHV	.6011	.5914	.5799	.5649
Energy Balance Confidence Value	.8827	.8951	.8805	.8999

HEAT PUMP MAPPING

AVERAGE DATA SUMMARY

95 DAY CONDITION
DATE: JAN 7, 1986

10 CS MINERAL BASE
REFRIGERANT 22

Displacer Stroke(MM)	21.88	19.99
Compressor Stroke (MM)	16.25	15.65
Frequency - avg (Hz)	56.73	56.78
Heater Head Temp - avg (Deg C)	712.9	700.0
Eng. Cooling Water In Temp (Deg C)	-1.779	-1.966
Mean Engine Pressure (BAR)	60.04	60.00
Combustor Exhaust Temp (Deg C)	131.4	130.1
Combustor LHV Firing Rate (KW)	12.23	11.31
Engine Cooling Water Heat (KW)	8.601	7.593
Displacer Phase Angle (Deg)	92.65	90.36
Displacer Motor Power (Watts)	648.1	341.5
Engine PV Power - avg (Watts)	2248.	2047.
Piston Power Loss (Watts)	301.5	353.8
Oil Temperature - avg (Deg C)	46.40	47.11
Compressor PV Power (Watts)	1882.	1654.
Compressor Suction Pressure (Psia)	90.82	91.23
Compressor Suction Temp (Deg F)	59.59	61.83
Compressor Discharge Press. (Psia)	278.5	278.0
Compressor Discharge Temp. (Deg F)	188.8	189.5
Subcooled Refrigerant Temp. (Deg F)	93.33	96.55
Refrigerant Mass Flowrate (Lb/Hr)	395.7	365.0
Transmission Efficiency (%)	83.71	80.80
Compressor Isentropic Power (Watts)	1462.	1350.
Compressor Efficiency (%)	77.67	81.68
Lower End COP	3.818	3.837
System Capacity (BTU/Hr)	29281.	26708.
System COP - HHV	.6313	.6247
Energy Balance Confidence Value	.8972	.8846

APPENDIX C

FPSE DATA ACQUISITION SYSTEM

C.1 Hardware

The computer system (Figure C-1) centers around an HP1000 XL computer with 516 kilobytes of memory. Peripherals include a 28 megabyte hard disk with a cartridge tape unit for streaming tapes, two floppy disk drives, an HP2631G graphics printer, an HP Think Jet printer, five terminals and six ASIC (Asynchronous Serial Interface Cards), five HPIB controllers (plus two with bus extenders), and the following instruments:

- (2) HP3456A digital voltmeters
- (1) HP5316A frequency counter
- (1) HP5328A universal counter
- (4) HP3437A system voltmeters
- (8) HP3495 scanners

A data acquisition system based around an HP9825A calculator is also linked via an RS232 serial link to the main computer. This satellite system includes:

- (1) HP3455A digital voltmeter
- (1) HP3495A scanner
- (1) HP59309A relay actuator
- (1) HP59309A digital clock
- (1) FX-80 Epson printer

The hard disk is divided into 11 regions. These are:

- LU14 for system files and major program modules
- LU15 for parts database programs and files
- LU16 for general storage
- LU40 for storage of latest HP software revisions, libraries
- LU41 for cell 1 programs, data
- LU42 for cell 2 programs, data
- LU43 for cell 3 programs, data
- LU44 for cell 4 programs, data
- LU45 for cell 5 programs, data
- LU46 for cell 6 programs, data

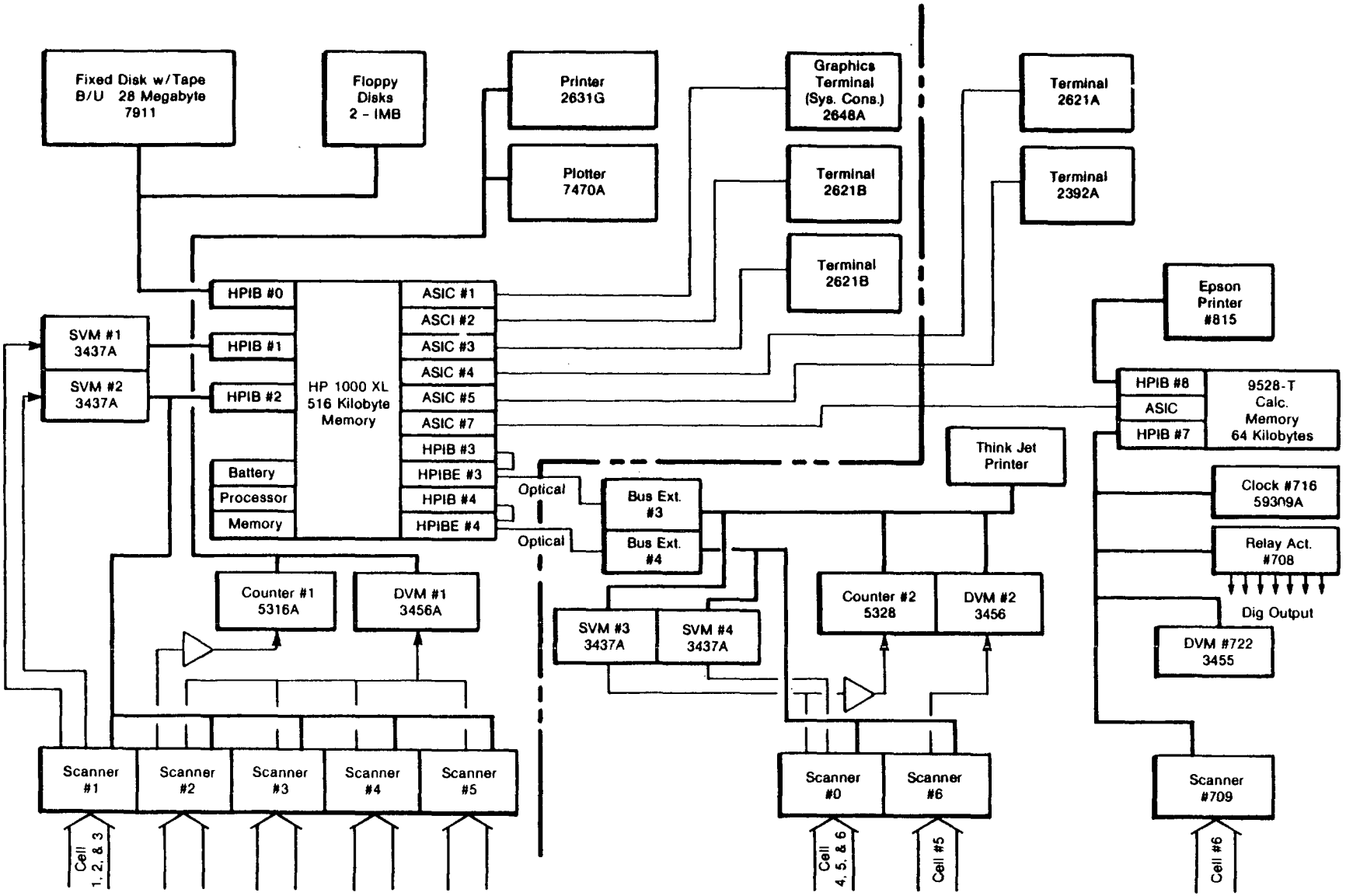

Figure C-1 Free-Piston Data Acquisition System

853498

- LU47 for use by system programmer as well as a general scratch area

C.2 Software

The FPSE Data Acquisition System software consists of four main programs:

1. ACQU - acquires the data from the instruments, writes the data to a file, and prints out a report.

2. PDUC - reads the data file and produces a full report, a summary report, and a data file for later plotting.

3. PLOT - generates graphic output of the raw data and/or calculated results.

4. CFIT - curve fit of data or calculated results.

ACQU: The ACQU program prompts the user for the names of two files - the current Channel Assignment File and the Data Storage File. For each sensor, the Channel Assignment File lists the scanner channel, the gain, the function and range setting for the voltmeter, and a label. This file also contains some constants which are used in later calculations; hence, these constants can be changed without recompiling and reloading the program.

ACQU reads in the Channel Assignment File and then takes an initial scan, reading the raw data from the voltmeters. The program converts this raw data into engineering units, performs the appropriate calculations (as specified in the subroutine CELL), and prints a report listing the converted raw data and the calculated results. The program then pauses and waits for the user to request that a scan take place and, at the user option, that the data be stored on disk in the Data Storage File.

The program takes both dynamic data and steady-state data. To take dynamic data, two HP system voltmeters are used: one connected to the reference channel X_D (displacer stroke) and the other connected to the channel being measured. The frequency is read first (from a frequency counter) and the voltmeters are each then programmed to read 99 points over four cycles. These data are stored in a system buffer and a harmonic analysis program, called

HANAL, is started. This program reads the raw data, computes the amplitude of both signals, and the phase between their first harmonics. The phase is computed from the difference of the ordinate crossings between the measured and reference signals. These results are then sent back to the ACQU program. This process continues through all of the dynamic channels. For steady state channels, the voltage is read and then multiplied by gain or put through the appropriate algorithm to convert to engineering units.

PDUC: The data reduction program asks the user for the name of the Data Storage File which contains the data in question. Then the user is asked which scans are to be summarized and what form the summary is to take. All of the data can be printed or selected variables can be summarized in column fashion. In addition, summary files can be created for later plotting. For each scan requested, the program reads the raw data from the Data Storage File and performs the calculations which appear in the CELL subroutine. The appropriate reports are then printed at the printer or terminal which was specified by the user.

PLOT: The plotting program asks the user for the name of the plot file containing the data. The labels, linetypes, data markers, etc., are then specified by the user. Multiple data sets can be placed on the same plot specified by different markers, and of course, the scale can be set by the user or computed automatically. A curve fit option is available as well.

CFIT: The curve fitting program uses a standard least squares algorithm to perform a polynomial curve fit. In addition, an exponential curve fit can be chosen, which uses a linear fit on the natural logorithms of the data.

A key issue in the data acquisition of dynamic data is the accuracy of phase measurements. A test has been performed to verify the accuracy of these phase readings. A 60-Hz signal with a peak amplitude of 0.5 volts was fed into two channels connected to two different system voltmeters. With one signal being the reference, dynamic data were acquired and a harmonic analysis was performed to compute the phase between the two signals. Twenty data points were taken with this input voltage. The test was repeated for input values of 0.1, 1.0, 1.5, and 1.75 volts. The resulting plot of the phase difference between the two signals versus input voltage appears in Figure C-2. Note that

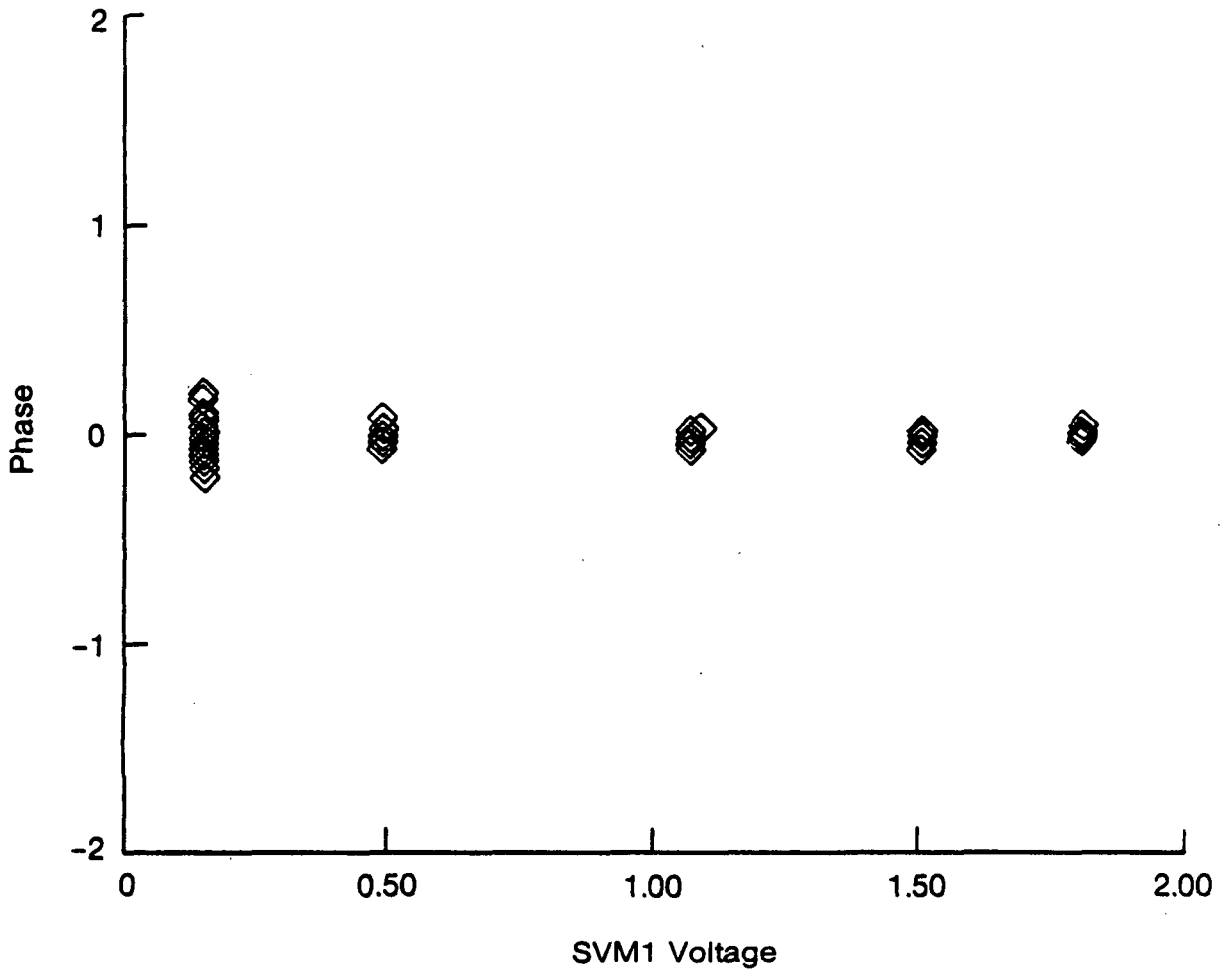

Figure C-2 Error Associated with DAS Phase Angle Calculations

853497

when taking engine data, most dynamic signals are above 0.5 volts into the system voltmeters, yielding very low phase angle measurement errors.

C.3 DAS Output Parameters

Displacer Gas Spring Calculations

CGSPE	CGSPB	CGSPA	CTOT	GSPOW
KGSPE	KGSPB	KGSPA	KTOT	---
PV DISP	PMOTI	PMOTO	ALPHA	PUMPPOW

Combustor Energy Flow

FUEL FLOW	AIR FLOW	AF	QRATE	MFUEL
MAIR	MTOT	TEXHST	ETARECP	QHEADC
QHEADE	QC-QE	ETACCOM	ETACENG	--

Engine PV Performance

PVKUL	PRWN	TAVGS	PFD	TAVGH
QREJ	QCYC	PCV-PM	PFP	COUNT
ETAENG	ETACYC	XDSINPHI	PV/XP**2	SIGMA

Lower End Drive Performance

PVU-OIL	DUCTLOS	PVL-OIL	PLHVP	PRHVP
AISLOSS	PPGS	TAVGOIL	EFFLE	CPIST
XPCAL	—	—	--	--

Lower End Dynamics

KUD	KLD	KMECTOT	KCMPLH	KCOMPRH
KPPGS	KSCPCE	KTOTAL	MP-EFF	--

Compressor Performance

TSUC	TDIS	CVR-LEFT	CVR-RT	MDL-CALC
MDR-CALC	MDL-DATA	MDR-DATA	ETAVOLL	ETAVOLR
ETAISNL	ETAISNR	PR-RATIO	--	--

Performance Calculations

GAS	PGAS	TFLIQ	DDAY	EFFTRA
EFFLE	ENERIN	ENEREG	CONFID	CAP
COP	AR8	ENERCW	ENERFR	AR5
GASFLO	CP	ENERFL	ENEROT	ENGPV
POWISNM	POWISNP	EFCOMPM	EFCOMPP	--

C.4 DAS Parameter Definitions

Displacer Gas Spring Calculations

CGSPE - Gas spring cavity E damping (N sec/m)
CGSPB - Gas spring cavity B damping (N sec/m)
CGSPA - Gas spring cavity A damping (N sec/m)
CTOT - Total gas spring damping (N sec/m)
GSPOW - Gas spring power (watts)
KGSPE - Gas spring cavity E spring stiffness (N/m)
KGSPB - Gas spring cavity B spring stiffness (N/m)
KGSPA - Gas spring cavity A spring stiffness (N/m)
KTOT - Total gas spring stiffness (N/m)
PVDISP - Displacer PV power from cycle (watts)
PMOTI - Engine motor input power (watts)
PMOTO - Engine motor shaft power (watts)
ALPHA - Engine motor alpha angle (°)
PUMPPOW - Engine displacer pumping power (watts)

Combustor Energy Flow

FUELFLOW - Combustor fuel flow (scfh)
AIRFLOW - Combustor air flow (scfh)

AF - Air fuel volume flow ratio
QRATE - Combustor firing rate (kW)
MFUEL - Fuel mass flow rate (kg/sec)
MAIR - Air mass flow rate (kg/sec)
MTOT - Total mass flowrate (kg/sec)
TEXHST - Combustor exhaust temperature (°C)
ETARECP - Combustor preheater efficiency
QHEADC - Heater head flux from combustor energy balance (kW)
QHEADE - Heater head flux from engine energy balance (kW)
QC-QE - Difference in energy into heater head (kW)
ETACCOM - Combustor efficiency (combustor balance)
ETACENG - Combustor efficiency (energy balance)

Engine PV Performance

PVKUL - Engine PV power (watts)
PRWN - Net cycle power (watts)
TAVGC - Average cooler temperature (°C)
PFD - Displacer pressure factor
TAVGH - Average heater head temperature (°C)
QREJ - Heat rejected (cooling water) (watts)
QCYC - Net cycle heat rejection (watts)
PVC-PM - Mean pressure difference between PBP and PMEAN
PFP - Engine pressure factor
COUNT - Number of TC's used in TAVGH calculation
ETAENG - Engine efficiency
ETACYC - Cycle efficiency
XDSINPHI - Displacer stroke x sin of displacer phase angle (mm)
PV/XP**2 - Stroke coefficient
SIGMA - Standard deviation of TC's used in TAVGH calculation

Lower End Drive Performance

PVU-OIL - PV power upper oil cavity (watts)
DUCTLOS - Delta PV power (upper compressor space-upper oil cavity)(watts)
PVL-OIL - PV power lower oil cavity (watts)
PLHVP - PV power refrigerant compressor - left piston (watts)

PRHVP - PV power refrigerant compressor - right piston (watts)
PISLOSS - Loss across piston (watts)
PPGS - PV power piston gas spring (watts)
TAVGOIL - Average oil temperature (°C)
EFFTRA - Transmission efficiency
CPIST - Damping coefficient of piston losses
XPCAL - Calculated piston stroke from gas spring data (mm)

Lower End Dynamics

KUD - Stiffness of upper diaphragm (N/m)
KLD - Stiffness of lower diaphragm (N/m)
KMECTOT - Total mechanical stiffness (N/m)
KCMPLH - Stiffness of refrigerant compressor - left
KCOMPRH - Stiffness of refrigerant compressor - right
KPPGS - Stiffness of power piston - gas spring
KCSPCE - Stiffness of engine
KTOTAL - Total stiffness
MP-EFF - Effective dynamic piston mass (kg)

Compressor Performance

TSUC - Refrigerant suction manifold temperature (°F)
TDIS - Refrigerant discharge manifold temperature (°F)
CVR-LEFT - Clearance volume ratio - left cylinder
CVR-RT - Clearance volume ratio - right cylinder
MDL-CALC - Calculated refrigerant compressor mass flow - left cylinder
MDR-CALC - Calculated refrigerant compressor mass flow - right cylinder
MDL-DATA - Estimated refrigerant compressor mass flow - left cylinder
MDR-DATA - Estimated refrigerant compressor mass flow - right cylinder
ETAVOLL - Volumetric efficiency-refrigerant compressor - left cylinder
ETAVOLR - Volumetric efficiency-refrigerant compressor - right cylinder
ETAISNL - Isentropic efficiency-refrigerant compressor - left cylinder
ETAISNR - Isentropic efficiency-refrigerant compressor - right cylinder
PR-RATIO - Refrigerant-compressor - pressure ratio

Performance Calculations

GAS - Combustor gas flow rate (acfm)

PGAS - Combustor gas flowmeter pressure (in H_2O)

TFLIQ - Refrigerant calorimeter liquid temperature (°F)

DDAY - Degree day condition (°F)

EFFTRA - Transmission efficiency (%)

EFFLE - Lower end efficiency (%)

ENERIN - System energy input (watts)

ENEREG - Upper end energy output (watts)

CONFID - Energy out - energy in ratio

CAP - Refrigerant compressor capacity (BTU/hr)

COP - System coefficient of performance

AR8 - Combustor exhaust gas energy (watts)

ENERCW - Cooling water rejected energy (watts)

ENERFR - Refrigerant compressor energy output (watts)

AR5 - Combustor air inlet energy (watts)

GASFLO - Combustor gas flow rate (scfm)

CP - Cooling water specific heat (BTU/lbm °F)

ENERFL - Energy input from the fuel gas based on LHV (watts)

ENEROT - System energy output (watts)

ENGPV - Average measurement of engine PV power (watts)

POWISNM - Compressor isentropic power, manifold conditions (watts)

POWISNP - Compressor isentropic power, plenum conditions (watts)

EFCOMPM - Compressor efficiency, manifold conditions (%)

EFCOMPP - Compressor efficiency, plenum conditions (%)

ORNL/Sub/86-47985/1
Dist. Category UC-95d

INTERNAL DISTRIBUTION

1. F. C. Chen
2. F. A. Creswick
3. N. Domingo
4. P. D. Fairchild
5. S. K. Fischer
6. W. Fulkerson
7. F. P. Griffin
8. M. A. Kuliasha
9. F. C. Maienschein
10. S. H. McConathy
11. R. W. Murphy
12. G. T. Privon
13. C. D. West

14–33. Energy Conservation Distribution, 9102-2, Room 218

34–35. Central Research Library

36. Document Reference Section
37. Laboratory Records—RC

38–39. Laboratory Records

40. ORNL Patent Section

EXTERNAL DISTRIBUTION

41–52. R. A. Ackermann, Mechanical Technology, Inc., 968 Albany-Shaker Road, Latham, NY 12110

53. William Beale, Sunpower, Inc., 6 Byard Street, Athens, OH 45701
54. Glendon M. Benson, Energy Research and Generation, Inc., Lowell and 57th Streets, Oakland, CA 94608
55. Don Beremand, NASA–Lewis Research Center, 21000 Brookpark Road, Cleveland, OH 44135
56. Dick Bloomquist, Code 2752, David W. Taylor Naval Ship R&D Center, Annapolis, MD 21402
57. T. A. Braun, Tectonics Research, Inc., 9556 West Bloomington Freeway, Minneapolis, MN 55431
58. J. P. Budliger, Battelle-Geneva, 7 route de Drize, 1227 Carouge (Geneva), SWITZERLAND
59. J. M. Calm, Electric Power Research Institute, P.O. Box 10412, Palo Alto, CA 94303
60. J. G. Carbonell, Associate Professor of Computer Science, Carnegie-Mellon University, Pittsburgh, PA 15213
61. Stig C. Carlqvist, Societe ECA, Boite Postale 16, 92194 Meudon Cedex, FRANCE
62. Dick Cawley, Lennox Industries, Inc., 1600 Metrocrest Drive, Carrollton, TX 75006
63. W. S. Chiu, General Electric Company, P.O. Box 527, King of Prussia, PA 19406
64. M. Clinch, Gas Research Institute, 8600 West Bryn Mawr Avenue, Chicago, IL 60631
65. E. H. Cooke-Yarborough, Lincoln Lodge, Longworth Nr Abingdon, Oxfordshire, OX13, 5DU, ENGLAND
66. J. G. Daley, Argonne National Laboratory, 9700 South Cass Avenue, Argonne, IL 60439
67. D. K. Darooka, General Electric Company, P.O. Box 527, King of Prussia, PA 19406
68. R. L. Demler, Foster-Miller Associates, Inc., 350 2nd Avenue, Waltham, MA 02254
69. G. R. Dochat, Mechanical Technology, Inc., 968 Albany-Shaker Road, Latham, NY 12110

70. J. E. Dudenhoefer, NASA–Lewis Research Center, 21000 Brookpark Road, Cleveland, OH 44135
71. T. Finkelstein, Stirling Associates International, P.O. Box 643, Beverly Hills, CA 90213
72. R. J. Fiskum, Energy Conversion Equipment Branch, CE-112, GF-217/FORS, U.S. Department of Energy, 1000 Independence Avenue SW, Washington, DC 20585
73. M. Foster, Homach Systems, Ltd., Hargreaves Road, Groundwell Industrial Estate, Swindon Wilts, SN2, 5AZ, ENGLAND
74. A. A. Frank, Department of Electrical and Computer Engineering, University of Wisconsin–Madison, 1500 Johnson Drive, Madison, WI 53706
75. S. Freedman, Gas Research Institute, 8600 West Bryn Mawr Avenue, Chicago, IL 60631
76. M. Fukiwake, Agency of Industrial Science and Technology, Ministry of International Trade and Industry, 1-3-1 Kasumigaseki, Chiyoda-Ku, Tokyo, JAPAN
77. D. R. Gedeon, Gedeon Associates, Box 141 A, South Canaan Road, Athens, OH 45701
78. Ted Gilles, Lennox Industries, Inc., Promenade Towers, P.O. Box 400450, Dallas, TX 75240
79. S. M. Gillis, Dean of the Graduate School, Duke University, 4875 Duke Station, Durham, NC 27706
80. L. Goldberg, University of Minnesota, Department of Civil and Mineral Engineering, 500 Pillsbury Drive SE, Minneapolis, MN 55455
81. B. S. Goldwater, Mechanical Technology, Inc., 968 Albany-Shaker Road, Latham, NY 12110
82. A. C. Harvey, Foster-Miller Associates, Inc., 350 2nd Avenue, Waltham, MA 02254
83. R. E. Hise, Consolidated Natural Gas Research Company, 11001 Cedar Avenue, Cleveland, OH 44106
84. Bob Holtz, Argonne National Laboratory, 9700 South Cass Avenue, Argonne, IL 60439
85. R. C. Hundt, Lennox Industries, Inc., 1600 Metrocrest Drive, Carrollton, TX 75006
86. P. Huntley, Borg-Warner Research, 1200 South Wolf Road, Des Plaines, IL 60018
87. B. C. Hwang, Code 2722, David W. Taylor Naval Ship R&D Center, Annapolis, MD 21402
88. H. S. Izawa, Northern Natural Gas Company, 2223 Dodge Street, Omaha, NE 68102
89. L. N. Johansson, Stirling Power Systems, 7101 Jackson Road, Ann Arbor, MI 48103
90. F. R. Kalhammer, Vice President, Electric Power Research Institute, P.O. Box 10412, Palo Alto, CA 94303
91. T. Kapus, CE-113, Building Equipment Division, U.S. Department of Energy, 1000 Independence Avenue SW, Washington, DC 20585
92. K. P. Lee, Aspen Systems Inc., 275 Boston Post Road, Marlborough, MA 01752
93. Dr. Martin Lessen, Consulting Engineer, 12 Country Club Drive, Rochester, New York 14618
94. Bengt Lundquist, Swedish Council for Building Research, Sankt Goransgatan, S-11233 Stokholm, SWEDEN
95. A. R. Maret, Gas Research Institute, 8600 West Bryn Mawr Avenue, Chicago, IL 60631
96. J. C. Mayor, Swiss Federal Institute for Reactor Research, CH-5303 Wurenlingen, SWITZERLAND
97. R. C. Meier, General Electric Company, P.O. Box 527, King of Prussia, PA 19406

98. R. J. Meijer, Stirling Thermal Motors, Inc., 2841 Boardwalk, Ann Arbor, MI 48104
99. N. P. Nightingale, Mechanical Technology, Inc., 968 Albany-Shaker Road, Latham, NY 12110
100. Herbert Nilsson, United Stirling AB, P.O. Box 856, S-201 80 Malmo, SWEDEN
101. L. B. Penswick, Sunpower Inc., 6 Byard Street, Athens, OH 45701
102. W. H. Percival, United Stirling, Inc., 1800 Diagonal Road, Alexandria, VA 22314
103. B. Qvale, Laboratory for Energetics, The Technical University of Denmark, DTH Building 403, DK-2800 Lyngby, DENMARK
104. E. A. Reid, Jr., Columbia Gas System Service Corporation, 1600 Dublin Road, Columbus, OH 43215
105. P. Riggle, Joint Center for Graduate Study, University of Washington, 100 Sprout Road, Richland, WA 99352
106. J. D. Ryan, Energy Conversion Equipment Branch, CE-112, GF-217/FORS, U.S. Department of Energy, 1000 Independence Avenue SW, Washington, DC 20585
107. J. G. Schreiber, NASA–Lewis Research Center, 21000 Brookpark Road, Cleveland, OH 44135
108. J. R. Senft, Department of Mathematics/Computer Science, University of Wisconsin, River Falls, WI 54022
109. J. G. Slaby, NASA–Lewis Research Center, 21000 Brookpark Road, Cleveland, OH 44135
110. J. L. Smith, Jr., Mechanical Engineering Department, Massachusetts Institute of Technology, Cambridge, MA 02139
111. P. F. Swenson, The East Ohio Gas Company, East 9th Avenue at Superior, P.O. Box 5759, Cleveland, OH 44101
112. D. R. Taylor, Royal Naval Engineering College, Manadon Plymouth, Devon PL5 3AQ, ENGLAND
113. W. P. Teagan, Arthur D. Little, Inc., 20 Acorn Park, Cambridge, MA 02140
114. R. C. Tew, NASA–Lewis Research Center, 21000 Brookpark Road, Cleveland, OH 44135
115. W. M. Toscano, Aspen Systems, Inc., 275 Boston Post Road, Marlborough, MA 01752
116. V. J. Van Griethuysen, Air Force Wright Aeronautical Laboratories, Wright-Paterson Air Force Base, OH 45433
117. D. A. Vaughn, ATTN: STRBE-EMP, Belvoir R&D Center, Ft. Belvoir, VA 22060
118. G. Walker, University of Calgary, Department of Mechanical Engineering, 2500 University Drive NW, Calgary, CANADA T2N1N4
119. B. P. Wang, Mechanical Engineering Department, University of Texas at Arlington, P.O. Box 19023, Arlington, TX 76019
120. M. A. White, University of Washington, Joint Center for Graduate Study, 100 Sprout Road, Richland, WA 99352
121. L. Williams, Logan Lewis Library, Research Division, Carrier Corporation, Carrier Parkway, Syracuse, NY 13221
122. J. Wurm, Institute of Gas Technology, 3424 South State Street, Chicago, IL 60616
123. Y. Yamashita, New Energy Development Organization, Sunshine 60 29F, 101 3-Chome Higashi-Ikebukuro, Toshima-Ku, Tokyo 170 JAPAN
124. Institute for Energy Analysis, ORAU Library, Oak Ridge, TN 37831
125. Office of the Assistant Manager for Energy R&D, U.S. Department of Energy, Oak Ridge Operations, Oak Ridge, TN 37831

126–341. Given distribution for Category UC-95d

☆U.S. GOVERNMENT PRINTING OFFICE 1987—548-118/60125